Australian Government
Department of Defence
Defence Science and
Technology Organisation

Exploration of Questions Regarding Modelling of Crack Growth Behaviour under Practical Combinations of Aircraft Spectra, Stress Levels and Materials

P. Jackson, C. Wallbrink, K. Walker, D. Mongru and W. Hu

Air Vehicles Division
Defence Science and Technology Organisation

DSTO-RR-0368

ABSTRACT

Questions regarding the boundries of validity of crack growth modeling tools in aircraft structural analysis have been asked of the Methods and Standards Group within AVD. Continuing the Group's previous endeavours along these lines, this report commences by stating the questions that will be explored and then individually examining the issues using both experimental data from coupon tests run under typical aircraft spectra and results from various crack growth prediction models. The findings, particularly those regarding the likely boundaries of validity of different crack growth modelling techniques are then discussed. Conclusions are drawn regarding the implications of the findings of the work for fatigue practicioners within DSTO and for future work within the Methods and Standards Group. The Defence Outcome is the more effective and efficient assessment of aircraft strutural life.

RELEASE LIMITATION

Approved for public release

Published by

Air Vehicles Division
DSTO Defence Science and Technology Organisation
506 Lorimer St
Fishermans Bend, Victoria 3207 Australia

Telephone: (03) 9626 7000
Fax: (03) 9626 7999

AR-015-053
July 2011

Conditions of Release and Disposal

Exploration of Questions Regarding Modelling of Crack Growth Behaviour under Practical Combinations of Aircraft Spectra, Stress Levels and Materials

Executive Summary

Modelling of fatigue crack behaviour in metallic aircraft structures has traditionally been split into a nucleation phase and a growth phase. The growth phase starts when the crack becomes observable, when the crack is said to have initiated. As the fundamental nature of each stage of nucleation and growth of a fatigue crack is still not understood well enough to allow successful constitutive mechanistic modelling, empirical models are by far the most dominant means for predicting fatigue life and crack growth. Whilst empirical modelling has been successful in significantly improving aircraft safety and reducing accidents, the current models are not without their limitations and difficulties. For example, it is not always easy to determine the 'transference' of a particular model from one problem or set of input values to another. Inefficiencies in research work or inaccurate life estimates are a potential result of using models outside a set of verified limits.

The Methods and Standards Group within Aircraft Structures Branch of Air Vehicles Division has been asked by the Directorate General Technical Airworthiness (DGTA) to provide advice on the accuracy of different fatigue life estimation approaches by exploring their boundaries of applicability or validity and evaluating their advantages and disadvantages in what has been defined as the 'Mapping of the Problem Space and the Method Space'. In order to provide the advice sought by DGTA and the aircraft structural integrity community a number of questions need to be asked. When are the traditional approaches to crack growth valid and when are they not? Where do they need improvement? Where would experimentally based methods be more suitable and/or more applicable? As the potential 'problem space' is made complex by factors such as material, stress and load sequence and structural configuration, the above questions are only being asked in the context of most interest to Aircraft Structures Branch, that is, of high strength aluminium alloys and stress spectra associated with fatigue sensitive locations on typical RAAF aircraft.

This report continues the Group's endeavours on this issue and starts by stating the questions that will be examined, namely; what trends in crack growth behaviour can be observed from tests under practical aircraft spectra used within DSTO; and what issues influence the ability of traditional models to successfully make predictions for crack growth under both combat and transport aircraft type spectra. The findings, particularly those regarding the need to both calibrate traditional models and validate any predictions, as well as the likely boundaries of applicability of different crack growth modelling techniques are then discussed. A new and insightful way of looking at data as it is being used within a particular existing crack growth model is presented.

One conclusion is that traditional fracture mechanics based crack growth models are suitable for use for all aircraft types such as F/A-18, F-111 and P-3, however care must be taken in their calibration and the use of input data. Importantly, the research shows that

continued improvement in the understanding of the growth of very small cracks and the availability of near-threshold crack growth rate data is required. Some new and insightful ways of looking at the data being processed by crack growth models is presented and this has helped improve the understanding of researchers, giving an opportunity to improve the accuracy of crack growth modelling work within DSTO. The work continues the effort aimed to provide guidelines for selecting and applying the best tools for analysis of fatigue cracking in RAAF aircraft structures.

Authors

P. Jackson
Air Vehicles Division

Philip Jackson graduated from the Royal Melbourne Institute of Technology (RMIT) in 1981 with a Bachelor of Aeronautical Engineering (with distinction). He spent the next 15 years as an engineering officer with the Royal Australian Air Force in both squadron and staff engineering posts specialising in aircraft structural integrity and fatigue management. In 1988 he completed a Masters of Science in Aerospace Vehicle Design at Cranfield Institute of Technology, UK and from 1991-94 was attached to the Canadian National Research Council, Ottawa, Canada as part of the F/A-18 International Follow-On Structural Test Project. He joined DSTO in 1997 and has been the technical and program lead for the DSTO contributions to the international P-3 Service Life Assessment Program (SLAP). He is currently Head, Helicopter and Transport Aircraft Structural Integrity in the Aircraft Structures Branch of Air Vehicles Division as well as leading the divisional research effort on airworthiness and aircraft design standards.

C. Wallbrink
Air Vehicles Division

Chris Wallbrink graduated in 2005 with a PhD from Monash University in the department of Mechanical Engineering. He then held the position of research fellow at Monash University until the end of 2006 where his research interests included, modelling of fatigue crack growth, infrared NDT technologies and fibre optic corrosion detection devices. He joined DSTO in 2007 in the Air Vehicles Division and is currently conducting research into methods of fatigue crack growth modelling and airworthiness standards.

K. Walker
Air Vehicles Division

Kevin Walker graduated in 1983 with a Bachelor of Aeronautical Engineering (with distinction) from Royal Melbourne Institute of Technology (RMIT). He then served for eight years with the Royal Australian Air Force, including a posting to the USA where he gained a Master of Science in Aeronautics and Astronautics from Purdue University. He then worked for three years in private industry before joining DSTO AVD in early 1994. His work at

DSTO has included fatigue crack growth and damage tolerance analysis studies (mainly related to the F-111 aircraft), evaluation of fatigue monitoring systems, development, design, validation and substantiation of bonded composite repairs, and development of improved fatigue crack growth analysis software. He is currently Science Team Leader for surveillance aircraft including the P3 Maritime Patrol and the Boeing 737 based AEW&C aircraft.

D. Mongru
Air Vehicles Division

David Mongru graduated from RMIT in 1990 with a Bachelor of Aerospace Engineering (Honours). He commenced work at DSTO in 1994 working on loads development and fatigue interpretation for the PC9 fatigue test. He joined the F/A-18 International Follow-on Structural Test program at DSTO in 1996 performing fatigue analysis of critical components on the aft fuselage of the F/A-18. In 2001 he commenced work on the P-3 Service Life Assessment Program at DSTO. As part of that program he spent two years working with Lockheed-Martin, Matietta, GA. His primary functions included fatigue test interpretation and provision of technical support to the P-3 empennage test. He spent several years working in the airworthiness standards and fatigue mechanisms group before joining the DSTO enabling research program.

W. Hu
Air Vehicles Division

Weiping Hu joined DSTO in 1998 as a research scientist. He is currently a senior research scientist leading the development of modelling capabilities for the analysis of structural integrity of aircraft structures.

After obtaining his PhD degree in 1993 at Dublin City University Ireland, he has held various academic positions at Dublin City University, Monash University and Deakin University. His current research interests include fatigue crack growth in aircraft structures, constitutive models and plasticity, and numerical methods in engineering.

Contents

1. Introduction

Modelling of fatigue crack behaviour in metallic aircraft structures has traditionally been split into a nucleation phase and a growth phase. The growth phase starts when the crack becomes observable, when the crack is said to have initiated. As the fundamental nature of each stage of nucleation and growth of a fatigue crack is still not understood well enough to allow successful constitutive mechanistic modelling, empirical models are by far the most dominant means for predicting fatigue life and crack growth in engineering practice. In this report, fatigue life refers to the time endured by a structural element subjected to fatigue loading from the initial or as-made state through to failure, where failure could be either a predefined crack length, a percentage change in compliance or the total fracture of the element. In contrast, crack growth life, or simply crack growth, refers to the time history of the crack length. The fatigue life of an aircraft structure has traditionally been assessed using stress-life or strain-life approaches, and the crack growth has been mainly predicted using linear elastic fracture mechanics (LEFM). While these approaches have been successful in significantly improving aircraft safety and reducing accidents, they are not without their limitations and difficulties.

The Methods and Standards Group in the Air Vehicles Division (AVD) of DSTO has been asked to provide advice on the applicability of different fatigue life estimation approaches by exploring their boundaries of validity and evaluating their advantages and disadvantages in what has been defined as the task of 'Mapping of the Problem Space and the Method Space'. This report aims to initiate investigations into several aspects of the problem, thereby potentially identifying the directions in which more in-depth work could take to tackle the task.

Examining the behaviour of fatigue cracks leads to clues about how to best model this failure mechanism. Using these clues, empirical models have historically been developed, tested and refined, but due to their empirical nature, the boundary of validity of this type of models is generally limited to the cases for which they were developed. Subsequent extrapolation of the boundary of validity generally proceeds (or should proceed) cautiously. For example, most classical models assume that the crack growth behaviour under spectrum loading may be adequately modelled using crack growth rates generated under constant amplitude loading data. These models do have known limitations that are often reflected in the way they are used, and in the methodologies that are implicit in the overall airworthiness regulations. Furthermore, the acceptable bounds of validity of a model or methodology are often influenced by the purpose and resource limits associated with the analysis.

Experimentally, fractography has provided a means to examine cracks down to very small sizes. It has been observed that plots of logarithm of crack size versus time for some cracks in aircraft components and coupons of aluminium alloy have shown linear relationships, down to a definable initial flaw size. Other experimental results have shown more complicated relationships, including an initial period of negligible or very slow growth followed by accelerated growth, or the reverse, depending on the geometry of the crack configuration and the load level. One of the challenges for fatigue crack growth modelling is to be able to represent these different growth behaviours in a consistent manner.

In order to provide the advice sought by the aircraft structural integrity community in AVD and the Directorate General Technical Airworthiness (DGTA), a number of questions can thus be asked. When are the different approaches to crack growth applicable and when are they not? Where do they need improvement? What are the relative strengths and limitations of the models based on constant amplitude data and those based on variable amplitude data? When are they more suitable and/or more applicable? Are there limitations to the use of these approaches? As the potential 'problem space' is huge, made complex by factors such as material, stress and load sequence and structural configuration, the above questions are only being asked in the context of most interest to Aircraft Structures Branch of AVD, i.e. within the scope of high strength aluminium alloys and stress spectra associated with fatigue sensitive locations on typical RAAF aircraft. This report continues the Group's endeavours along the same lines as previous work [1], [2].

Focussing on aspects of so-called traditional models, this report addresses two questions taken from the work that commenced in a previous discussion paper [3, 4]. The findings, particularly those regarding the performance of traditional crack growth models are then discussed. Conclusions are drawn regarding the implications of the findings and for future work within the Fatigue Methods and Standards Group.

1.1 Fatigue and Fatigue Crack Growth

The fatigue process can be roughly divided into three stages: cyclic hardening/softening, crack nucleation, stable crack propagation and then a final overload leading to unstable fracture and failure. The propagation period itself can also be broken down into a period of growth and coalescence of microcracks, and a period of growth of macro-cracks which can itself be broken into stages. In flaw-free materials, a significant amount of the total lifetime is spent during crack nucleation and growth of microcracks. At low load amplitudes the nucleation stage can occupy the majority of the lifetime. Conversely, at high amplitudes nucleation is usually accomplished within a small fraction of the fatigue life. Another fraction of the lifetime is needed for propagation of the microstructurally small cracks (cracks small compared to microstructural size scales) to reach the size of the physically small cracks (*i.e.*, ~0.5-1.0 mm). Again, this fraction can be quite high at low load amplitudes. While the propagation of physically small cracks and long cracks can be described by LEFM, there is no generally agreed quantitative description of the nucleation process, and there are a number of concepts for the propagation of microstructurally small cracks.

Fatigue would thus appear to be a complex phenomenon, influenced significantly by the material in which it occurs. Initiation of fatigue cracks has been observed to occur along slip bands, at grain boundaries, in second-phase particles, and at inclusion or second-phase interfaces with the matrix phase. The mode of fatigue crack initiation observed in any particular circumstance depends on which occurs most easily. Fortunately, if we limit ourselves to the problems of most concern within Aircraft Structures Branch, those relating to common aircraft materials, stress levels and surface finishes, the problem space can be simplified. In aluminium alloys and steels used in aircraft structures the constituent particles present in Al alloys or inclusions present in steels are the primary source of initiation.

Surface breaking constituent particles, sometimes removed by processes such as etching or cracked during machining have been shown by DSTO researchers [5] to play a dominant role in the formation of 'normal' fatigue. Whilst DSTO has been prominent recently in the research in this area, the notion that cracking occurs not long into the life of aluminium aircraft components from surface or near surface constituent particles is generally accepted[1]. The cracking of the aluminium alloy coupons described in the previous Discussion Paper [4] and again in this report showed the same behaviour, i.e. initiation at surface breaking constituent particles (or their voids left by etching) in the parent material. Coupons from sheet aluminium material clad by a thin corrosion protective pure aluminium layer showed a slightly different mechanism, with cracking initiating in the clad layer.

1.2 Crack Initiation

In contrast to the metallurgically-based breakdown of the fatigue process described in Section 1.1 above, engineers often use the terms of 'crack initiation' and 'crack growth' or 'established crack growth', which when added together give 'total fatigue life'. For practical or engineering purposes, it is useful to define the 'initiation stage' as that portion of the lifetime before a crack is detectable by usual non-destructive evaluation (NDE/NDI) techniques. This is typically 1.00-2.00 mm (0.050 – 0.100 inches). As the resolution of inspection instruments increases, the portion of the fatigue lifetime ascribed to fatigue crack 'initiation' decreases. For example, if the NDE technique of magnetic rubber is used, the size of detectable crack can be as small as 0.20 mm (0.010 inches). It should be noted that for life assessment, the chosen value for crack initiation (i.e. the crack size defined as the point at which initiation is said to have occurred) or initial crack size a_i should be compatible with the capability of the crack growth model used for subsequent analysis.

1.3 Crack Growth

The inference from the earlier description of the stages of the fatigue process is that after mircocracks have nucleated, they must initially grow in an environment dominated by non-homogeneous material effects and local strain concentrations. At a certain size the microcracks become large enough to enter a phase of more stable and repeatable growth dominated by stress intensity factor ΔK. Towards the end of crack growth, things again become more complicated as changes in stress state, stable tearing and the material fracture toughness all become influential. The final stage of growth leading to unstable fracture is generally given less attention when performing life assessment, simply because it typically takes up very little of the overall life, but it is crucial for residual strength consideration.

1.4 Other Literature

In his comprehensive review [6] of the historical developments in the science of fatigue J. Schijve thought it useful to consider the fatigue life as consisting of two phases:

[1] Presentation at DSTO by J. Newman, Professor Mississippi State University, May 2010.

- *The crack initiation period,* including crack nucleation and microcrack growth
- *The crack growth period,* covering the growth of a visible crack until final failure

Schijve shows these phases in a block diagram, see Figure 1, with the associated stress related factor that researchers believed drives the crack growth. The percentage of time in the initiation period verses the growth period will depend upon the stress in the material and the initiating defect or notch. There is also an obvious question of defining the transition from the initiation period to the crack growth period.

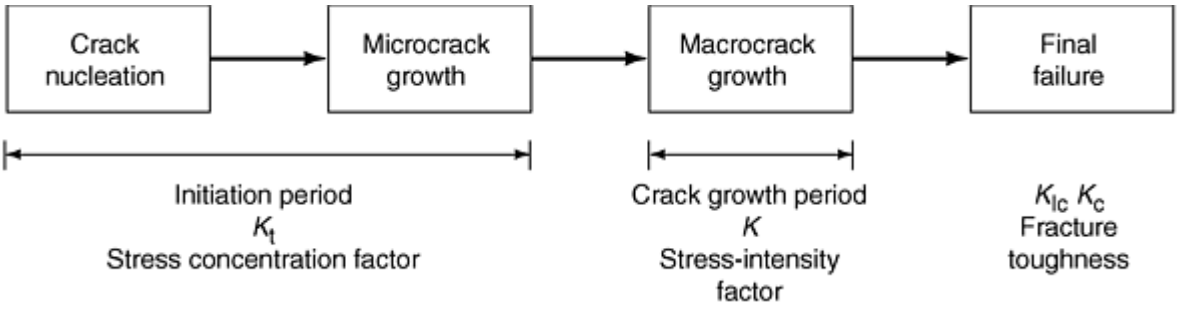

Figure 1: Different phases of fatigue life and relevant factors, after [6]

Whilst Schijve's diagram describes linear-elastic factors, the underlying mechanisms involved significant non-linear plastic considerations that can and do contribute to the complexity of the problem.

The study of the growth of fatigue cracks as a macrocrack and their propagation through a structure offers some advantages to the researcher in that the 'established crack growth' can be more readily observed. The use of techniques such as fractography, however, is opening up the world of the microcrack to researchers as never before.

1.5 What Questions are being Addressed in this Report

Using the advantages provided by fractography and focussing on the types of materials, spectra and stress levels that are of practical interest to the platform tasks this report seeks to address two questions originally raised in [4] that remained open following the application of both traditional methods and the EBA method to the recent F/A-18, F-111 and P-3 test interpretation programs conducted in DSTO. The first question concerned the identification of trends in crack growth behaviour and the second concerned the calibration of classical LEFM based crack growth models. These two questions will be address in Section 4 and 5, respectively, of this report. A remaining question regarding the effect of notches and notch plasticity on crack growth will be addressed in a separate report.

1.5.1 Trends in Crack Growth Behaviour

Growth proportional to ΔK^{exp} is the behaviour typically assumed (and modelled) for most fatigue cracks in their 'established growth phase'. What happens before this observed

established growth is more open to argument. The growth of cracks from the first applied load spectrum block, colloquially referred to as 'day one' has been observed for the high stress scenarios in F/A-18. This 'instant cracking' behaviour has sometimes been observed to have a linear behaviour of growth (log of crack size v time). Yet, other non-linear crack growth and delayed 'initiation' behaviour has been observed and reported in the DSTO and international literature. The questions that then arise are: what actually is the area or boundary of applicability of the 'cracks start at day one' observation? What other types of behaviour are observed? And, from the fractography data held at DSTO, what can we say about 'what's going on at the bottom' of the crack growth curve, *i.e.*, at the very early stages of crack growth?

1.5.2 Traditional Crack Growth Model Calibration

Traditional crack growth modelling approaches are empirical and hence necessitate the calibration of the models being used for the particular spectra, material and stresses being examined. Any calibration process may have its limitations, either in the range of crack sizes or other significant parameters such as material thickness that it is valid for, or the range of applied spectra over which the predictions can be made with confidence. The use of traditional models in the recent DSTO test interpretation work for F/A-18 and F-111 was rejected in favour of EBA due to inconsistencies between experiment and modelling [7] and difficulties in achieving a standardised and calibrated model that was considered valid for the necessary range of stresses and spectra. Inconsistency between experiment and prediction was also seen at small crack sizes during the P-3 program and any possible limits to practical calibration need to be examined and understood in order to determine which models may be most suited for particular applications. The FASTRAN code is used in this report as an example of a traditional, constant amplitude data based model.

2. Crack Growth Modelling

The inference from the earlier sub-sections is that after microcracks have nucleated, they must initially grow in an environment dominated by non-homogeneous material effects and local strain concentrations. At a certain size the small cracks become large enough to move into a more stable and repeatable growth phase that is dominated by a homogeneous parameter *K* (stress intensity factor) and towards the end of their life things again become more complicated as stress states, stable tearing and the material fracture toughness become more influential. This means that modelling the entire growth phase is difficult and has resulted in researchers attempting to adjust their different empirical models in the different stages of growth. The final stage of growth leading to unstable fracture is generally given less attention simply because it typically takes up very little of the overall life. The period when cracks are small, however, can be a significant proportion of the life and it is in this stage that models have to be successful if they are to predict the total growth period with any accuracy. Yet it is the successful modelling of small cracks that has been the most difficult to achieve to date. Despite some progress in developing mechanistic models, e.g. [8], most methods that deal with the small crack regime thus far remain as empirical adjustments to the original empirical models developed for large-crack problems.

2.1 Traditional Modelling of Crack Propagation

Traditional crack growth models are overwhelmingly based on the use of the empirical Paris equation,

$$\frac{\mathrm{d}a}{\mathrm{dN}} = C\Delta K^{m} \qquad (1)$$

which relates the crack growth rate $\mathrm{d}a/\mathrm{d}N$ to the crack tip stress intensity range ΔK. This equation applies in the so-called *K*-dominated region, or Paris region as shown in Figure 2, and it explicitly defines a linear relationship on a $\log(\mathrm{d}a/\mathrm{d}N)$ versus $\log\Delta K$ scale. If experimental data do not show this linear relationship, then using this equation may lead to error. In addition, similitude is assumed to hold true in this region; i.e. the crack growth rate is uniquely defined by ΔK and different length cracks subject to the same ΔK cycle will grow at the same crack growth rate. To conduct a life assessment using the Paris equation, coupon tests are carried out under constant amplitude loading to obtain crack growth rates at the corresponding ΔK. These data can be fitted to Equation (1) to obtain the parameters *C* and *m*. Equation (1) can then be integrated from a selected initial size to a desired final size, to obtain the *a*-*N* relationship (better known as the crack growth curve) for a load spectrum.

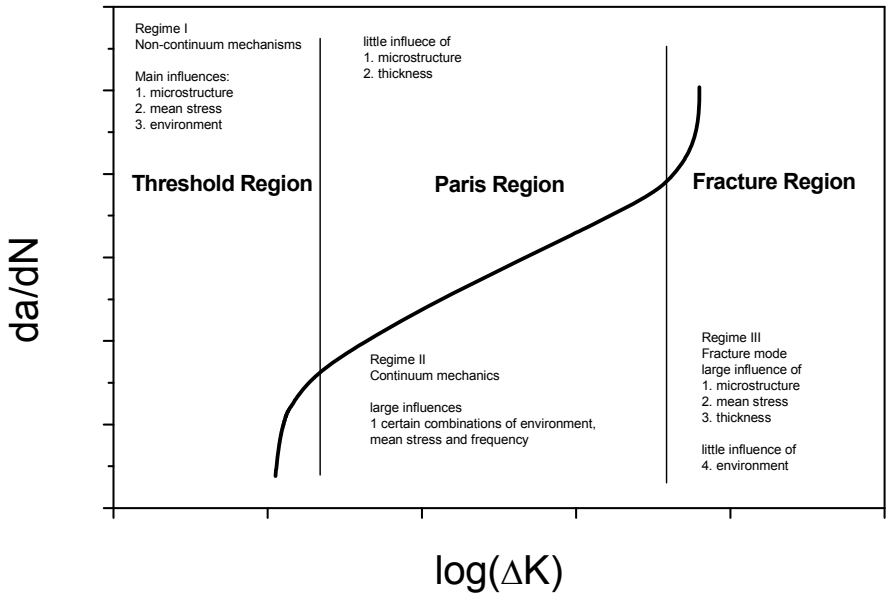

Figure 2: Constant amplitude crack growth behaviour typical for Al alloy, adapted from [9]

The basic Paris equation was later enhanced by introducing adjustable parameters to account for the effect of non-zero mean stresses (the Walker Equation [10], for example) and to represent the rapid increase in growth rate when the stress intensity approaches the material fracture toughness (Forman Equation [11], for example). All, however, are empirical models that fit equations to experimental data.

More detailed plots of $\log(\mathrm{d}a/\mathrm{d}N)$ - $\log \Delta K$ show that in fact, even within the Paris region, it is not a single linear relationship. The crack growth rate often shows several 'knees' or transition points with sharp changes in slope. Figure 3, taken from [12] shows an example. Section 5 of the same reference refers to two papers by Yoderl [13] and Wanhill [14] where these transitions are shown to correspond to load conditions where the resulting plastic zone sizes are equal to specific microstructural features such as grain size. The plastic zone is the region at the crack tip where the material has plastically deformed under a load, the size of which is given by the equation

$$r_p = \frac{K^2}{\alpha \pi F_{ty}^2}$$ where α=2 for plane stress and α=6 for plain strain

It is often noted by researchers that predictions of crack growth under variable amplitude loading using the Paris equation and rate data derived under constant amplitude loading are conservative. In reality the growth of a crack under a certain cycle is affected by the previous cycles. It has been observed, for example, that an overload can slow down or retard crack growth for subsequent smaller load cycles. This memory effect or load interaction effect is generally attributed to the residual stresses ahead of the crack tip, and/or the residual strains

behind the crack tip, generated by the overload, and it is the single most difficult issue in the modelling of crack growth under spectrum loading. Various models have been proposed to account for this effect, such as the retardation models based on the plastic zone size ahead of the crack tip and the crack closure models based on the residual plastic deformation left behind the crack tip.

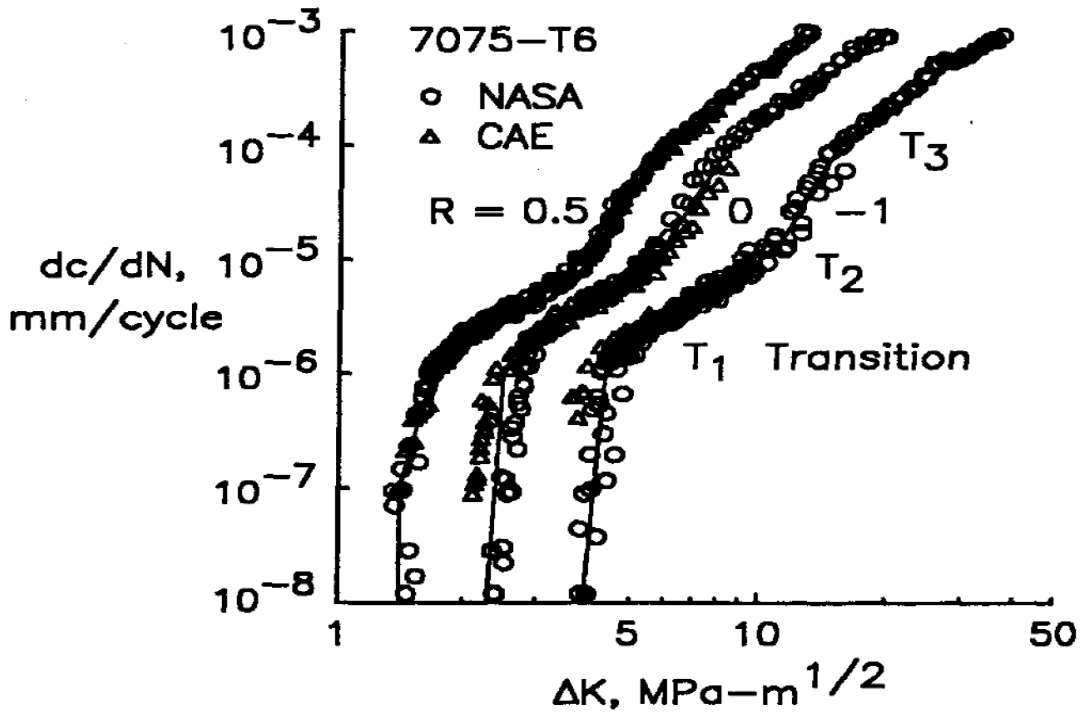

Figure 3: Crack Growth rate against ΔK for 7075-T6 Aluminium Alloy (taken from [14, 15] where these transitions are shown to correspond to load conditions where the resulting plastic zone sizes are equal to specific microstructural features such as grain size)

2.1.1 When is Small Crack Behaviour Important?

Small-crack behaviour is not an important issue for applications in which initial defects are large, such as welded civil engineering structures. Also, small cracks are generally not significant for many traditional mechanical and aeronautical designs and analyses based on damage tolerance concepts, because the initial flaw size and/or conventional NDE inspection limits of 0.050″ (1.27mm) and above, is usually beyond the small-crack regime. However, damage tolerance methods are sometimes applied to more highly stressed structures where tolerable flaw sizes are much smaller and non-destructive evaluation requirements are stricter. Small-crack behaviour can be very important in these applications, which historically have been treated with fatigue life prediction methods based on strain-life or stress-life analyses. Note that the total life in many strain-life applications is often dominated by the growth of

microstructurally small cracks, especially in the low-cycle fatigue (LCF) regime where crack formation occurs very early in life and the allowable critical crack sizes are still relatively small. Therefore, the damage growth process in LCF, which is often treated as an 'initiation' problem, is often actually a small-crack growth process. Whilst this does not necessarily invalidate the conventional approaches, small-crack analysis techniques may provide valuable new insights into some difficult LCF lifing problems. However, before current crack growth models can be used for estimating total life a number of advances in their ability to predict small crack growth need to be made. Small-crack phenomena, especially micro-crack arrest, are also thought by some researchers to be the key to high-cycle fatigue (HCF) behaviour, including the fatigue limit, but a practical treatment of HCF based on small cracks is not yet available. Small cracks are important for fracture mechanics-based durability assessments in which an equivalent initial flaw size (EIFS) is back-calculated from fractographic data or from a prediction of total life. This EIFS is often well within the physically small-crack regime of typically up to 1 mm and below the usual NDE thresholds, thus making crack size predictions in this region difficult to verify. The often observed sensitivity of crack growth life prediction to EIFS by current models is also an indicator that the current state of the art is not yet satisfactory.

2.1.2 Difficulty in Modelling Small Crack Behaviour

Fatigue cracks are small for a significant fraction of the total life of some engineering components and structures. The growth behaviour of these small cracks is generally significantly different from what would be expected based on conventional (*i.e.*, large crack) fatigue crack growth (FCG) rate test data. Small fatigue cracks are often observed to grow faster than corresponding large cracks at the same nominal value of the crack driving force, represented by correlating parameters such as ΔK. Small cracks have also been observed to grow at non-negligible rates when the nominal applied ΔK is less than the long-crack threshold value, ΔK_{th}, determined from traditional large-crack test methods. Therefore, a structural life assessment based on large-crack analysis methods can be non-conservative if the life is dominated by small-crack growth. In contrast to large-crack growth rates, which generally increase with increasing ΔK, small-crack growth rates are sometimes observed to increase, decrease, or remain constant with increasing ΔK. A variety of typical small-crack growth rate behaviours are illustrated schematically in Figure 4.

The existence of a number of possible crack growth rates for the same value of ΔK suggests a lack of similitude and/or errors in the calculation of the actual ΔK operating at the crack tip. Although nominally-calculated ΔK values for large and small cracks may be the same, we can speculate that the actual (resultant) driving force and/or resisting force for crack growth may well be different due to the effects of localized plasticity, crack closure, micro-structural influences on crack-tip strain, or localised crack-tip chemistry. In some cases, the basic continuum mechanics assumptions of material homogeneity and small-scale yielding may be violated for small-crack analysis.

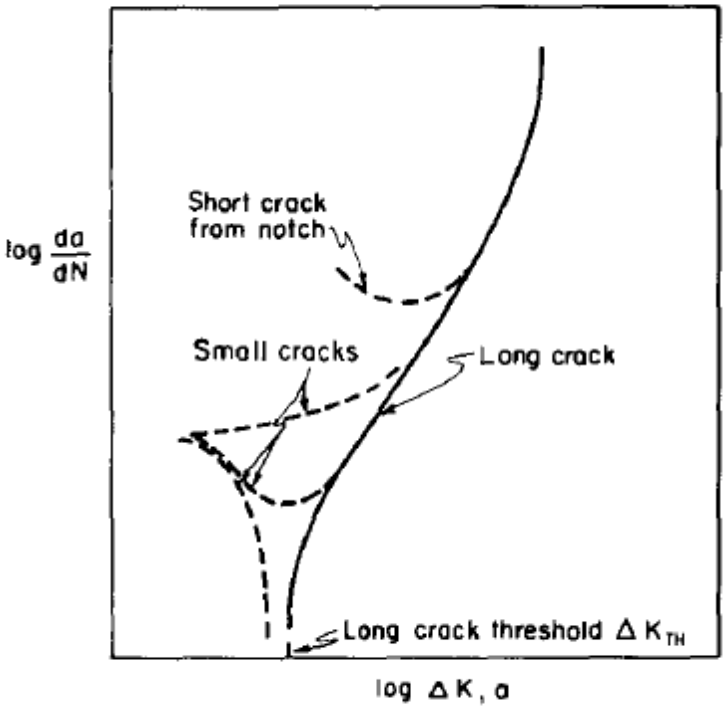

Figure 4 A sketch of small-crack growth rate behaviours, in comparison to typical large-crack behaviour, from [16, 17]

Small-crack behaviour is a complex subject, due to the variety of factors that may affect small cracks and the variety of microstructures used in engineering structures. Many researchers have published small-crack data and offered various explanations and models to rationalize these data, and apparent disagreements are not uncommon in the literature. A survey of several of the approaches taken is in [1], including the approach by El Haddad and co-workers in which the stress intensity factor K is increased by adding a value a_o to the actual crack size a

2.2 Direct Experiment based Crack Growth Methodologies

With the problems besetting traditional crack growth models, such as load interaction, sometimes proving to be difficult for certain situations, more empirical methods that rely primarily on variable amplitude (VA) experimental evidence also have a place in practical crack growth prediction work. For a fatigue crack subjected to a fairly short and repetitive load sequence, an effective stress approach (ESA) has been used to analyse its growth [18, p. 192]. The essence of the approach is to treat the whole spectrum as an effective constant amplitude cycle, which is characterised by a reference stress intensity factor,

$$K_{\text{ref}} = S_{ref}\beta\sqrt{\pi a}\,. \qquad (2)$$

The reference stress for a given spectrum can be the maximum peak stress, the average stress, or the root-mean-square value of stress per block, etc. Importantly, the choice of reference stress needs to be consistently applied for a given case.

To use this method, one would first conduct baseline fatigue crack growth experiments using coupons representing the geometry and the material of the component to be analysed, subjected to the variable amplitude (VA) load spectrum (to be) experienced by the component. The crack growth rate, in terms of crack increment per block of loading $\mathrm{d}a/\mathrm{d}B$, from the coupon test is then correlated to the effective stress intensity factor using the following Paris-type equation,

$$\frac{\mathrm{d}a}{\mathrm{d}B} = F\left(K_{\mathrm{eff}}\right), \tag{3}$$

where $F\left(K_{\mathrm{eff}}\right)$ is any crack growth rate model, such as the Paris law. The crack growth life in terms of the number of blocks of loading may be obtained by integrating the above equation,

$$B = \int_{a_0}^{a_f} \frac{\mathrm{d}a}{F\left(K_{\mathrm{eff}}\right)}, \tag{4}$$

where a_0 and a_f are the initial and final crack length, respectively.

The concept has been tried in earlier times [19], [20], and Grandt has referred to this approach as an *effective stress approach* [18, p. 192], and stated that it is limited to *short, repetitive load histories that do not exhibit significant amount of growth retardation*. Furthermore, it presumes a unique scalable relationship between the material behaviour and the VA spectrum, which is usually not the case.

DSTO researchers (see [1] p63 for a full list and references) have for some time observed that fatigue cracks under the Nz based spectrum loads of fighter aircraft grow at approximately a constant exponential rate, i.e.

$$a = a_i e^{\beta_L N}$$

where a is the crack depth, a_i is the initial crack depth, N is the crack growth life in cycles and β_L is a regression parameter. This is similar to findings from other researchers for constant amplitude (CA) loading (again, see [1] p64 for references). In examining potential crack growth models that would match the exponential data observed in coupons under F/A-18 spectra McDonald and Molent *et al* [21] proposed an *effective block approach* (EBA) using either the Front and Dugdale 'log-linear' (exponential) crack growth relationship based on crack length a, or the Paris-based stress intensity (and thus √a based) relationship similar to Equation 1. The crack growth rate equation for the Paris-type version of the EBA is,

$$\frac{\mathrm{d}a}{\mathrm{d}B} = C_B K_{\mathrm{ref}}^{m_B}.$$

where C_B and m_B are *spectrum-specific* material constants.

The key difference of the EBA approach is that rather than attributing VA effects such as load sequence interaction to an effective stress, it attributes VA effects to the standard material model constants C and m. This potentially allows a wider range of validity compared to the ESA.

The first technical issue for the EBA is the rational and consistent determination of the constants C_B and m_B for a given spectrum for which experimental data exists. Given that the derived rate data can be satisfactorily expressed by the EBA rate equation such that the original crack growth curve can be self-predicted, the next possibility is that the constants can be predicted for other stress scale levels, thereby allowing crack growth predictions to be made without having to conduct experiments in every case.

Furthermore, whilst the EBA has no predictive ability of the VA effect on C and m for different spectra, the use of third party crack growth prediction models could also allow the calculation of constants for different spectra. Assuming a fixed m_B, the following hypothesis was put forward for the determination of $C_{B,S2}$ for an untested spectra from the value $C_{B,S1}$ obtained from a tested spectra,

$$\frac{C_{B,S2}}{C_{B,S1}} = \frac{C_{B,S2}^{(num)}}{C_{B,S1}^{(num)}}, \tag{5}$$

where the superscript "*(num)*" indicates the numerical value obtained from a software tool such as AFGROW or FASTRAN, and the subscripts '*S1*' and '*S2*' indicate the 'tested' and 'untested' spectrum, respectively, hence $C_{B,S1}$ is known. To determine $C_{B,S2}$, the following procedure is followed [21];

1) conduct a cycle-by-cycle fatigue crack growth analysis of the specimen subjected to the tested and untested spectrum, respectively, using software tools such as AFGROW or FASTRAN;
2) for each case, convert the crack growth curve to the growth rate curve;
3) for each case, plot $\log\frac{da}{dB}$ versus K_{ref} to obtain $C_{B,S2}^{(num)}$ and $C_{B,S1}^{(num)}$, respectively;
4) calculate $C_{B,S2}$ from

$$C_{B,S2} = \frac{C_{B,S2}^{(num)}}{C_{B,S1}^{(num)}} C_{B,S1}.$$

The initial EBA work on F/A-18 low K_t coupons showed that the exponent m in the EBA equation was equal to or close to 2. However, data from F-111 [22], P-3 [2] and F/A-18 data for other than low Kt specimens [23] showed that m could take other values. Subsequently, Wallbrink [2] and Zhuang [22] independently developed derivations that enabled variable m values to be predicted in concert with the C coefficient using the equation

$$m_{\mathrm{B,S2}} = m_{B,S2}^{(num)} - m_{B,S1}^{(num)} + m_{\mathrm{B,S1}}$$

The simplicity and practicality of the EBA approach is its attractiveness. However, the important gain of EBA over the traditional Paris based approach, being the 'lumping' of VA effects such as load sequence into two growth rate constants, is also its biggest limitation in terms of fatigue problem applicability. To allow predictions to be made, if necessary, over a range of stress levels

that depart from the levels at which the spectra specific data has been gathered, the EBA process requires that the exponent m, which governs the shape of the crack growth curve either remain the same or be recalculated. Development of model parameters at stress levels below the yield stress of the material and then applying those same parameters for higher values of K may be inappropriate if it is believed that the VA sequence effect is influenced by the size of the LEFM plastic zone size which is a function of K^2 rather than K.

Furthermore, if total fatigue life predictions are being made then the assumed initial flaw size a_i also needs to be invariant with stress and spectra otherwise an alternately defined flaw size needs to be used. This limitation is no different to the EIFS concept referred to in Section 2.1.1.

3. Crack Growth Data

There have been numerous coupon test programs performed at DSTO in support of research and platform related activities. This section will describe several test programs which have been conducted in recent times using F/A-18, P-3 and F-111 spectra, selected data from which have been used in this report. The coupon designs and test information are provided in Appendix A.

3.1 F/A-18 Coupon Tests

A series of coupons were tested using a single F/A-18 Y488 bulkhead spectrum denoted IARPO3a. Three different coupon configurations were tested, namely a low K_t coupon (dog-bone configuration) with a K_{tn} of 1.037 and a thickness of 6.35 mm; a medium K_t coupon (notched) with a K_{tg} of 2.26 and a thickness of 10 mm; and a high K_t coupon (open hole) with a K_{tg} of 3.32 and a thickness of 10 mm. The coupons were machined from 7050-T7451 aluminium plate. Different surface treatments were investigated including etched and as- machined. Different stress levels were also examined. Fractography was used to obtain crack growth data. Marker cycles in the form of five underloads were added to the spectrum to enable fractography. Further details regarding coupon design, spectrum details, test matrix and results may be found in [24], [25], [26], [23]. A large number of the low K_t coupons were also tested by using a number of different wing root bending spectra in both as-machined and etched surface conditions.

3.2 F-111 LITV Tests

Numerous F-111 spectra were tested as part of the F-111 Loads Interpretation and Truncation Validation (LITV) coupon test program [27]. The program used a symmetrical notched coupon with a K_t (gross) of 2.5, a thickness of 8 mm and machined from 2024-T851 etched aluminium plate cut from an F-111 wing panel. Several wing spectra were tested and for one spectrum the program included tests at a nominal stress level and ±10% of that stress level. Different truncation levels were also investigated. Coupon crack growth data were obtained via fractography. In this case, the cold proof load test (CPLT) load, which is applied to the F-111 aircraft at regular intervals, also served as a 'marker band' to assist fractography, so no extra marker cycles were inserted into the test spectra.

3.3 P-3 Spectra Tests

In 2003, the National Aerospace Laboratory (NLR) of the Netherlands tested a series of P-3C spectra using a high K_t coupon ('double-ear') with a gross K_t of 5 made from 7075-T6 aluminium sheet with a thickness of 2 mm. Spectra derived for different fatigue critical areas (FCA) along the wing and different fleet usage (USN, RAAF etc) were used in the tests. Crack growth data were acquired via Direct Current Potential Drop (DCPD) readings [28]. However, the accuracy of the NLR DCPD data for crack lengths less than 0.01" (0.254 mm) was later questioned at DSTO during preparation of [4]. Consequently, in 2007 a number of double-ear coupons were tested at DSTO by the Methods and Standards Group using P-3C and F/A-18 spectra. These

coupons were 3.175 mm thick and made from 7075-T6 aluminium sheet. The aim of these tests was to examine the effectiveness of the newly acquired DSTO DCPD system and obtain crack growth data for small cracks (<0.01”). The crack growth data obtained from the DCPD system were compared to those obtained from fractography. Marker cycles were added to each of the P-3C spectra to assist with fractography. The conclusion was that the DCPD system coupon provides accurate data on crack length for part through cracks down to a certain size limit as long as the correct equations for calibration were used in the data acquisition process.

3.4 Methods and Standards Group Ad-hoc Tests

A series of ad hoc coupon tests were conducted in 2008 which included a study of the effect on life of different stress levels for the F/A-18 spectrum using the DSTO P-3 type double-ear 7075-T6 coupons described earlier. Both DCPD and fractography were utilised to obtain crack growth data. The ad hoc test program also examined the effect on fatigue life of using different notch-type coupons and examined the effect on crack growth of etched versus as-machined coupons for a P-3C spectrum. Several F-111 spectra were used for this investigation and two coupon types, namely the double-ear coupon described earlier, and an open hole coupon made from 7075-T6 aluminium Alclad sheet (thickness of 3.05 mm) and with a K_t of 3.24. Fractography was utilised to obtain crack growth data.

4. Trends in Crack Growth Behaviour

4.1 Graphical Comparisons of Behaviour

To observe trends in crack growth, the actual measured crack data in coupons of relevant material, stress levels and spectra are examined graphically. The aim of the examination is to reveal relationships between behaviour and inputs such as stress level and spectrum type rather than seeking the fundamental reasons why the cracks are behaving as they do. This approach is similar to the field of epidemiology in the medical sciences. Tools include statistics and logic, with the caution that: correlation does not imply causation. From these observations of relationships research can then move on to developing empirical models and/or target specific relationships to gain more fundamental understandings that can explain the observed behaviours. A weakness in the proposed approach is that the sample size is often small; therefore conclusions have to be cautious. Trends in behaviour, however, can be at least observed and then identified for larger experiments if needed.

The following sub-sections provide a graphical comparison of crack growth behaviour due to different effects. Note that where multiple coupons have been tested under the same conditions, in some graphs only one 'average' crack growth curve has been plotted to allow easier identification of any trends in the data.

Note also that the crack growth data plotted were measured relative to the edge of the notch or the bore of the hole in the coupon. In some of the plots, an estimate of the size of the discontinuity from which the crack initiated has been included. Also included in these plots is the type of crack, i.e., a surface crack denoted by an 'S' or a corner crack denoted by a 'C'.

4.1.1 Effect of Surface Condition

Surface condition is known to influence fatigue life and the influence is traditionally regarded as being in the nucleation/initiation stage. The examination of many types of surface condition is possible. However, the two surface conditions for which data was available from the programs identified was 'as-machined' and 'etched', with etched referring to a DSTO process that imitated one of the surface treatments applied to certain F/A-18 components during manufacture.

Figure 5 shows the effect on crack growth of etched and as-machined surface finish for F/A-18 high K_t 7050-T7451 coupons. The coupons were tested with a single F/A-18 Y488 bulkhead sequence at several stress levels. For clarity not all available results are reproduced.

Figure 6 shows a similar comparison, for a single spectrum (RAAF P-3 FCA351) and stress level, between etched and as-machined finishes using thin 7075-T6 double-ear coupons. The double-ear coupons were etched in the same manner as the F/A-18 coupons following the procedure described in [23].

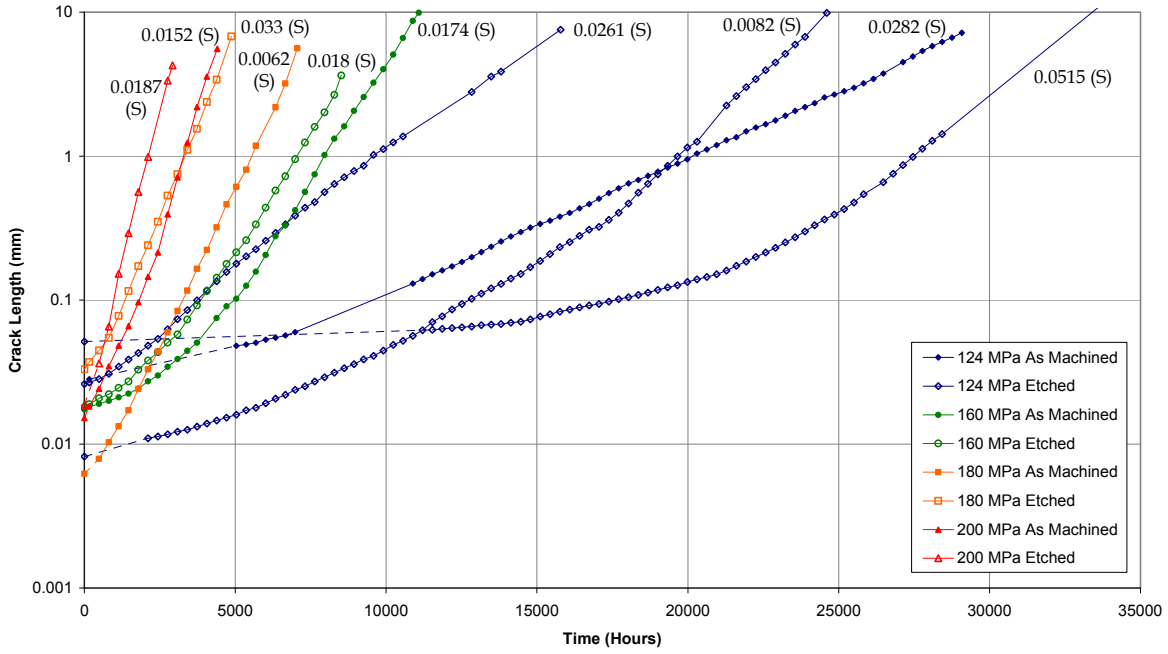

Figure 5: Etched versus As Machined Crack Growth Comparison – F/A-18 High K_t Coupon

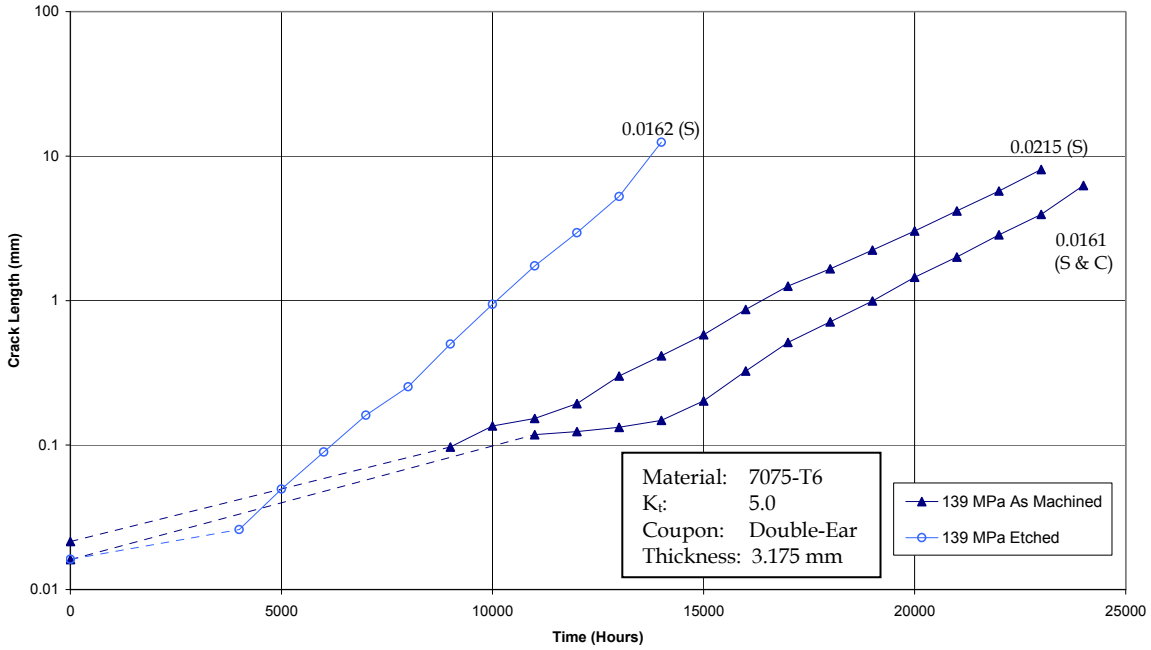

Figure 6: Etched versus As Machined Crack Growth Comparison – P-3C Double-Ear Coupon

4.1.2 Effect of Stress Level

The effect of stress level on fatigue and crack growth lives is well known; for the same spectra, lower stress levels produce longer fatigue lives and longer crack growth lives. What is of interest is the variation in crack growth shape with changing stress level. Figure 7 shows, for 'high' K_t etched coupons under an F/A-18 spectrum with peak stress levels varying from 124 MPa (18ksi) to 200 MPa (29ksi), a orderly lengthening of crack growth time with reducing stress, whilst retaining early commencement of crack growth and a (nearly) log-linear crack growth shape.

In contrast Figure 8 shows that a 30% increase in stress level to a P-3 spectrum applied to a notched coupon resulted in a significant shortening of the unobserved 'initiation' period with a more moderate decrease in the period of observed crack growth.

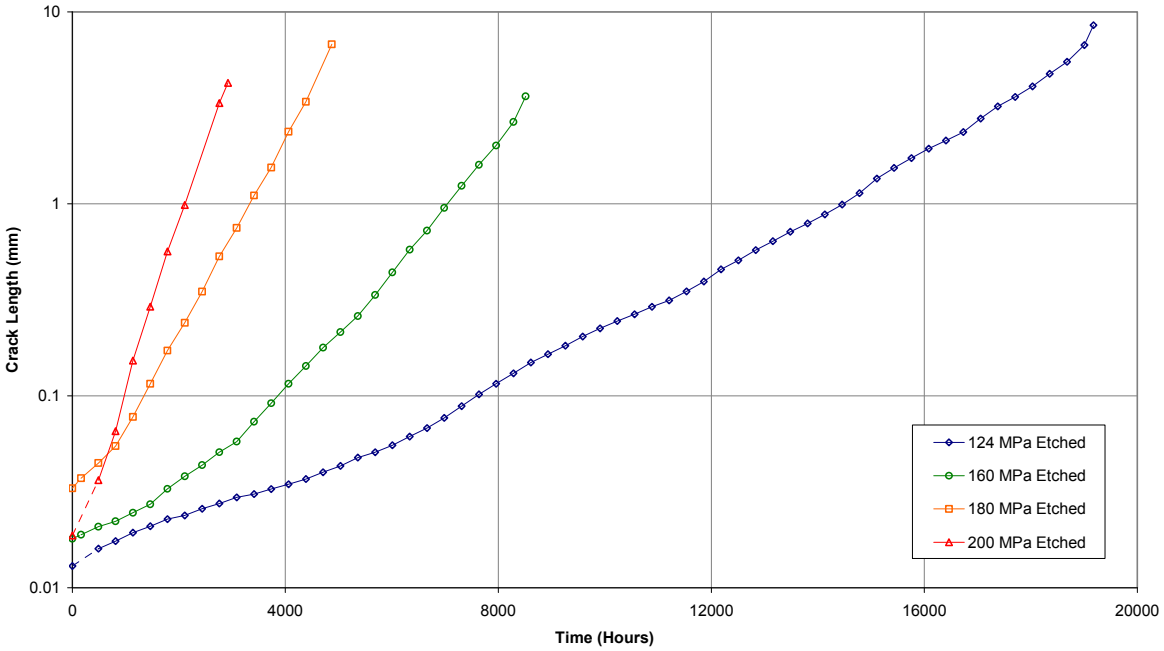

Figure 7: Crack Growth variation with Stress Level - F/A-18 'high' Kt (K_t=3.32) Etched Coupon

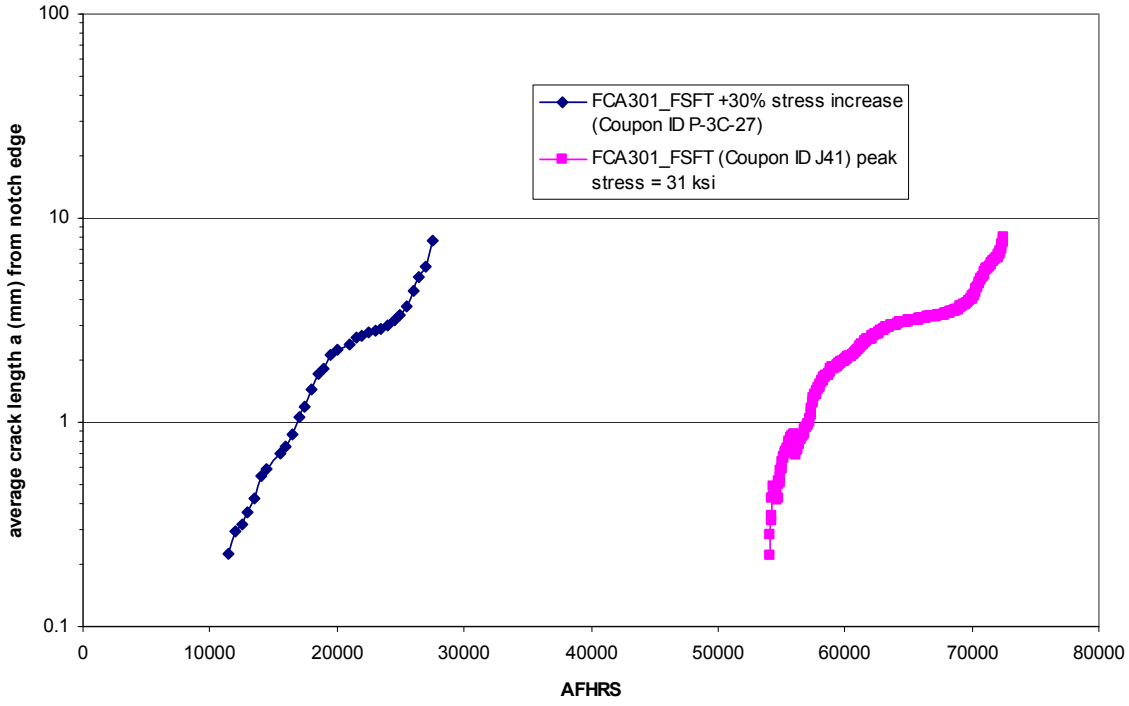

Figure 8: Crack growth variation with stress level – P-3 K_{tg}=5 double ear coupons

4.1.3 Different Spectra within the Same Aircraft Program

One of the issues of interest was the natural variation in test lives that had to be accommodated within a program due to individual aircraft usage variations within the fleet under study. This type of data puts into perspective the amount of adjustment that the crack growth models need to make in order to successfully produce reliable crack growth predictions over the range of spectra being examined in a test interpretation program. Different spectra may also show different crack growth shapes. Coupon configuration, particularly if it results in changes in stress state, may also be influential. Variation in notch type and structural configuration is also of interest but the scope of the coupon programs being studied in this report only allowed variations in input spectra to be examined.

Figure 9 shows the crack growth curves for different F-111 spectra at the wing splice location for the 7075-T6 double-ear coupons. Significant differences in life and crack growth curve shape between the spectra are noted for these notched and relatively thin coupons.

Figure 10 shows the crack growth curves for three different F-111 spectra at FASS 226 for the double notched 2024-T851 coupons of the LITV test program. Life ratios between the different spectra are of the order of three with crack growth shapes similar.

Figure 11 provides the crack growth curves for different F/A-18 wing root spectra for the low K_t 7050-T7451 coupons. The graph shows in-service and full scale test spectra covering the range from what was regarded as the most severe usage on aircraft A21-103 through to the most benign, A21-055 with an overall range in lives of a factor of two. The peak spectrum stresses are high at about 390 MPa (56 ksi) and the final crack growth length is of the order of the specimen thickness.

Figure 12 shows the crack growth curves for different P-3C spectra (FSFT and RAAF) at two locations along the P-3 wing; FCA301 and FCA351 obtained from 7075-T6 double-ear coupons. Both the spectra and location differences result in different peak stress levels

Figure 13 shows the crack growth curves for four different P-3C spectra (FSFT, RAAF, CF and RNLN) at FCA301 for the 7075-T6 NLR centre crack growth coupons. Significant slowing of the crack growth rate is seen once the crack gets beyond a certain length.

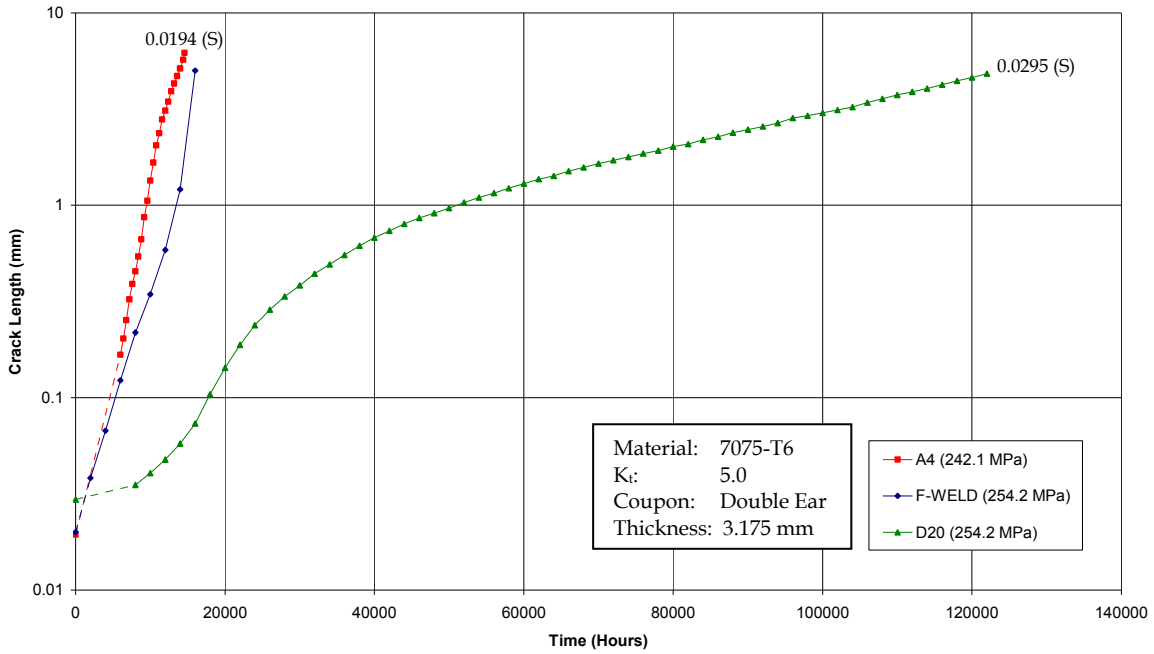

Figure 9: Crack Growth for different F-111 Wing Splice Spectra – Double-Ear Coupons

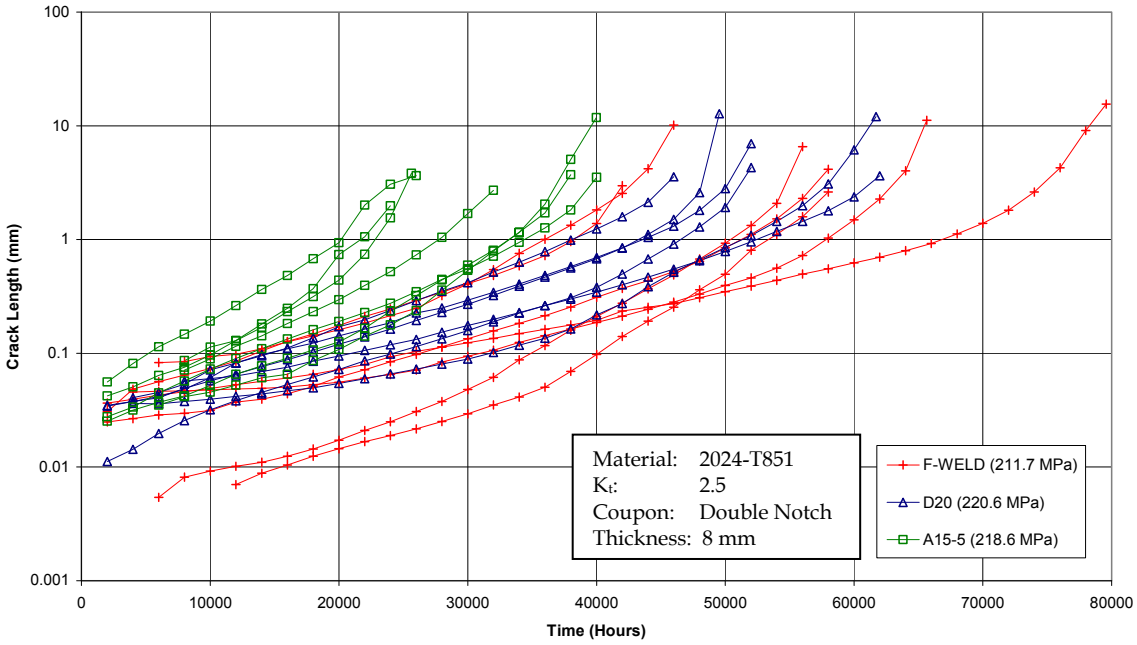

Figure 10: Crack Growth for different F-111 FASS 226 Spectra – Double Notched Coupons

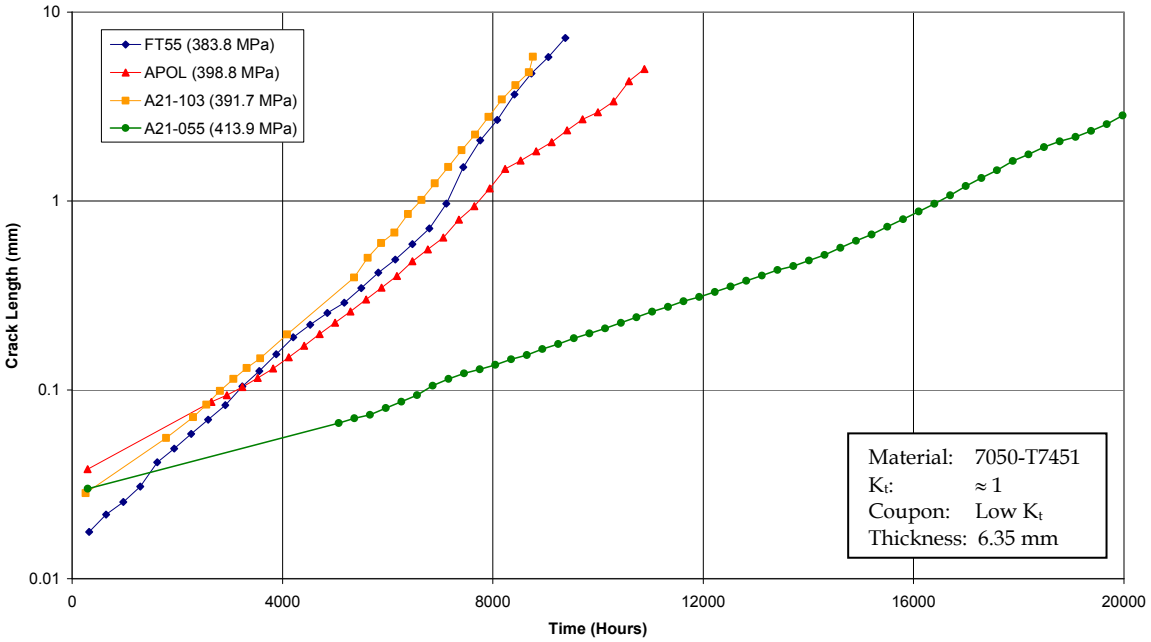

Figure 11: Crack Growth for different F/A-18 Wing Root Spectra – Low K_t Coupons

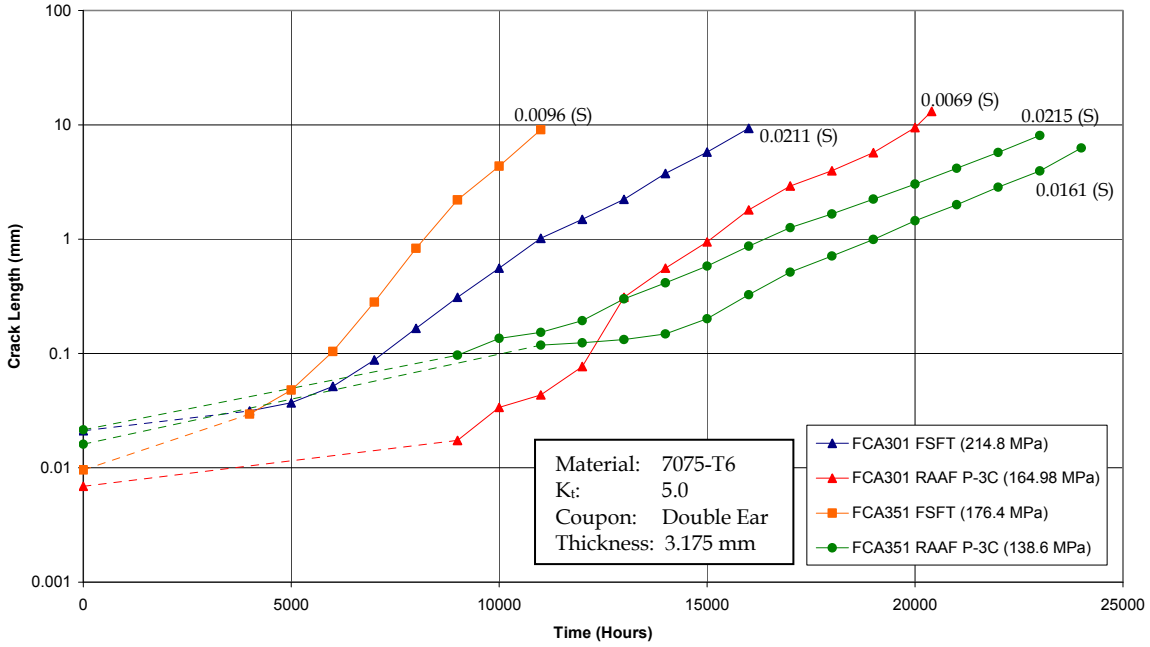

Figure 12: Crack Growth for different P-3C FCA301 and FCA351 Spectra – Double-Ear Coupons

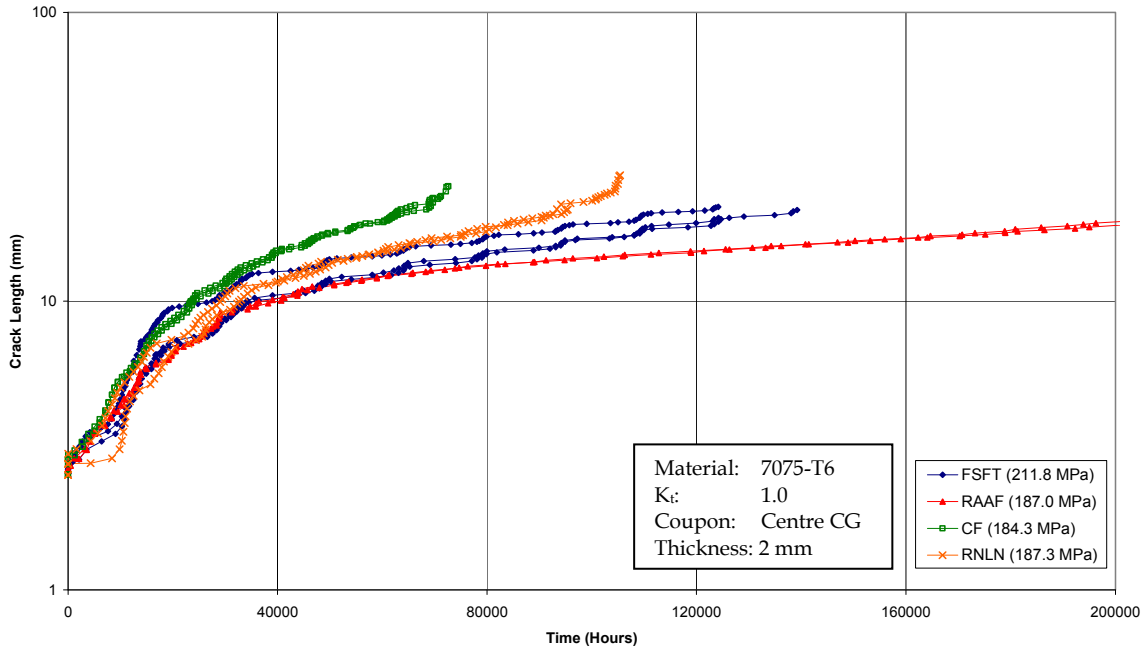

Figure 13: Crack Growth for different P-3C FCA301 Spectra – Standard Centre Crack Growth Coupons also known as middle tension (MT) coupons with a central saw cut of 5mm (not included in Appendix A)

4.1.4 Variability in Fatigue Life and Crack Growth Curves

This F/A-18 coupon series examined in [23] provides a comprehensive set of results for a fighter type spectrum at different K_t values and different stress levels. The effects of stress level and K_t can be seen in the results, and the variability in crack growth lives within the sub-sets can also be examined.

Figure 14 shows the variability in crack growth for etched and as-machined high K_t coupons at a stress level of 124 MPa (18 ksi). The coupons were tested with an F/A-18 Y488 bulkhead sequence and the plots contain all repetitions. Examining the graph one can see that whilst the sizes of the estimated initial defects of the etched and as-machined coupons may fall in the same range, the scatter in lives for the as-machined coupons appears less whilst the average life is longer. It can be seen for the as-machined specimens in particular, the lowest life specimens contained cracks that were relatively log-linear in behaviour, whilst specimens with longer lives had slower initiation and/or general curved type shapes. The fastest growing cracks have sometimes been called 'lead cracks' by researchers [5].

Figure 15 re-plots the data for the lowest stress level, 124 MPa, with the curves re-set to zero hours at a size of 0.1 mm. The reduction in variation in final lives with respect to Figure 14 suggests much of the variability in crack growth for the etched coupons at least occurs when the cracks are less than 0.1 mm.

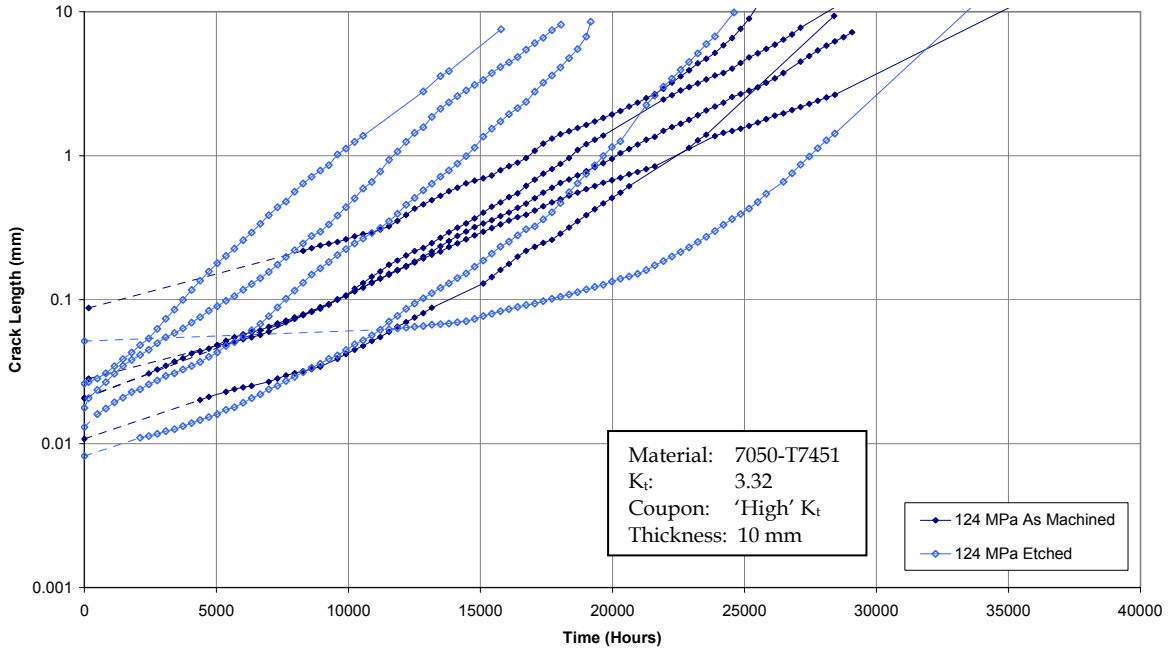

Figure 14: Crack Growth Variability for High K_t Coupons at 124 MPa – F/A-18 Spectrum

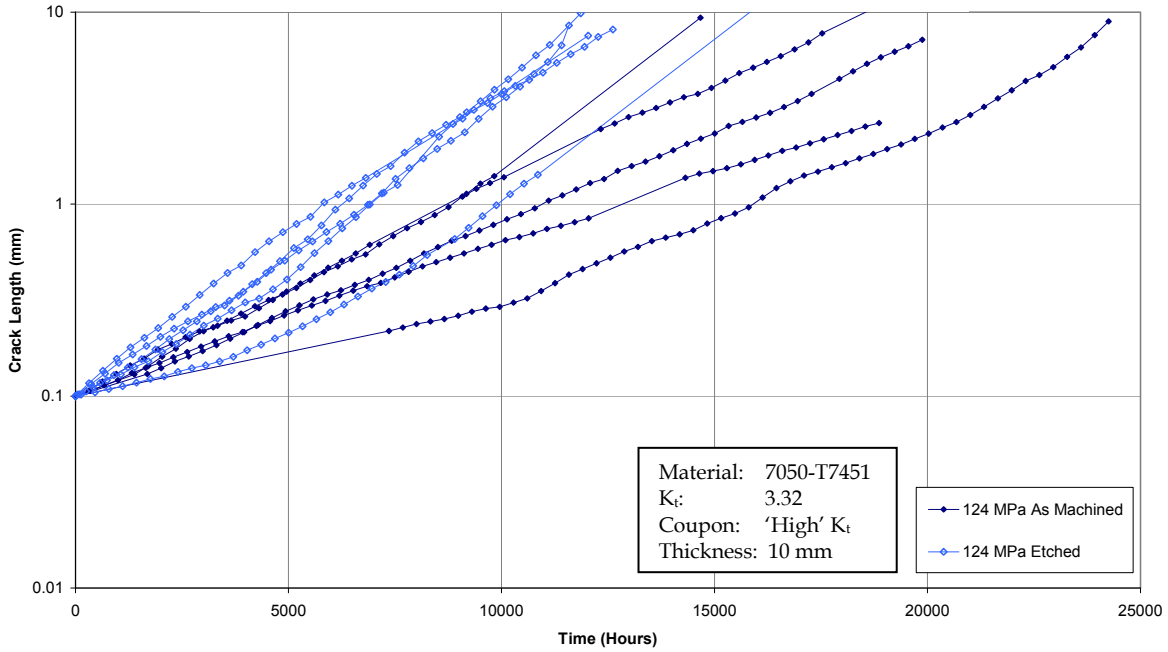

Figure 15: Crack Growth Variability for High K_t Coupons at 124 MPa – F/A-18 Spectrum (for crack lengths greater than 0.1 mm)

Crack growth variability for the double-ear coupons tested at NLR for the P-3C FSFT and RAAF spectra at FCA361 is shown in Figure 16. This crack growth data is based on DCPD readings for which the data was deemed unreliable below about 0.1 mm. For each spectrum the tests displayed remarkably consistent crack growth curves with almost all the scatter in the final lives associated with the unobserved growth or initiation below approx. 0.2 mm (0.008 inches).

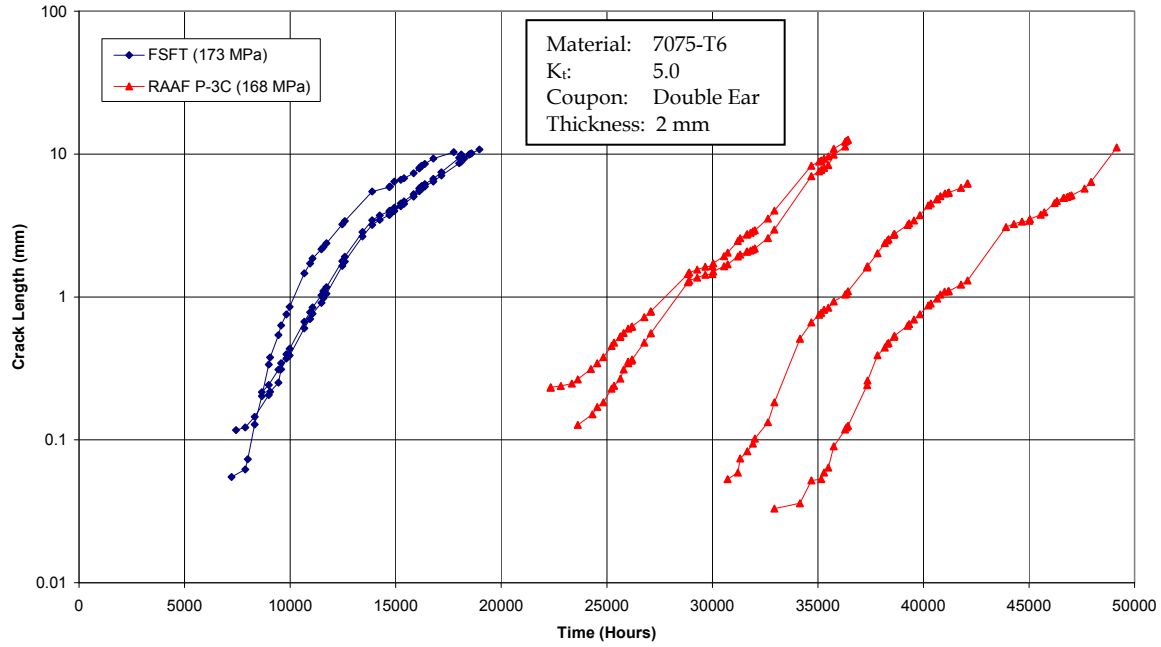

Figure 16: Crack Growth Variability for Double-Ear NLR Coupons – P-3C Spectra

4.2 Discussion

The effect of two different surface conditions, etched and as-machined, is explored using F/A-18 High-K_t results and P-3 coupons from the ad hoc program. Of most interest is the observation that there is a difference between etched and as-machined results, not just in the 'initiation' or small crack end of the curve, but in the slope of the entire crack growth curve. This is shown best in Figure 6 and Figure 15. The surface condition seems to affect the rate of crack growth for the full life of the crack. This could be explained by the effect that the etching process has on the surface of the material. It produces many more (but not necessarily larger) initiating sites than that would normally be the case for the as-machined surface with the result that larger numbers are well oriented to the prevailing stress. Shorter lives from these 'optimal sites' are therefore more likely. However, the prevalence of such sites (perhaps with their own micro-cracks), the interaction between them and their link-up on the material surface ahead of the advancing crack could also explain the faster crack growth seen in the etched coupons over the full life of the cracks in both the F/A-18 and P-3C examples. Other effects such as the interaction of any retained etching fluid with the plain stress crack growth behaviour at the surface may also be responsible. *Care is therefore needed to be taken to ensure that the accelerated cracking promoted by etching is appropriately accounted for in any analysis.*

The F/A-18 program coupon results show crack growth curves that range from log-linear (linear on a log of crack size versus linear time plot) to a more general power relationship curve resulting from a Paris-like rate equation, depending upon spectrum type, stress level and notch type. The F-111 results showed varying crack shapes for similar spectra applied to a single notch

type, as shown in Figure 10. The P-3 spectra tests show established growth curves that are broadly either log-linear (exponential) or Paris-like (note that log-linear is a special case of the Paris form with the exponent of 2), although in detail they show many variations in slope. However, for some spectra the established curve is preceded by a period of nucleation/initiation from the site of the initial feature or discontinuity, or perhaps a period of growth that is at a different rate to that when the cracks are large, see Figure 12 and Figure 16. In these cases, the ratio of the initiation period to the period of established crack growth was observed to be dependent on the type of spectrum and stress level.

Figure 13 shows coupon results for centre crack specimens. For these coupons, the through-thickness crack length becomes large relative to the coupon thickness. In this configuration there is the phenomena of changing stress state, due to the loss of through thickness constraint as the crack grows, observed by the transition of the crack face from 'flat' to 'slant'. It is clear that different spectra with their different peak loads can result in different crack growth rate retardation in these cases. Such behaviour cannot be modelled by a single empirical CG rate exponent.

4.3 So What is Going on at the Bottom (of the Crack Growth Curve)?

The data presented thus far in the figures of this section are mostly obtained from fractography. Some DCPD data have been used when correlated with fractography and optical measurements. The markings on the fracture surfaces generated by certain repetitive spectra (such as the F/A-18 spectra and the F-111 A4 spectra) have generally been easier to read than those from the longer non-repetitive spectra. Marker cycles can help the process but that does not mean that all cracks can be traced back to their beginnings. The result is that often, crack growth has been tracked down to between 0.1 and 0.01mm (0.004" to 0.0004"). For many of the F/A-18 coupons, particularly those tested at the higher stresses, this is sufficient to track the crack growth right back to time zero at the size of the identified initiating flaw. The F-111 double notch coupon type resulted in high net stress with similar observations for many, but not all, of the spectra tested. This is consistent with the general view that at higher stress levels, crack initiation takes up an ever smaller portion of the total fatigue life. For some coupons subjected to the F-111 spectra, the characteristic markings in the fractography could not be distinguished below 0.2 to 0.6 mm. For the P-3 coupons, 0.02~ 0.1 mm seemed to be the practical limit, and it is noted that often the longer the coupon life the less successful the fractography at the lowest sizes. The measurements of the smallest crack lengths are limited by the tools used to measure the position of the marker bands and the condition of the fracture surface. For some cases, the lack of data in the early stages of crack growth means that the validity of prediction methods can not be adequately assessed.

For the F/A-18 coupons and F-111 coupons at the highest gross stresses, it is clear that cracking starts almost immediately and proceeds in a log-linear or general Paris-like manner until failure. What is also clear is that there are a number of cases (see Figure 12 and Figure 16) where the established crack growth is preceded by a period of nucleation or growth of the micro or small crack that cannot be combined with the observed established growth into a curve with a single exponential form. Unfortunately, what is going on exactly in terms of crack growth in this initial period cannot always be directly observed by the current techniques, including DCPD and

fractography. The cracking process can be described in visual terms, however, from what we can deduce from the observations, see Figure 17.

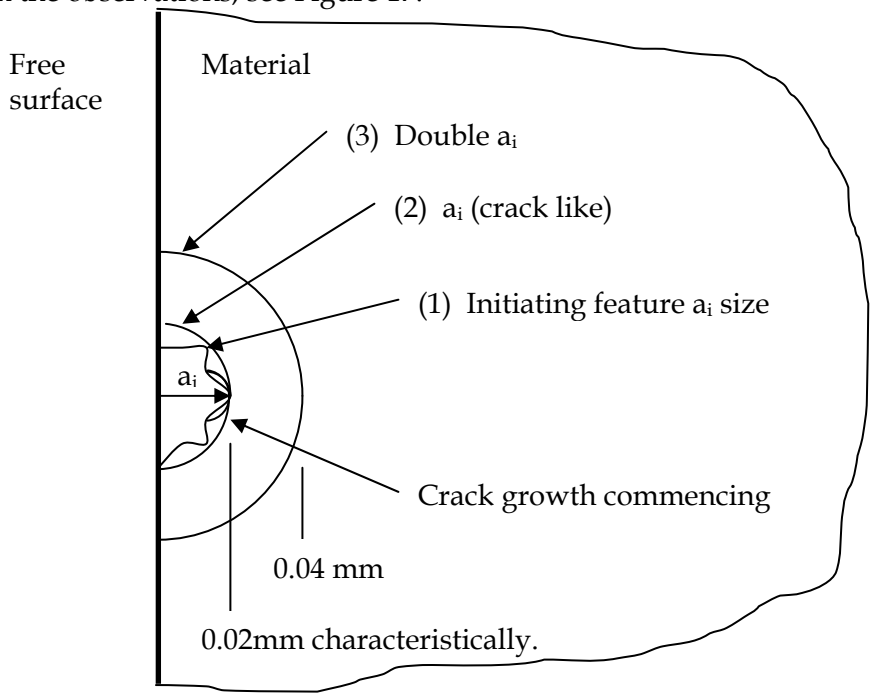

Figure 17: Crack commencement visualisation in stages (1), (2) and (3)

The process is described as follows; an initiating feature of characteristic size a_i is located at the free surface or very close to it, as a result, cracking nucleates and grows (not necessarily uniformly) around the feature such that the feature becomes a crack of size a_i. This crack of size a_i then grows in a more regular fashion under fatigue loading. The initiating defect for high strength Al is most often a constituent particle or, in the case of an etched surface, a pit or fissure. Appendix B of [5] provides a very good description of the range of material features and manufacturing defects that can act as initiating discontinuities. In terms of their ability to initiate fatigue growth, different features do not necessarily act the same way. Sharp or crack-like features such as etch pits could be expected to generate cracking faster than, say, a score or a dint. This effect, along with defect size, shape and orientation to the principal stress field explains some of the variability in crack behaviour seen at very small crack sizes. By looking at some of the coupon crack growth data identified in this section, and using the Stages defined in Figure 17, different crack growth behaviours can be discerned between typical F/A-18 and P-3 cracking, see Table 1

Table 1: Comparison of Crack Development using the Figure 17 model and data from this Section

Stage	F/A-18 spectra (high stress) Al 7050 (10mm thick)	P-3 spectra Al 7075 (2mm thick)
(1) initiating defect a_i	≈ 0.02 mm (range from 0.01 - 0.1 mm)	≈ 0.02 mm (range from 0.01 – 0.1 mm)
(2) development of crack of size a_i	Very quick (for lead cracks)	Up to 50% of life
(3) growth to twice a_i	10-20% of life	

5. Calibration of Traditional Models

Traditional models that use cycle by cycle crack growth integration and constant amplitude crack growth rate data often need calibration for the task at hand for a number of reasons including;

a. Restricted availability of data. Test limitations may prevent the acquisition of appropriate material data, or library data may not be available for the material therefore data for 'the nearest substitute' may be necessary. Similarly data may not be available for the specific material orientation, product form, thickness, environment and surface treatment.

b. Load interaction and cycle mean stress. Crack growth retardation or acceleration due to load interaction are stress and spectrum dependent, and models often have parameters that allow adjustments to be made empirically so that variable amplitude predictions can be improved. Similarly, the effect of cycle mean stress may be available from data but in its absence there are a number of empirical models that may also work.

c. Accuracy of stress levels and stress states. As growth rates generally relate to the third power of stress amplitude, the local stress level is important. Knowledge of the local (principal) stress for coupons is typically good, but for real cracks in complex aircraft parts the local stress levels are often not accurate. Similarly, for models that make adjustments of crack growth from calculations of plastic zone sizes, the estimation of the local stress state (plane stress, plane strain), affects these calculations and could well be inaccurate.

d. Residual stress. Residual stress as a result of the manufacturing process or from local notch plasticity effects may be present, and these can significantly influence crack growth behaviour.

Thus traditional models in use today can range from simple 'Paris equation' (stress intensity K) based integrations, to models that provide for empirical adjustments for mean stress and load interaction, through to the more complicated crack-closure based models. For sake of brevity, we show how calibration is used in just one example – the FASTRAN code used in P-3 SLAP project. FASTRAN is a crack closure code.

5.1 P-3 SLAP and FASTRAN

Starting with what is assumed to be the best available material data, FASTRAN allows adjustments to be made to both the rate data and to the stress state (via the parameter alpha, α, which represents the extent of out-of-plane or through-thickness constraint) to enable the program to match particular variable amplitude spectra results. Figure 18 shows centre crack coupon results from [29] for a particular spectrum called '85%' with the FASTRAN predictions for the same spectrum before calibration and after. Note that this type of calibration uses through-thickness crack data from centre cracked coupons for a half crack length of 2 to 10 mm (approx. 0.1 to 0.4 inches). The calibration was checked against results for spectra at several wing locations to ensure the chosen parameters provided some robustness.

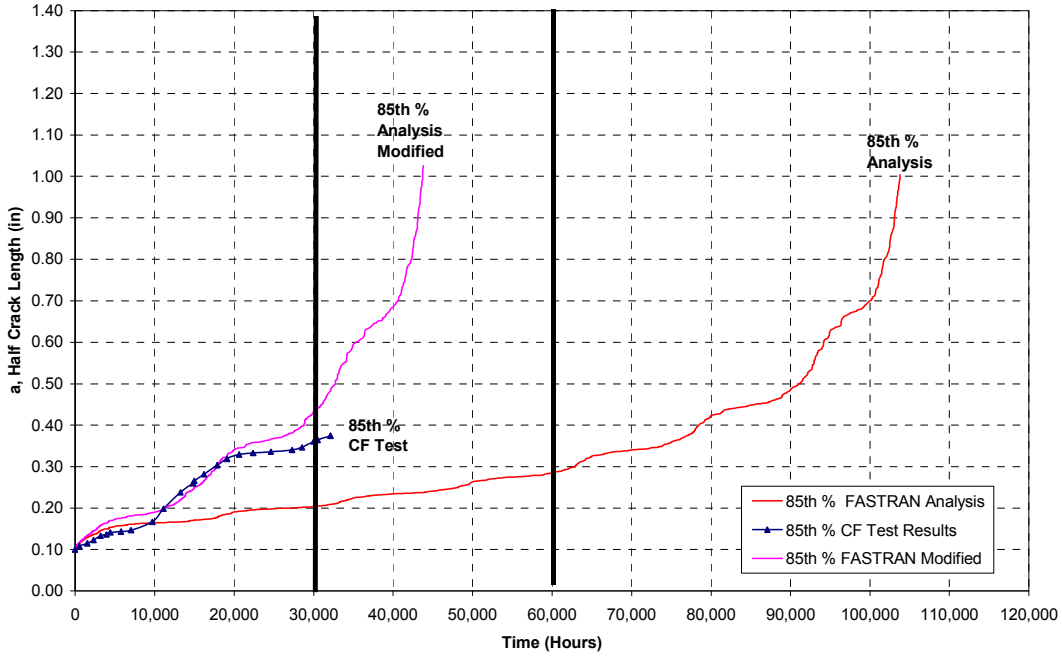

Figure 18: Centre Crack Coupon Results at FCA301 for the '85%' spectrum used on the P-3 SLAP Full Scale Fatigue Test along with initial and final predictions after modifications to alpha

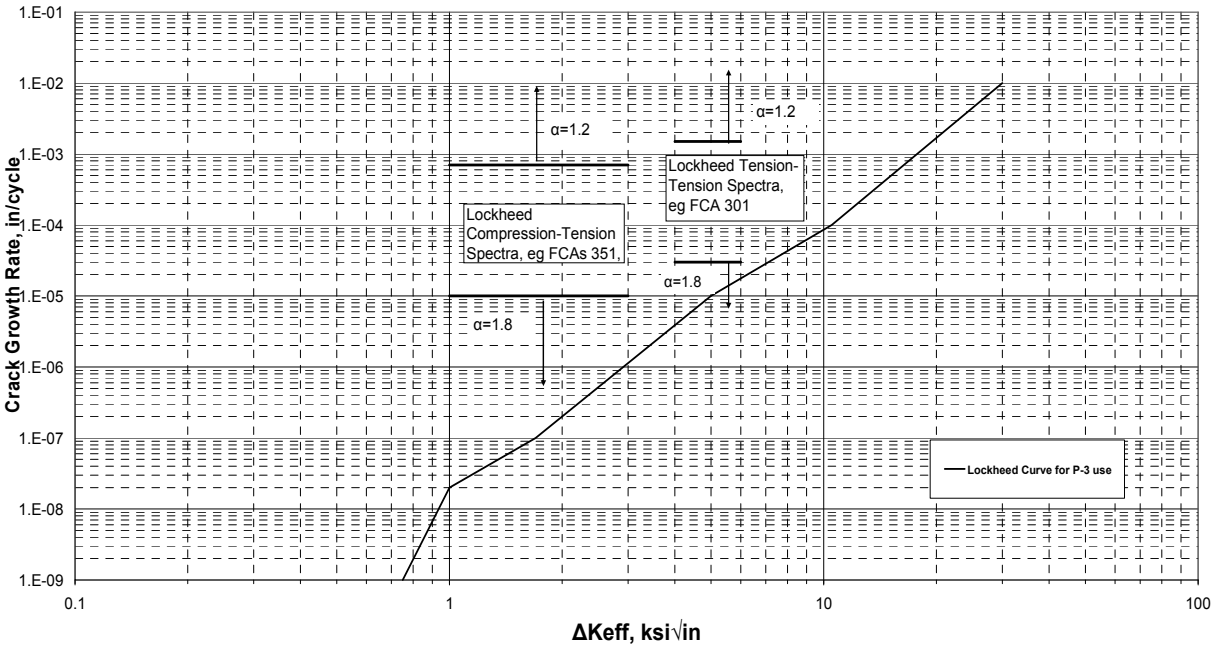

Figure 19: Crack Growth Rate versus dK_{eff} Data for Al 7075-T6 used for P-3 test interpretation

The resulting da/dn versus ΔK_{eff} data and values of constraint factor α used in the subsequent test interpretation analysis is shown in Figure 19. For the crack growth rates between the fixed values of α, the analysis uses a value of α on a sliding scale between the upper and lower values.

The analyses of cracks in aircraft are typically conducted in notched features, and the parameter used to account for the notch effects on the local stress field is the geometry factor β. Figure 20 shows the ability of FASTRAN, previously calibrated to match centre crack (through thickness) coupon results such as in Figure 18 between 1 mm (0.040 inches) and 10 mm (0.4 inches), to predict crack growth in a K_{tg}=5 notched coupon 2 mm thick and for a quarter circle crack transitioning to a through thickness crack over the same crack length range. The only additional input being the use of a β factor appropriate to the notch and the crack shape. The FASTRAN curve has been adjusted by manipulating the initial crack size a_i so that the final crack growth life matches the experimental life of the coupons. The Stress Factor (SF) referred to on the graph represents an adjustment to the stress level of the applied spectra (both experiment and prediction) in order to match full scale test stress survey results.

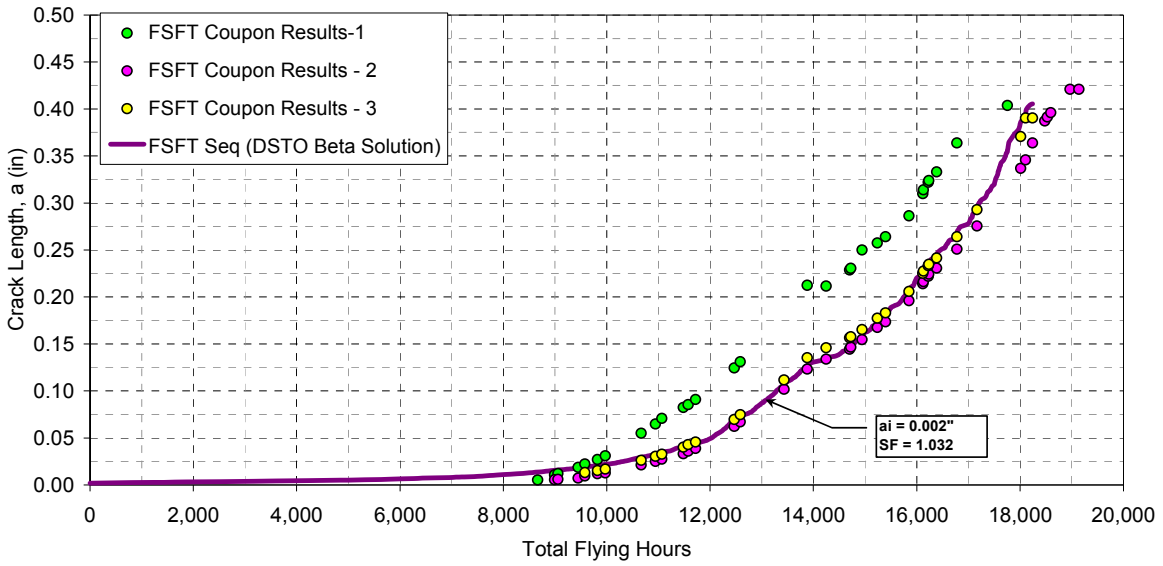

Figure 20: Comparison of Experimental and FASTRAN Crack Growth Data at FCA361 for the P-3 SLAP Full Scale Fatigue Test Spectrum

The usefulness of any calibration however is also measured by whether it can be used to accurately predict crack growth for a range of related load spectra. In the P-3 program the range of spectra included different spectra at different locations along the wing such as FCA301 and FCA 361 as well as different fleet usages (USN, RAAF etc). Figure 21 shows the performance achieved by the model in predicting crack growth under the RAAF P-3C sequence (with differences in peak stress levels as well as spectra) having been calibrated to the Full Scale Fatigue Test (so called 85 percentile) spectrum. The ability to predict to about 25% (on the conservative side) relative to a 300% difference in test life between the two spectra was judged to be satisfactory during the test interpretation work.

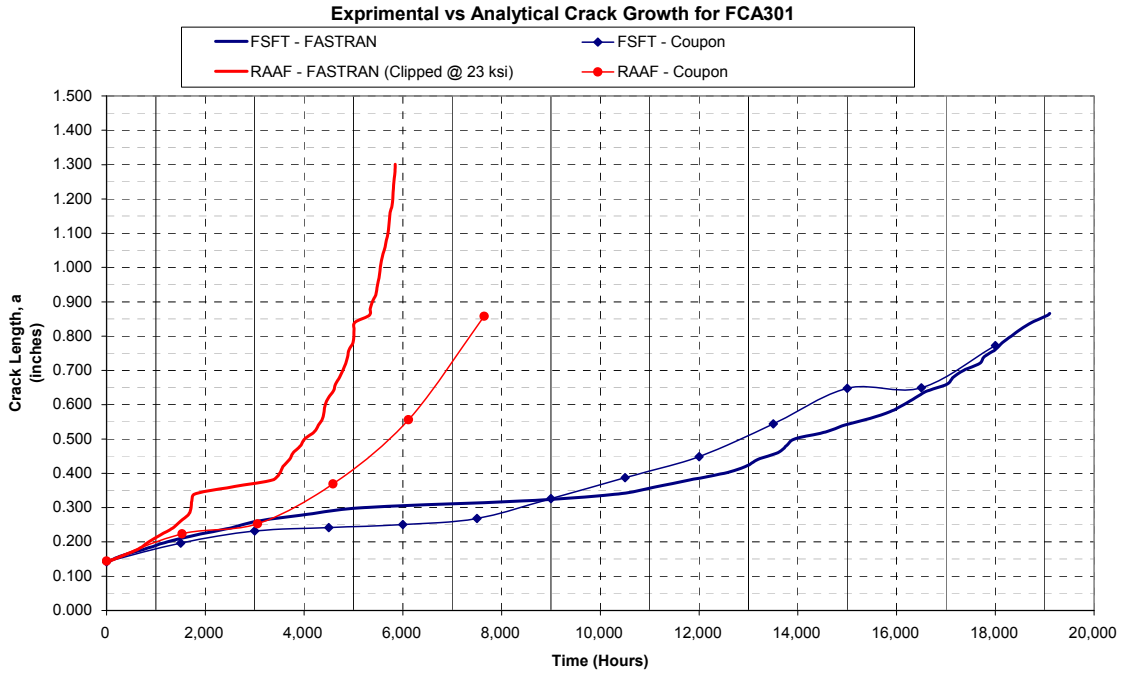

Figure 21: Comparison of Experimental and FASTRAN Crack Growth Data at FCA301 (Figure 29 from [30])

The P-3 SLAP test interpretation proceeded on the above basis, however, it was recognised that not all the issues had been resolved. The first of these was the ability of FASTRAN to make accurate predictions for crack sizes below about 0.5 mm (0.020 inches). This was not an issue during test interpretation as the interpretation methodology separately estimated a crack initiation period (up to 0.050 inches in the DSTO methodology, up to 0.010 inches for the USN methodology) using a strain life model. However, FASTRAN based equivalent initial flaw size (EIFS) values could of course still be estimated by fitting coupon or test article results to the FASTRAN analysis under the FSFT spectra and then using these same EIFS values in making full life predictions for other spectra. DSTO coupon test and analyses at the time of the P-3 SLAP work showed that FASTRAN full life predictions conducted this way could not be made with any accuracy and could be out by up to 100%. An example is shown in Figure 22. There was obviously something wrong with the crack growth estimations made using very small crack sizes. The use of long-crack growth rate experimental data supplied with the model for very small crack sizes was suspected as one of the problems.

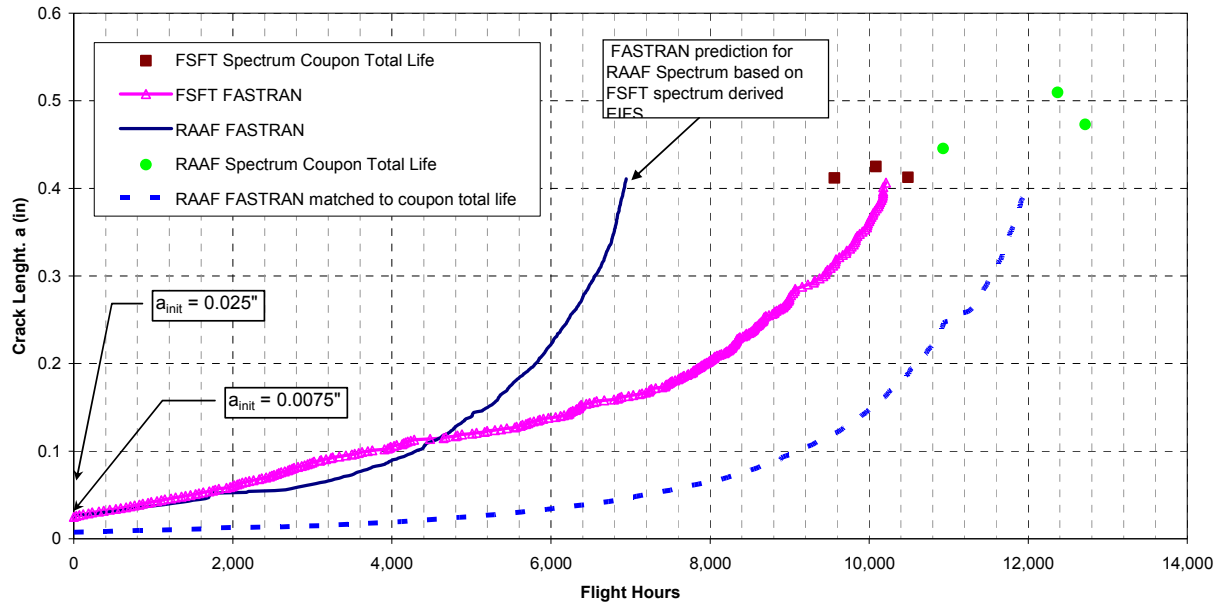

Figure 22: Evaluation of FASTRAN Predictions at FCA361 for RAAF Spectrum

As the influence of the beta value is crucial in the process of transferability between notch types for traditional LEFM models, efforts to improve the prediction of stress intensity factors were also undertaken. Replacement of theoretical or handbook derived solutions with those from FEM resulted in some improvement, particularly at the small crack sizes, see Figure 23 where the initial beta solution from Lockheed-Martin (L-M) was replaced by a solution developed by DSTO.

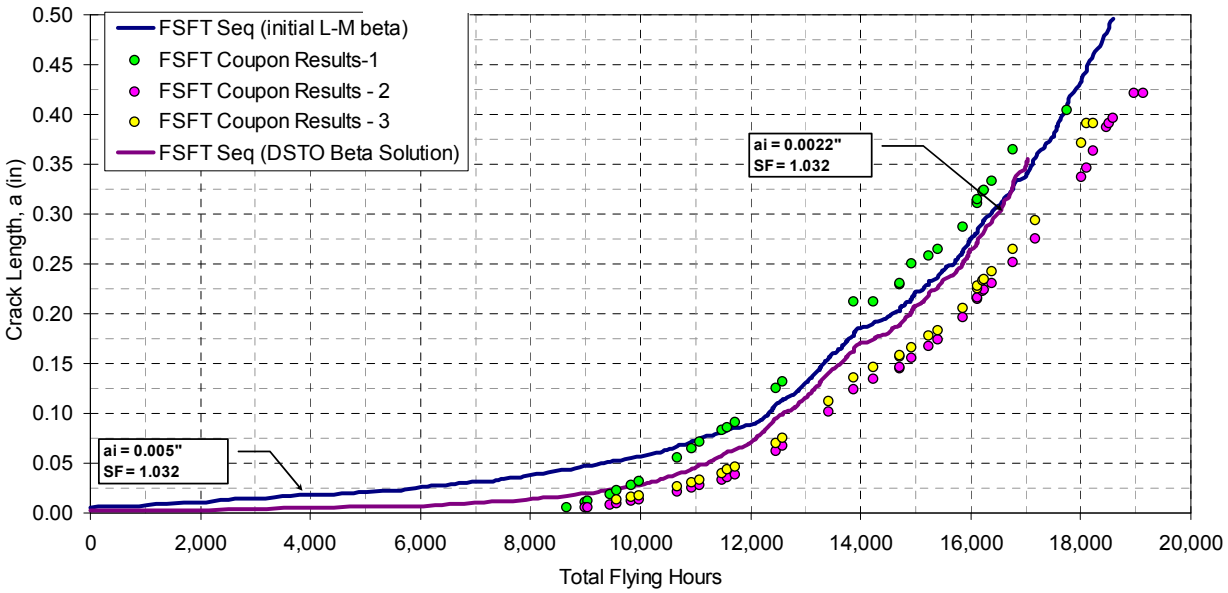

Figure 23: Comparison of FASTRAN Crack Growth for Different Beta Solutions and Experimental Data at FCA361

But there are limitations still. For example, the definition of the long crack rate threshold and the satisfactory use of short crack rate data is a problem that still needs to be solved and the current state of the art is not yet satisfactory. And then, when the cracks are physically small, there are simply the physical limitations such as the possible variations in sizes and orientations of stress concentrations and nucleation features that make a unique beta for each coupon test a possibility. Finally, there is the issue of notch plasticity. These issues could potentially limit the use of the current traditional models to crack sizes that are outside the influences of notch plasticity and non-homogeneous material effects. The P-3 data suggested that FASTRAN (at least in the configuration and with the CA material data used during the P-3 SLAP) cannot provide reliable total life estimates where the initial flaw size is less than 0.020 to 0.040 inches (0.5 to 1 mm). Clearly, improvements are necessary.

5.2 Reported Results from Previous F/A-18 Work

Previous attempts [21] to model F/A-18 coupon test results using traditional models including uncalibrated AFGROW and FASTRAN codes produced what were considered poor results given the shape of the predicted curves in particular. Examples are shown in Figure 24 and Figure 25 below (from [21]). Figure 24 came originally from [31], which is the earliest found example of this comparison for aluminium alloy, although earlier work conducted on AF 1410 steel in preparation for the F/A-18 spindle lifing work reported in [32] showed similar results. An investigation into this matter is underway and suggests that the problem, at least in the case of Al 7050, was caused by inadequate data in the threshold and near threshold region. When updated data for this region is used the comparison between analysis and test becomes very favourable. Full details of this work will be published in the near future. The first example that was examined in this current investigation is discussed in Section 5.2.2.

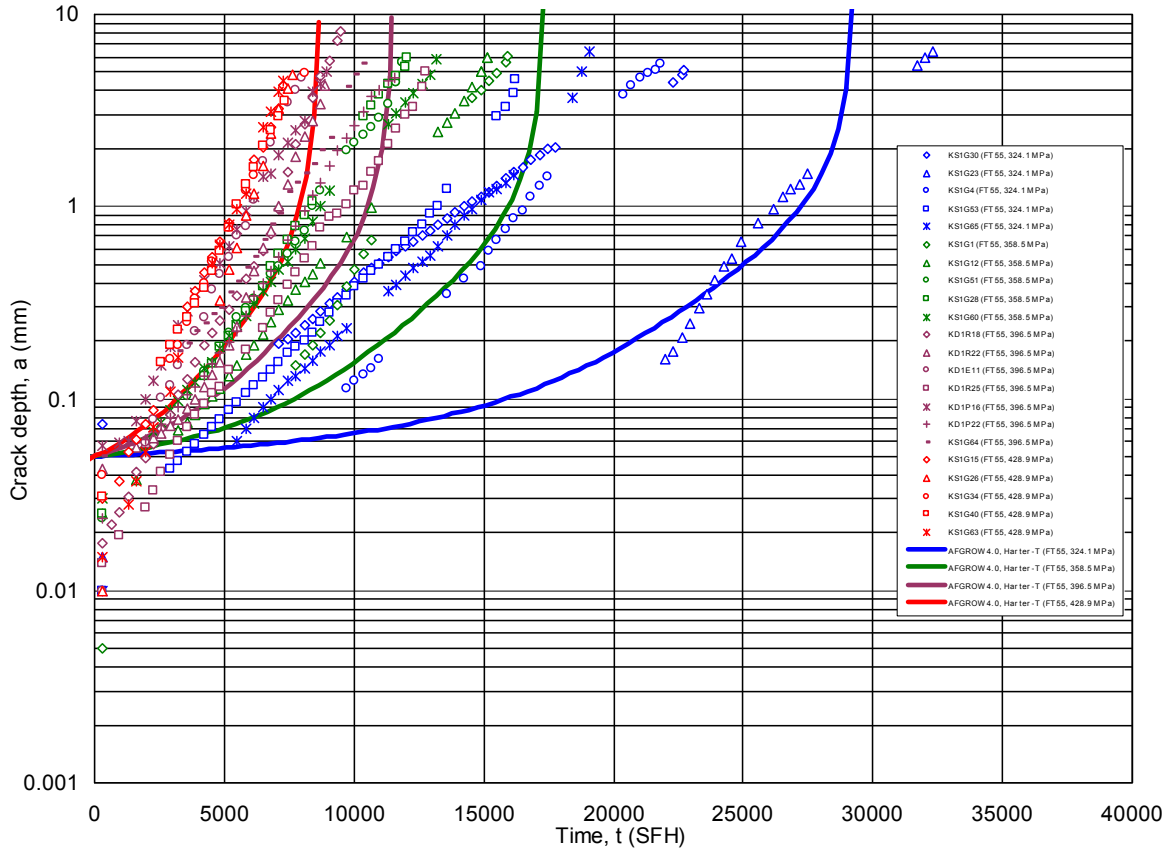

Figure 24: Comparison of Coupon test results against AFGROW analysis, from [21]

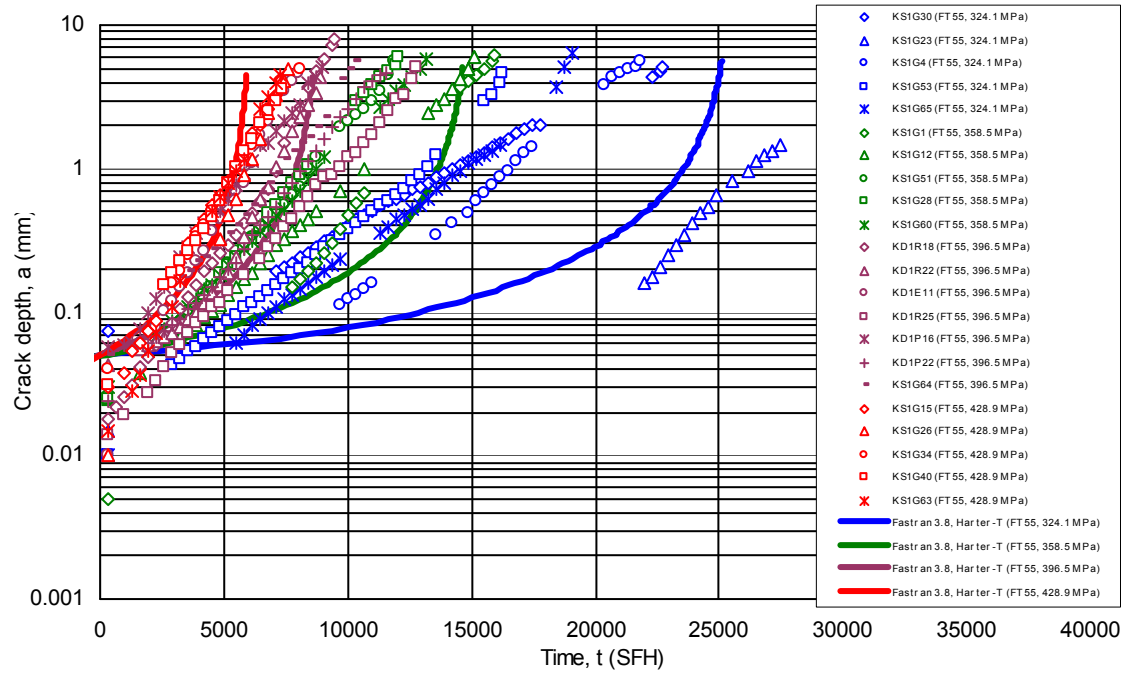

Figure 25: Comparison of Coupon test results against FASTRAN analysis, from [21]

5.2.1 F/A-18 Calibration using Variable Amplitude Data

As part of a project in January 2008 for a vacation student, Hui Chuan Ong, the F/A-18 low K_t coupon test results were analysed using CGAP. A spectrum-specific numerical calibration was conducted on one load case (one spectrum and stress level combination) to determine the parameters that define the crack growth curve, and this set of parameters was then used to analyse other cases. The motivation for this exercise, apart from helping the student to become familiar with the numerical tool and the procedure for crack growth analysis, was to see whether it was possible to reproduce the log-linear crack growth curves observed experimentally.

5.2.1.1 Numerical Calibration to Determine the Parameters

The following crack growth rate equation was used for this study:

$$\frac{da}{dN} = C\Delta K_{eff}^{m},$$

where ΔK_{eff} is the effective stress intensity range, $\Delta K_{eff} = K_{\max} - K_{open}$, and ΔK_{open} is the crack opening stress intensity. Iterative analyses were carried out to match the numerical results to one set of experimental results by modifying the parameters C and *m*. The case chosen for this purpose was a corner crack subjected to the APOL spectrum phase 1 at a stress level of 396.5 MPa.

The input details for the trial-and-error analyses were:

Geometry

Crack Configuration: Corner-crack in bar specimen under S

Width **w** = 0.014 m
Thickness **t** = 0.00635 m
Initial Crack Size **ci** = 2E-005 m
Initial Crack Depth **ai** = 2E-005 m
Final Crack Length **cf** = 0.00635 m
Notch Length **cn** = 2E-005 m
Notch Depth **an** = 2E-005 m
Notch Height **hn** = 0 m
Radius **R** = 0 m

Material
Material Name: Al 7050-T7451
Static Properties:
Young's Modulus = 71000 MPa
Poisson's Ratio = 0.33
Yield Strength = 450 MPa
Ultimate Strength = 521 MPa

Fracture Toughness Properties:
Elastic Fracture, Toughness = 35.4 MPa-m^(1/2)

Constraint Factor:
Constant Constraint Factor = 1.9

Load
APOL Phase I: 396.5 MPa

Trial-and-error shows that the parameters that produced the best correlation to the experimental data were ***C***=0.95E-9, *m*=2, (m/cycle, MPa√m units), and the correlation is shown in Figure 26.

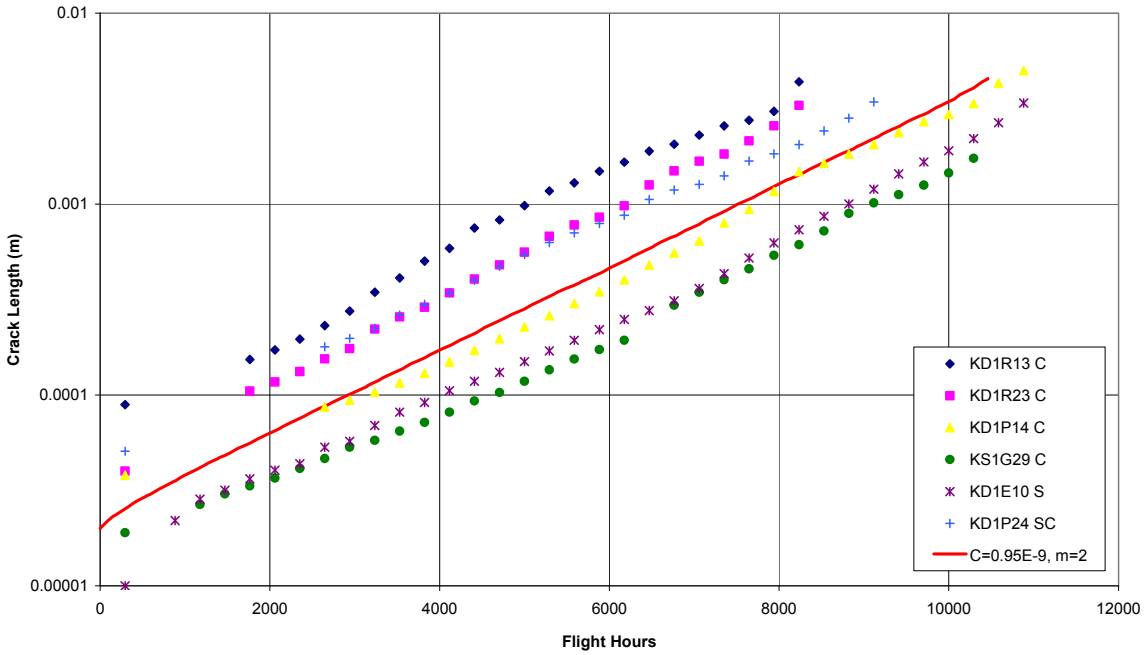

Figure 26 Numerical calibration of the crack growth rate equation using experimental data

5.2.1.2 Analyses of Other Cases

Once the crack growth rate model was calibrated, the other cases were analysed routinely. Figure 27 and Figure 28 plot some examples for the correlation between the CGAP results and the experimental results, for different spectra and different load levels.

Table 2 presents a summary of the extent of correlation for all the cases analysed using a qualitative assessment based on observations of prediction versus experiment.

From these figures and the table it can be seen that, for the experimental data considered, CGAP was able to give very reasonable predictions for crack growth curves, based on the crack growth rate equation obtained from numerical calibration. This outcome may indicate that: (1) the crack growth rate data used in the original AFGROW and FASTRAN analysis may not have been accurate, especially in the range of ΔK of interest; (2) the observed log-linear crack growth was due to the fact that crack growth mainly took place within a band of ΔK values which happened to have an m close to 2. Of course more investigation needs to be conducted to substantiate these observations as the trial could at this stage only be regarded as a demonstration, rather than a comprehensive validation involving multiple stress levels and diverse spectra.

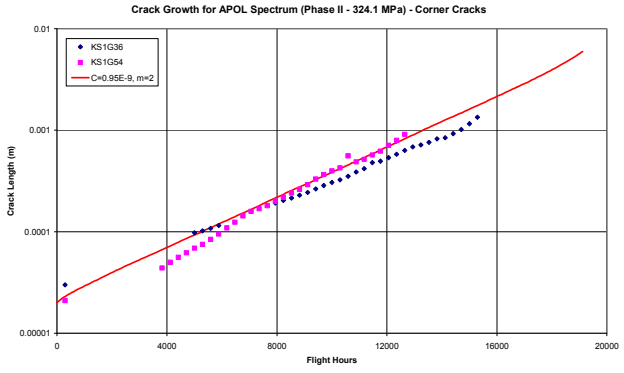

APOL 324.1 MP Corner Crack

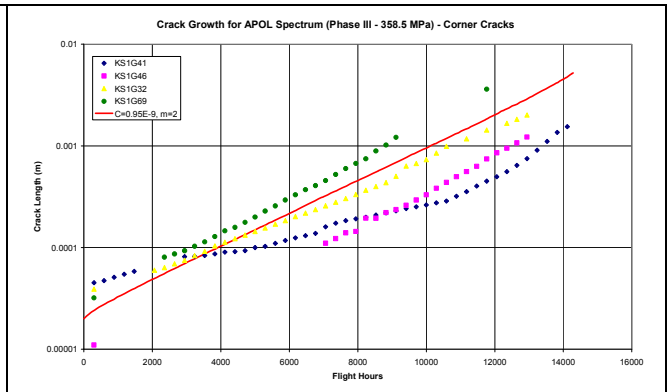

APOL 358.5 Corner Crack

Figure 27 Comparison of CGAP results and experimental results for APOL spectrum and corner cracks. Both results were considered 'good'.

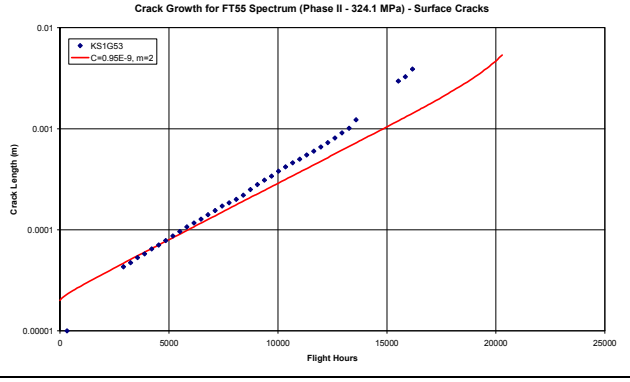

FT55 324.1 MPa Surface Crack

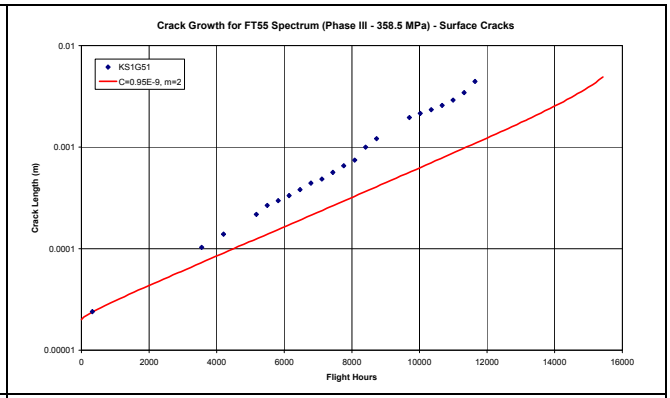

FT55 358.5 MPa Surface Crack

Figure 28 Comparison of CGAP results and experimental results for FT55 spectrum and surface cracks

Table 2 Summary of correlation of CGAP and experimental results using calibrated crack growth rate equation

Spectrum and Phase (Stress)	**Type of Crack**	**Qualitative Assessment of match**	**Notes**
APOL Spectrum Phase I (396.5)	Surface and Corner	N/A	Calibration
APOL Spectrum Phase II (324.1)	Corner	Good	See Figure 27
APOL Spectrum Phase II (324.1)	Surface	Poor	But correct gradient
APOL Spectrum Phase III (358.5)	Corner	Good	See Figure 27
APOL Spectrum Phase III (358.5)	Surface	Good	
APOL Spectrum Phase IV (428.9)	Corner	Very Good	
APOL Spectrum Phase IV (428.9)	Surface	Poor	
FT55 Spectrum Phase I (396.5)	Corner	Very Good	
FT55 Spectrum Phase I (396.5)	Surface	Good	
FT55 Spectrum Phase II (324.1)	Surface	Good	See Figure 28
FT55 Spectrum Phase III (358.5)	Corner	Good	
FT55 Spectrum Phase III (358.5)	Surface	Poor	See Figure 28
FT55 Spectrum Phase IV (428.9)	Corner	Very Good	
FT55 Spectrum Phase IV (428.9)	Surface	Poor	But correct gradient
A21-103 Spectrum Phase I (396.5)	Corner and Surface	Good	
A21-103 Spectrum Phase II (324.1)	Corner and Surface	Good	
A21-055 Spectrum Phase I (396.5)	Corner and Surface	Good	
A21-055 Spectrum Phase II (324.1)	Corner and Surface	Good	

5.2.2 Another Model Comparison Example – F/A-18 Bulkhead

Another comparison between the performance of a traditional model and an EBA type 'spectrum-specific calibration' model used experimental data from cracking in an F/A-18 bulkhead manufactured from 7050-T7451 material [33]. This journal paper put forward an example where a model developed by the authors (the C* model, a variant of the Frost-Dugdale log-linear model) worked well compared with a comparative FASTRAN analysis which did not compare well with the F/A-18 experimental data. The same case has been cited in several other papers [34-36]. The case was originally reported in [37]. The case involves spectrum loading (based on a mini-FALSTAFF spectrum) applied to an F/A-18 fuselage centre barrel. Details of the bulkhead and the analysis result from [33] are shown in Figure 29 to Figure 31.

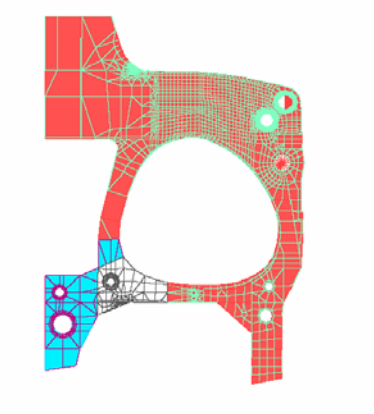

Figure 29: F/A-18 Bulkhead structure (original FE model by Chris Wallbrink) (from [33])

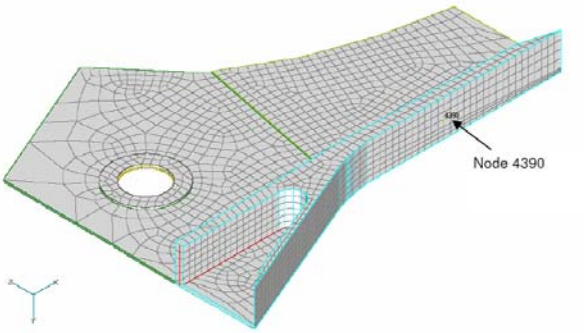

Figure 30: Crack location and local mesh (from [33])

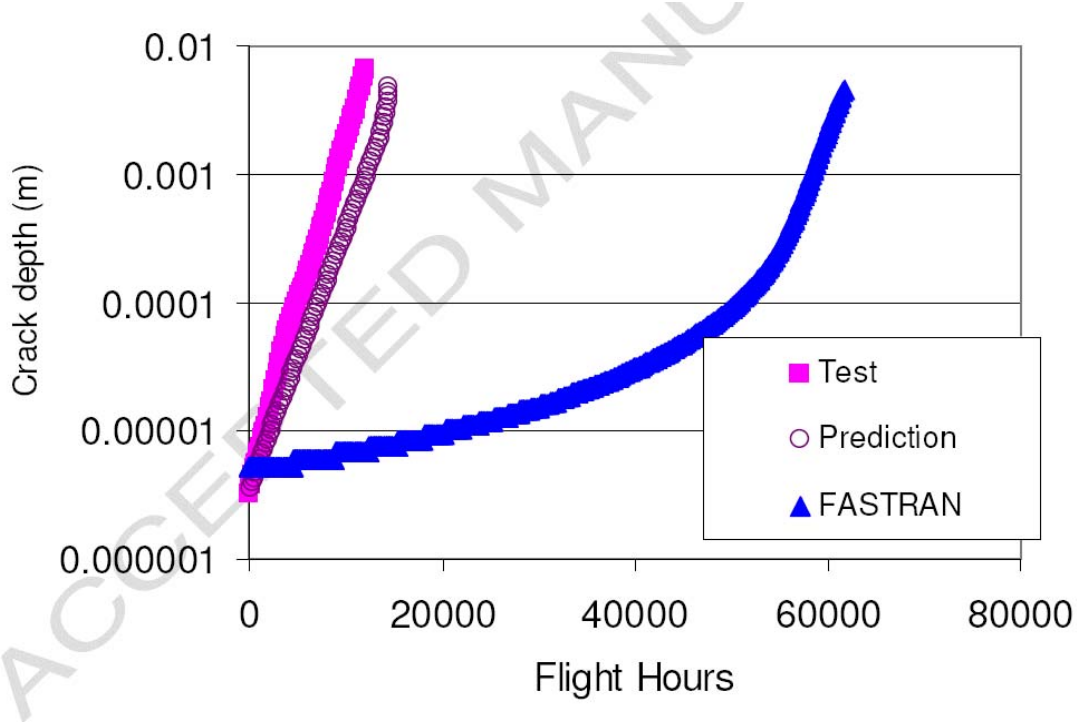

Figure 31: Experimental and predicted crack growth (from [33])

The original FASTRAN analysis has been reviewed more recently by DSTO. The first step was to re-produce the analysis as reported in [33]. Although it was difficult to do this precisely, the same basic trend as observed in [33] was obtained using values for crack growth rate data taken from the literature (see Figure 33). The next step was to investigate if improved analysis results could be obtained using FASTRAN with updated or improved crack growth rate data. An important aspect in the original conclusion of poor FASTRAN performance is that apart from the incorrect prediction of final life, the shape of the crack growth curve was also incorrect. The experimental result indicates log-linear or exponential crack growth, which is consistent with a

crack growth rate exponent, *m*, in a Paris type relationship of about 2.0, where the Paris equation is as follows:

$$\frac{da}{dN} or \frac{dc}{dN} = C\Delta K_{eff}{}^{m}$$

The FASTRAN analysis as per [33] used a Paris type fit for the crack growth rate equation with C=1.78 x 10^{-10} and m=3.36 (m/cycle, MPa√m units). The original data were sourced from [38], and it was noticed that there were no data for ΔK_{eff} values below 3.5 MPa√m, i.e. the data were missing in the threshold/near threshold region. It was thought that this near threshold area would be significant for this case.

An alternate source of 7050 data was found [39]. It was for a slightly different temper, T76 instead of T7451. However, it did include data between 1 and 3.5 MPa√m. The various rate data are shown in Figure 32. It is interesting to note that the new data is very similar to the data used in [33] for the region above 3.5 MPa√m, but below that point there is a distinct 'knee'. Using the green dashed curve as per Figure 32, a much improved FASTRAN result was produced as shown in Figure 33, although the experimental results were still underestimated somewhat.

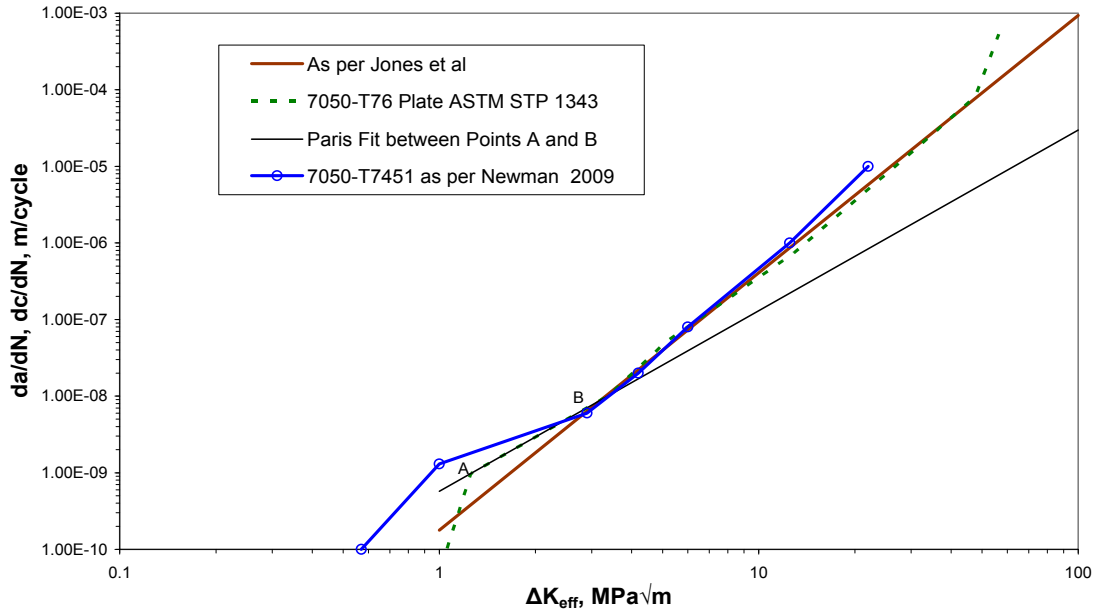

Figure 32: Comparison of crack growth rate versus effective stress intensity range curves for Al 7050

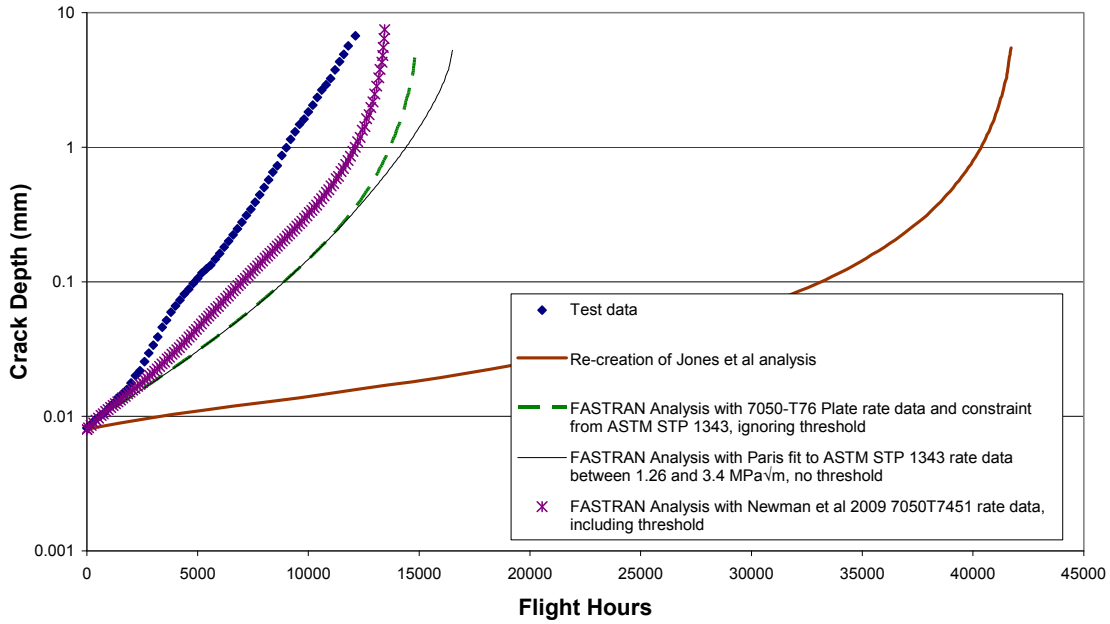

Figure 33: Revised analyses of F/A-18 Bulkhead Example. Note that the initial crack size is about 8 microns as per [37].

In order to investigate the importance of the section of the rate curve below 3.5 MPa√m, a case was analysed with a simple Paris type relationship based on the section of the crack growth rate curve between 1 and 3.5 MPa√m, i.e. points A and B as shown in Figure 32. The Paris constants were C=5.7 x 10^{-10} and m=2.36 (m/cycle, MPa√m units). The crack growth result as shown in Figure 33 did not change very much from the result obtained using the improved rate data, suggesting that the crack growth for this problem is dominated by the threshold or near threshold data, i.e. below 3.5 MPa√m. It also highlights the danger of relying (even inadvertently) on extrapolated rate data for this type of analysis.

In an even more recent analysis this same problem was run using crack growth rate data presented in 2009 in [40]. This data was similar to the previous ASTM data but had improved threshold and near threshold data obtained from using the compression pre-cracking constant amplitude (CPCA) technique. This technique is explained in [40] along with the use of a lower than expected value of constraint of α = 1.3 (an alpha value of 1 represents a plain stress condition). The result of the use of the more recent data was a further improvement in FASTRAN prediction verses experiment, see Figure 33.

If we accept that the growth of the crack in this example is dominated by the section of the da/dN versus ΔK_{eff} curve below 3.5 MPa√m in Figure 33, where the value of m for the Paris fit between points A and B is 2.36 it is not surprising that the resulting crack growth curve is approximately 'log-linear'. This would suggest that there is no inconsistency (for this example at least) between traditional modelling using underlying constant amplitude rate data and an

experiment that showed log-linear or exponential crack growth behaviour. This problem will again be revisited in the next section.

The key point that can be taken from this example is the need to ensure that the baseline material data used encompasses the range of the problem. Extrapolation of the crack growth rate curve, or over-simplification of it to a single constant Paris exponent as was done in [33] can lead to significant errors. To conclude that the error is with the model itself is not correct. The error in this case was with the input data.

5.3 Which Spectra Use What Part of the Crack Growth Rate Curve?

In Section 5.2 it was shown that the use of a short-crack-calibrated crack growth rate curve would significantly improve FASTRAN predictions. In fact a modification of just a segment of the rate curve can have a significant effect on the output. It is then of interest to know which segment of the rate curve is used within FASTRAN for a given load cycle and thus confirm or otherwise the importance of the near-threshold region. This may be examined by extracting the cycle-by-cycle crack growth information from FASTRAN.

The FASTRAN code was modified to output the required cycle-by-cycle information during the analysis. The modified code was used to analyse four spectra; the F-111 D20 wing slice spectrum, the FA-18 FT55m512 spectrum from the FT55 Wing Fatigue test, the spectrum used in the F/A-18 bulkhead example of Section 5.2, and the P-3C FCA361 FSFT spectrum. The exceedence curves for the four spectra are in Figure 34, showing the different spectra shapes, the proportion of negative and positive loads and, in the case of the F-111 and FT55m512 spectra the deliberately inserted overloads, the purpose of which is explained in the following sub-sections.

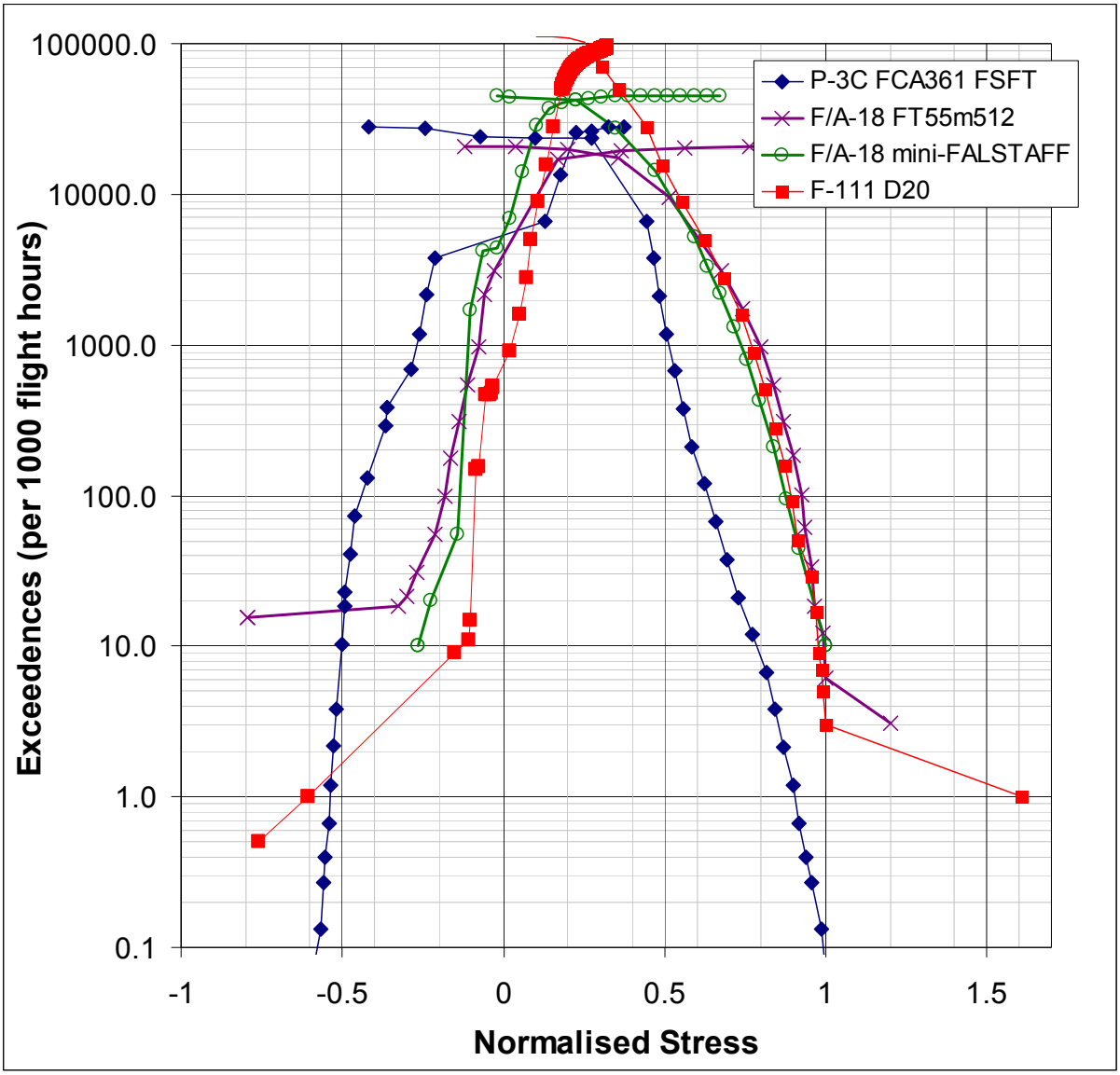

Figure 34: Exceedence curves for four spectra examined in Section 5.3

The F-111 and F/A-18 spectra were developed from flight recorded data and were completely variable with no constant amplitude cycles. The P-3C FCA361 FSFT spectrum was also a flight-by-flight spectrum but had periods of constant amplitude loading representing gust events within flights. These periods of constant amplitude loading were modified by very slightly altering every second cycle to coerce FASTRAN to output data for each cycle without altering the FASTRAN prediction. Subsequent testing showed that modification of the spectrum produced minimal change to the total crack growth prediction.

Analyses were conducted to determine the amount of crack growth and the number of cycles attributable to a ΔK_{eff} range for various portions of the predicted crack growth curve. Bar graphs were generated showing the proportion of crack growth for a given ΔK_{eff} range. The

number of cycles contributing to the crack growth at a given ΔK_{eff} range was also calculated and is presented on the graphs as a number above each bar. Only cycles that contributed to crack growth were considered in the analysis, *i.e.*, cycles with ΔK_{eff} ranges below the crack growth threshold were ignored as they produced no analytical crack growth. In this way the analysis provides an indication of the relative significance of the various portions of the input material crack growth rate curve.

Before the results are presented, it is useful to recall that the values of ΔK_{eff} and crack growth increment are those that are predicted by FASTRAN. It is not claimed that this exactly represents what has happened physically. The link to reality is through the match between the overall crack growth predicted by the code and the experimental results. For the F-111 and F/A-18 examples the correlation is reasonable, for the P-3 example the predictions are very close above 0.020" (0.5mm). It should also be noted that only in the P-3 analysis had FASTRAN been specifically calibrated. The crack growth rate curve for the 7075 coupon examples is shown within the P-3 example. All predictions for the coupon examples used a threshold in the crack growth rate curve of 0.68 MPa√m ΔK_{eff} whereas for the predictions for the F/A-18 bulkhead example no threshold value was used.

5.3.1 F-111 D20 Wing Splice spectrum

Due to the size of the output files generated by this particular spectrum only certain portions of the crack growth curve were selected for analysis. This spectrum contained a significant 'overload' called a cold proof load test (CPLT) load at the end of the spectrum after four programs of service loading. This load is important in the development of plastically-induced closure. The crack growth data along with the FASTRAN crack growth prediction is presented in Figure 35.

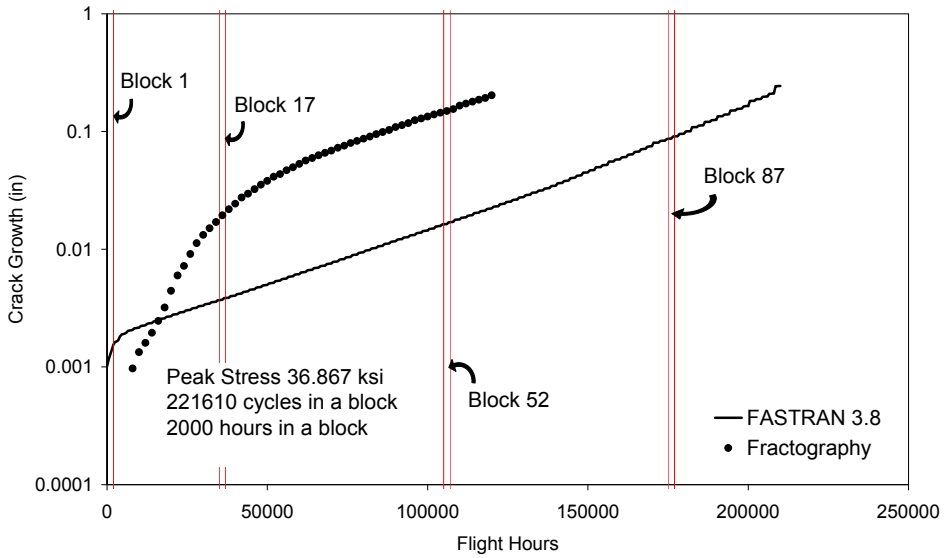

Figure 35: Experimental and FASTRAN predicted crack growth for F-111 D20 spectrum example

The analysis showing the combined contribution to crack growth of individual cycles (grouped into segments of the ΔK_{eff} range) is shown in Figure 36 whilst the information showing the number of cycles that FASTRAN determined to be contributing to crack growth (called 'active' cycles) is shown in Table 3. Figures 36a to 36d present information at various points in the total crack growth curve which are indicated in Figure 35. Each of these figures is presented with different axis scales that maximise readability but it should be noted when comparing figures. The data in Figure 36a shows the growth attributed to the ΔK_{eff} in the first block. This figure provides insight into how FASTRAN handles the application of very large loads. Since the CPLT load occurs at the end of the spectrum, a significant number of prior cycles are observed to contribute to crack growth. The CPLT load increases the opening stress and therefore reduces the number of active loads subsequent to the CPLT load. Also identifiable in this figure is the significant contribution to crack growth at very low ΔK_{eff} and also the large number of cycles contributing to crack growth. Figure 36b presents data taken from 17th repeat of the spectrum (block 17). At this stage the effect of the CPLT load is evident due to a reduced number of cycles contributing to crack growth. The CPLT load increases the crack opening stress evaluated by FASTRAN which reduces the number of active cycles contributing to crack growth. The two CPLT load cycles contributed a significant proportion of the crack growth while the remaining 3350 cycles that still contribute to crack growth all have ΔK_{eff} below 2.9 $\text{ksi}\sqrt{\text{in}}$. At the point where half the predicted life has elapsed Figure 36c is produced. Again a significant portion of crack growth is attributed to cycles with small ΔK_{eff} ranges. Indeed 85% of the cycles contributing to crack growth are below $2\,\text{ksi}\sqrt{\text{in}}$. Examining a block in the final third of the predicted crack growth life (Figure 36d) we see that the CPLT loads become very dominant in the calculated crack growth life. At this point the importance of the rest of the spectrum is greatly diminished. Only 0.7% of the cycles in the entire spectrum are contributing to the prediction of crack growth with the vast majority of crack growth due to the CPLT loads.

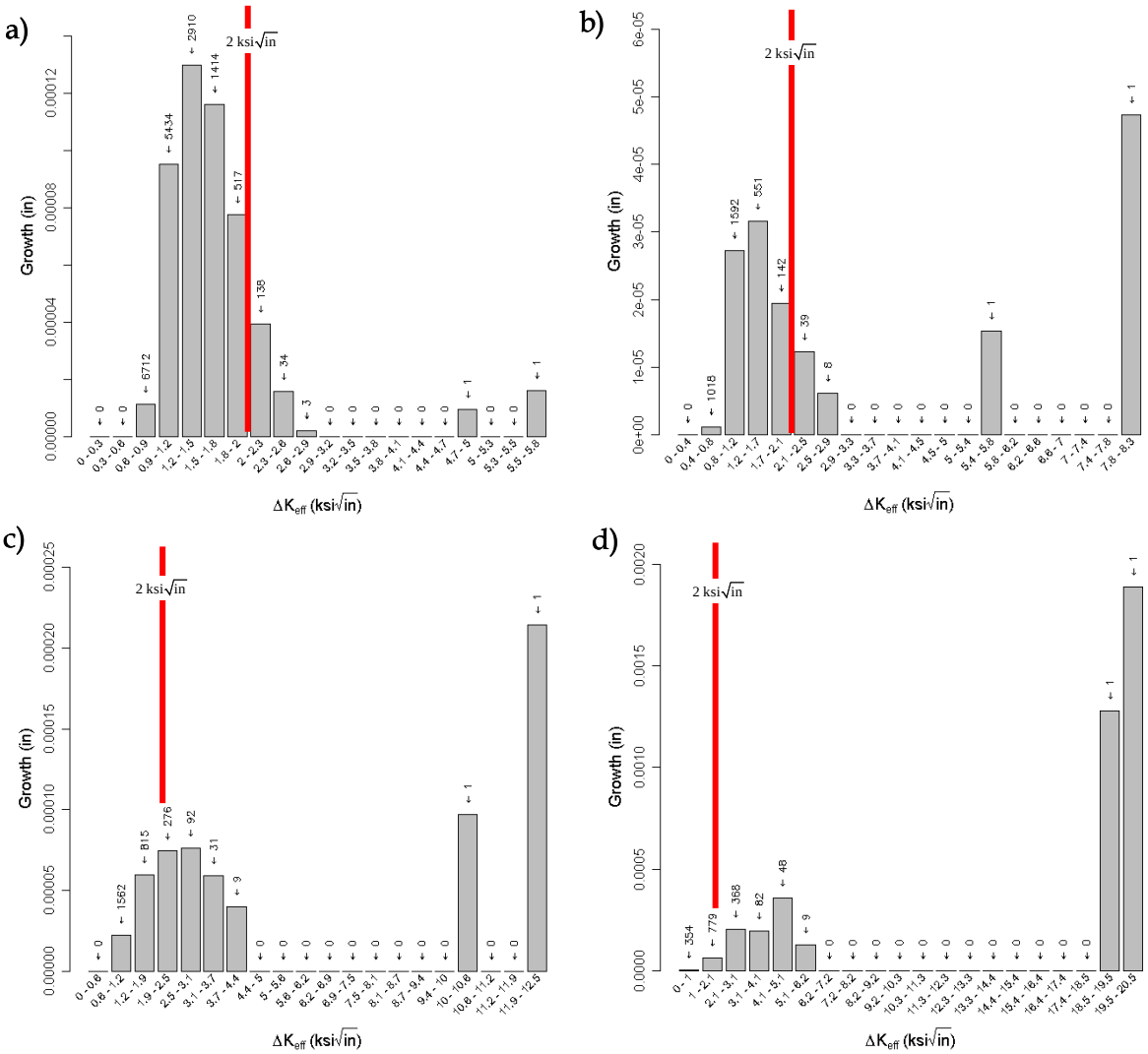

Figure 36: Growth and cycle counts attributed to different bands of ΔK_{eff} for crack growth under the F-111 D20 WS spectrum for a) block 1, b) block 17, c) block 52 and d) block 87

Table 3: Statistics on FASTRAN analysis of sections of the crack growth curve under D20

Proportion analysed	**Elapsed Flight Hours**	**No. of cycles in analysis**	**No of 'active' cycles**	**% of cycles 'active'**	**Total crack growth predicted**
Block 1	0	221610	17164	7.75	0.001550 in
Block 17	35000	221610	2801	1.26	0.003735 in
Block 52	105000	221610	2787	1.26	0.016467 in
Block 87	175000	221610	1642	0.74	0.088414 in

A key point to note in all the previous sub-figures is the contribution of growth attributed to cycles evaluated with small ΔK_{eff}. A significant portion of cycles active in producing crack growth have a ΔK_{eff} below 2 ksi$\sqrt{\text{in}}$. In the final third of the crack growth life the large crack

size is expected to raise ΔK_{eff}, yet 69% of the active cycles were still below $2\,\text{ksi}\sqrt{\text{in}}$, an effect likely to be due to the FASTRAN calculated crack closure effect of the CPLT loads

5.3.2 F/A-18 FT55m512 spectrum

FASTRAN cycle-by-cycle output for the F/A-18 FT55m512 spectrum was of a smaller size which also produced a smaller output allowing analysis of all the data. The F/A-18 FT55m512 spectrum contains a marker block consisting of five under loads followed by an overload of 1.2 times the maximum peak load in the spectrum [41]. Further information on the FT55 spectrum can be found in [42]. The crack growth life (Figure 37) was divided into thirds in an attempt to assess the behaviour of the crack growth model at different points in the life of the crack. Similar analyses (as used earlier) were performed to establish amounts of crack growth attributed to various ΔK_{eff}. The combined contribution to crack growth of individual cycles is shown in Figure 38 whilst the information showing the number of active cycles is shown in Table 4. Interestingly the FASTRAN prediction showed that over the first 2 thirds of the total predicted crack growth life, approximately 93% of all load cycles had a ΔK_{eff} below $2\,\text{ksi}\sqrt{\text{in}}$. As shown in Figure 38a, in the first third of crack growth life 99.0% of cycles contributing to crack growth had a ΔK_{eff} below $2\,\text{ksi}\sqrt{\text{in}}$ and contributed to 90.7% of the crack growth. In the second third of crack growth life 90.3% of cycles contributing to crack growth had a ΔK_{eff} below $2\,\text{ksi}\sqrt{\text{in}}$ which contributed to 43.3% of crack growth as shown in Figure 38b. The final third of crack growth still indicated that a considerable proportion of cycles 46.9% still had a ΔK_{eff} below $2\,\text{ksi}\sqrt{\text{in}}$, however these cycles now only contributed to 0.3% of crack growth, as shown in Figure 38c.

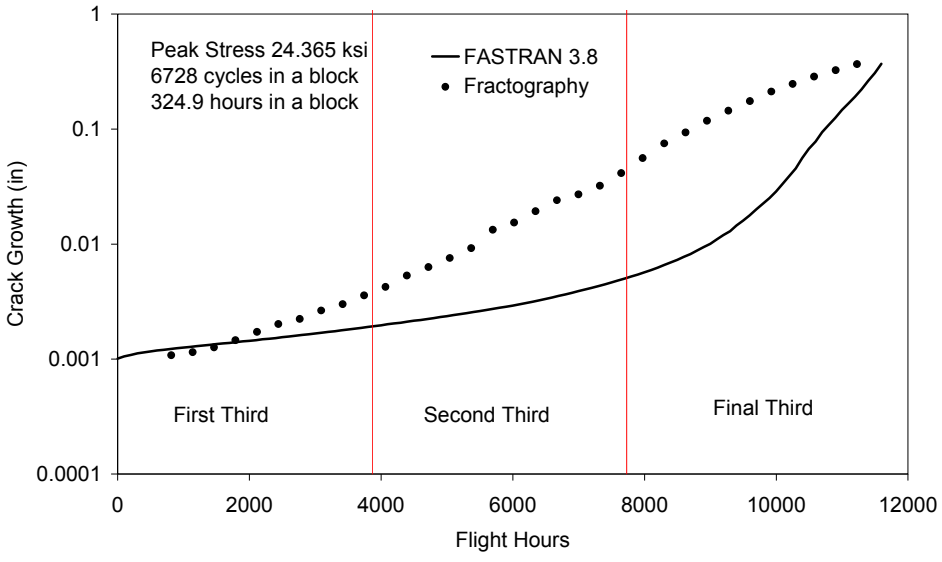

Figure 37: Experimental and FASTRAN predicted crack growth for F18 FT55m5 spectrum example

Table 4: Statistics on FASTRAN analysis of sections of the crack growth curve under F18 FT55m5

Proportion analysed	Analysis Flight Hours	No. of cycles in analysis	No of 'active' cycles	% of cycles 'active'	Total crack growth predicted
First third	0-3865	80279	29555	36.8	0.048 mm
Second third	3865-7730	80279	37046	46.1	0.127 mm
Final third	7730-11596	80279	51265	63.9	9.37 mm

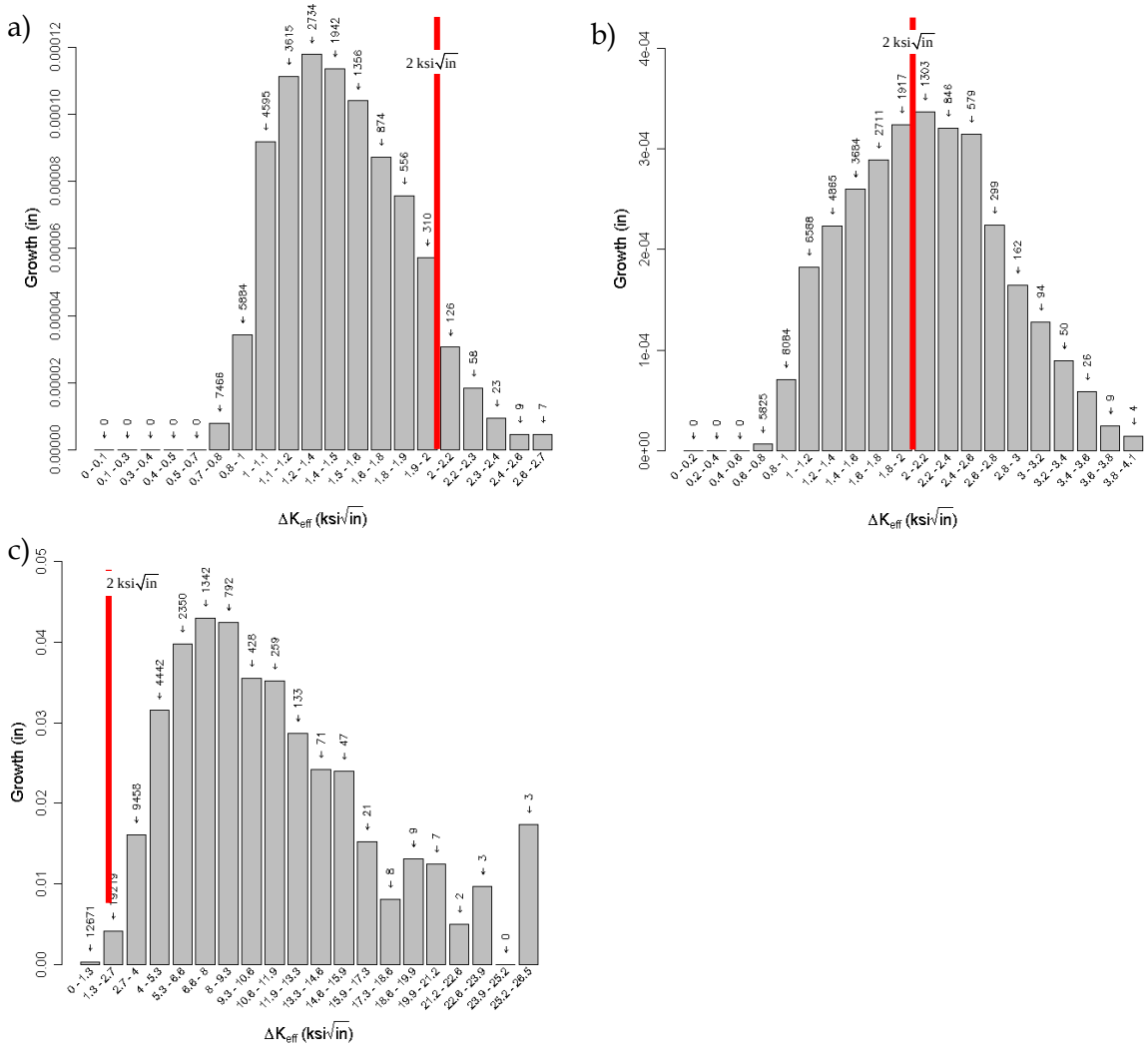

Figure 38: Growth and cycle counts attributed to different bands of ΔK_{eff} for crack growth under the F/A-18 FT55m512 spectrum for a) the first third of crack growth, b) the second third of crack growth and c) the final third of crack growth

5.3.3 F/A-18 Bulkhead problem

In this section we revisit the earlier problem considered in Section 5.2.2 and examine the FASTRAN results that used the ASTM material data. As was done in the previous F/A-18 example the crack growth prediction was divided into thirds. Analysis was performed to establish the amounts of growth attributed to various ΔK_{eff} values. Results are presented in Figure 39 and in Table 5. The crack growth data used in this analysis is from [39] and reproduced in Figure 32. The analysis in Section 5.2.2 focused on the region of the ΔK_{eff} curve below 3.5 $\text{MPa}\sqrt{\text{m}}$ which contained the observed knee in the crack growth rate curve that was not captured in earlier analysis. Concentrating on this region the present analysis reveals the importance of data in the region below 3.5 $\text{MPa}\sqrt{\text{m}}$. In the first third of crack growth, 100% of all the active loads contributing to crack growth had a ΔK_{eff} below 3.5 $\text{MPa}\sqrt{\text{m}}$ shown in Figure 39a. In the second third of crack growth, 99.996% of all active loads had a ΔK_{eff} range below 3.5 $\text{MPa}\sqrt{\text{m}}$ shown in Figure 39b. Thus, in the first two thirds of the crack growth prediction, close to 100% of all active loads contributing to the crack growth prediction were evaluated with ΔK_{eff} below 3.5 $\text{MPa}\sqrt{\text{m}}$. In the final third of crack growth, 88.2% of all the active loads contributing to crack growth had a ΔK_{eff} below 3.5 $\text{MPa}\sqrt{\text{m}}$. However, these loads only contributed to 3.7% of the total crack growth in the final third, indicating the remaining 11.8% of the active cycles contributed to the majority of crack growth (96.3%) as the crack reaches its critical length, as shown in Figure 39c. These results support the previous conclusions demonstrating the importance of an accurate input ΔK_{eff} data.

Table 5: Statistics on FASTRAN analysis of sections of the crack growth curve under mini-FALSTAFF spectrum

Proportion analysed	**Analysis Flight Hours**	**No. of cycles in analysis**	**No of 'active' cycles**	**% of cycles 'active'**	**Total crack growth predicted**
First third	0-4584	194659	191080	98.16	0.019 mm
Second third	4584-9169	194659	191079	98.41	0.098 mm
Final third	9169-13753	194659	191087	98.17	8.459 mm

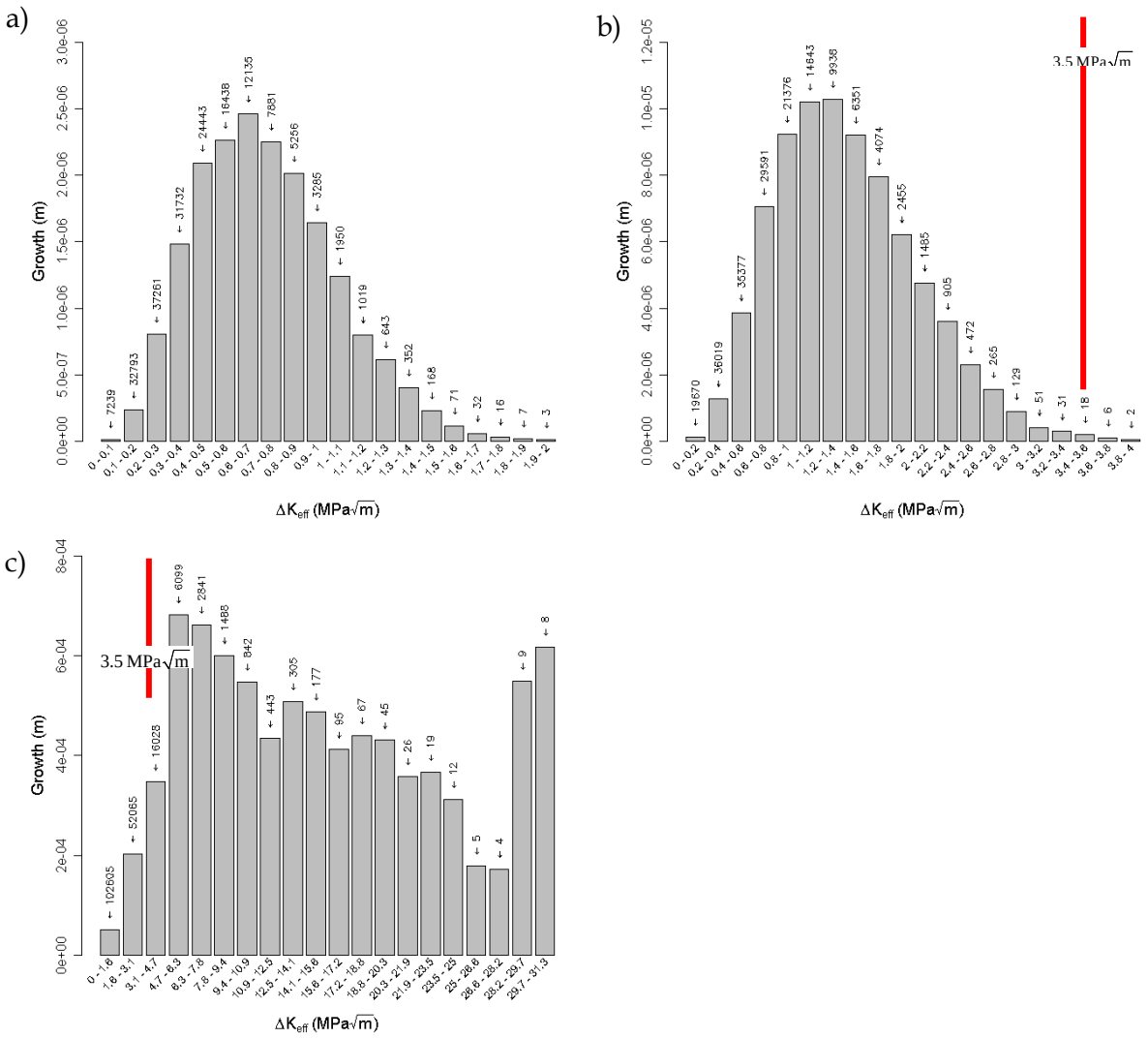

Figure 39: Growth and cycle counts attributed to different bands of ΔK_{eff} for crack growth under the F/A-18 mini-FALSTAFF spectrum for a) the first third of crack growth, b) the second third of crack growth and c) the final third of crack growth

5.3.4 P-3C FCA361 FSFT spectrum

The P-3C FCA361 FSFT spectrum was chosen to assess the output produced by FASTRAN for a typical transport/maritime aircraft wing spectrum and stress level combination. This spectrum consisted of 421545 cycles in a block with each block equivalent to 15,000 flight hours. The total predicted crack growth results from FASTRAN, see Figure 40, were divided into three equal sections. Analysis was again performed to determine the proportion of crack growth attributed to various ΔK_{eff}. The results are presented in Figure 41 and Table 6. In the first third of crack growth, 98.5% of cycles active in producing crack growth had a ΔK_{eff} below $2\,\text{ksi}\sqrt{\text{in}}$ which contributed to 74.9% of crack growth as shown in Figure 41a. This changed dramatically in the second third of crack growth, shown in Figure 41b. Here a considerable proportion of the cycles

(65.5%) still had a ΔK_{eff} below $2\,\text{ksi}\sqrt{\text{in}}$, but these cycles only contributed to 8.6% of crack growth. In the final third of crack growth 47.2% of cycles had a ΔK_{eff} range below $2\,\text{ksi}\sqrt{\text{in}}$ resulting in 0.9% of crack growth, as illustrated in Figure 41c.

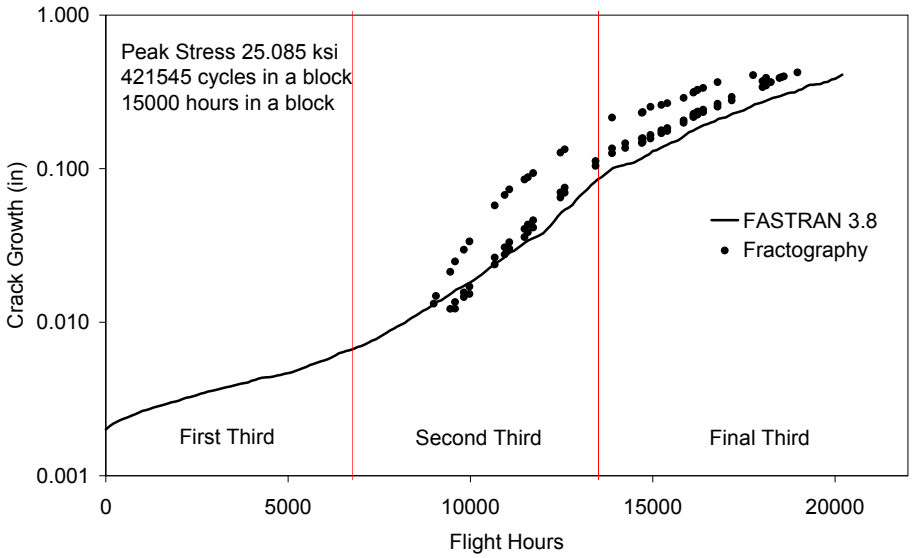

Figure 40: Experimental and FASTRAN predicted crack growth for P-3C FCA361 spectrum example

Table 6: Statistics on FASTRAN analysis of sections of the crack growth curve under P-3C FCA361

Proportion analysed	**Analysis Flight Hours**	**No. of cycles in analysis**	**No of 'active' cycles**	**% of cycles 'active'**	**Total crack growth predicted**
First third	0-6756	189,879	135,513	71.37	0.0066 in
Second third	6756-13513	189,879	143,941	75.81	0.0859 in
Final third	13513-20269	189,879	109,223	57.52	0.4109 in

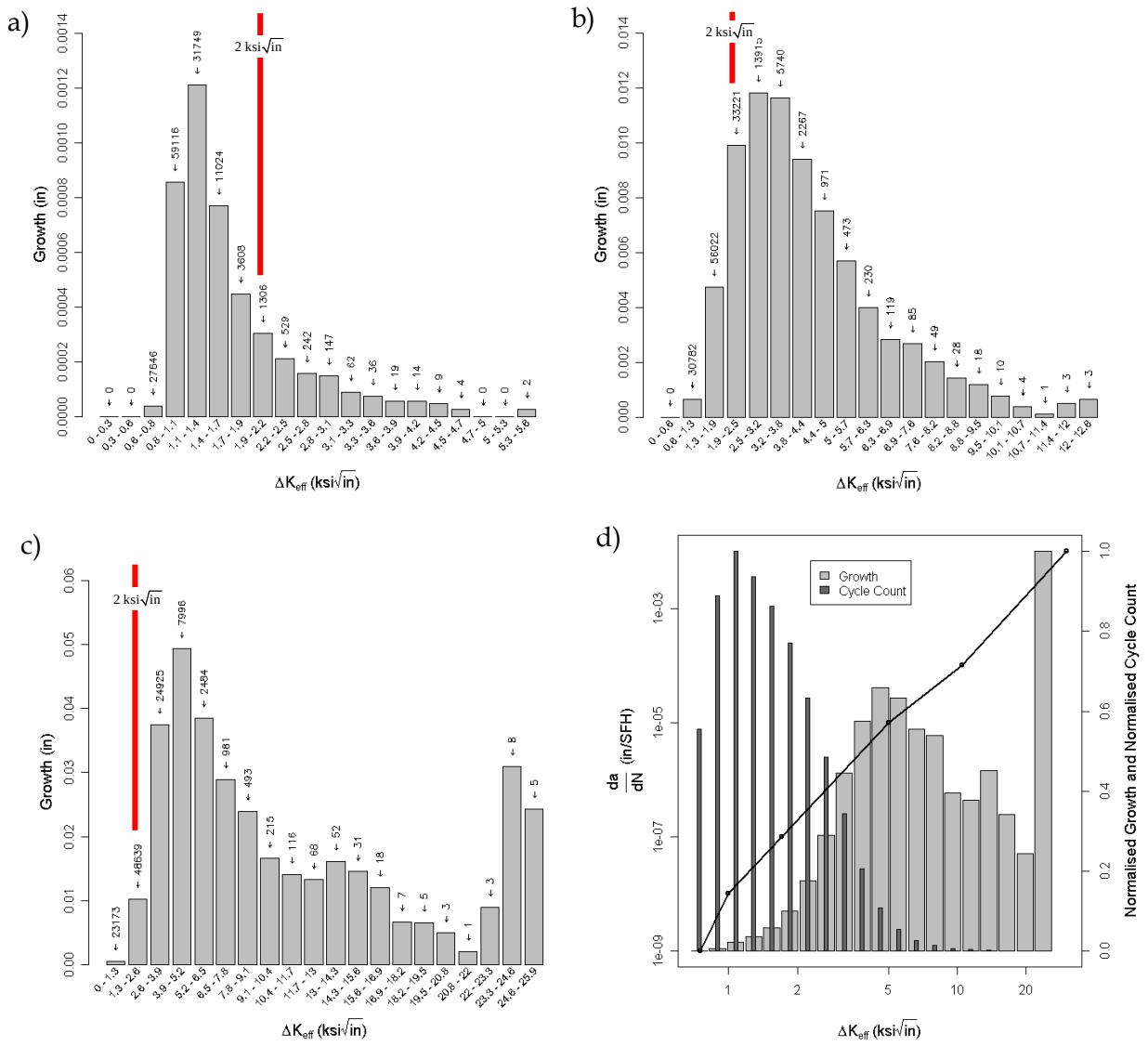

Figure 41: Growth and cycle counts attributed to different bands of ΔK_{eff} for crack growth under the P-3C FCA361 FSFT spectrum for a) the first third of crack growth, b) the second third of crack growth, c) the final third of crack growth and d) the total crack growth overlayed with the crack growth rate curve

The entire FASTRAN predicted crack growth was also analysed in a similar way and is presented in Figure 41d against the crack growth rate versus ΔK_{eff} curve used in FASTRAN. It shows that the lower part of the curve is used considerably more often in the analysis than the latter part of the curve. It also shows that the majority of the growth over the entire life is evaluated from the mid to later parts of the CGR versus ΔK_{eff} curve. However, it should be remembered that the later part of crack growth contributes significantly to crack growth and skews the growth distribution to the right. Thus Figures 41a-41c give a better indication of the importance of sections of the crack growth rate curve at different times in the modelled life of a

crack. Errors in the crack growth rate that are located in regions where either the cycle count is high or where cycles contribute to significant growth will affect the overall prediction as both have an impact on the shape of the crack growth curve and the prediction in life.

Another way to present the data in Figure 41a-41c is shown in Figure 42a and Figure 42b. Using the P-3C spectrum as an example, the counts for all three bands have been plotted in the same figure, Figure 42a. This figure shows the relative contribution of cycles from each band of ΔK_{eff}. The number above the bar indicates the total number of counts. Similarly the crack growth attributed to different bands of ΔK_{eff} is plotted together in Figure 42b. These figures do not provide the fidelity of earlier figures but allow, for each spectrum, a direct comparison of the contribution of cycles from each of the stages within the same band of ΔK_{eff}.

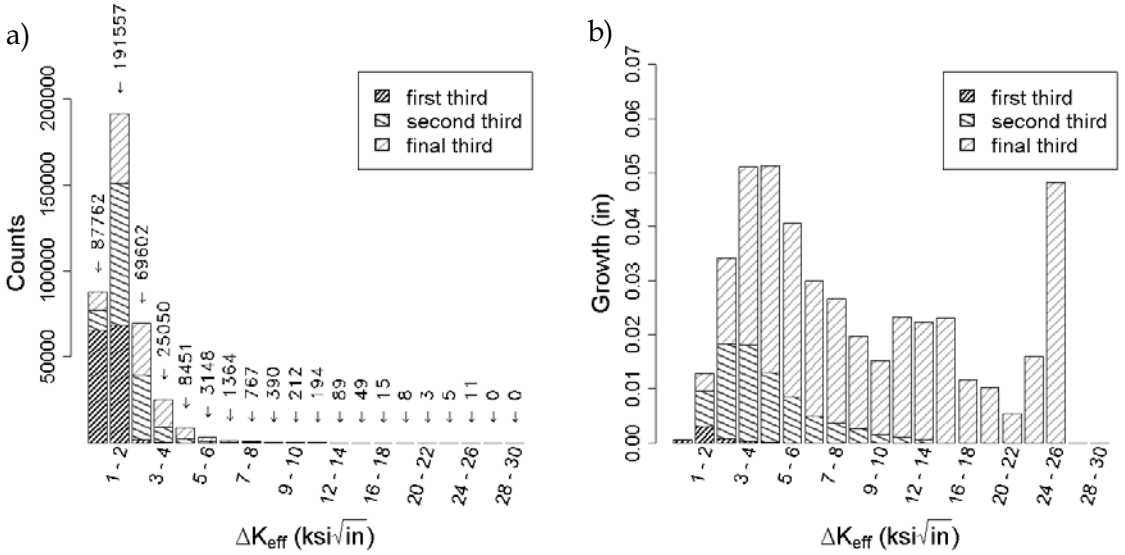

Figure 42: a) Growth and b) cycle counts attributed to different bands of ΔK_{eff} for crack growth under the P-3C spectrum

5.3.5 The probability of a cycle having a ΔK_{eff} value in the FASTRAN analysis

A probability density function that shows the probability of a certain ΔK_{eff} value being evaluated can be obtained with the present analysis. Probability density functions were developed for the three spectra considered. In Figure 43 a comparison of the probability density functions for the F-111, F/A-18 and P-3C crack growth analyses is presented.

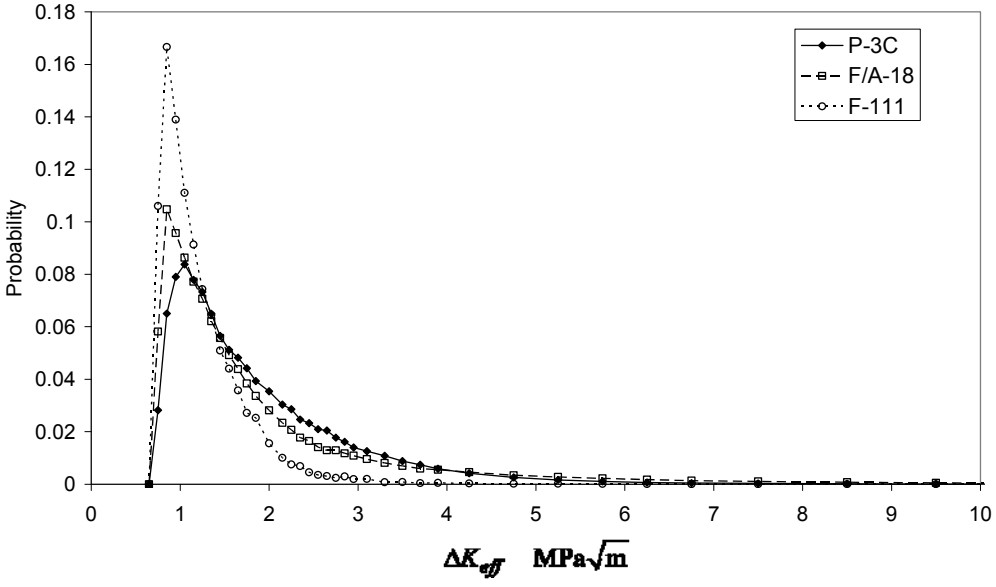

Figure 43: Probability density of ΔK_{eff} for crack growth under the F-111, F/A-18 and P-3C spectrums

Indeed the probability density functions predicted through FASTRAN in Figure 43 show considerable correlation. Not only are they closely correlated they show that most of the cycles will probably be evaluated with a ΔK_{eff} below $2\,\mathrm{ksi}\sqrt{\mathrm{in}}$.

5.3.6 Summary of Results

It should be noted that the analysis is conducted for the specific cases considered in this report. The modification to the FASTRAN code produces data that enables researchers to determine what part of the crack growth rate curve the code is accessing in order to produce its crack growth increments and thus its integrated crack growth verses time prediction. In the F-111 example it can been seen that prior to the application of the first cold proof 'overload', the region of the rate curve most accessed was below 2.0 $\mathrm{MPa}\sqrt{\mathrm{m}}$. The results following the overload show that the crack opening stress (and thus crack growth increments) calculated by the model were significantly impacted. As the crack opening stress increased, a considerable portion of the load cycles were not active in the crack growth prediction. With better estimates of the threshold stress intensity and a better understanding of the crack growth rate data in the threshold region it is feasible that predictions could be improved significantly.

It can be seen in the F/A-18 coupon example that for the majority of the crack growth prediction the key part of the rate curve was a ΔK_{eff} region close to a value of 2.0 $\mathrm{MPa}\sqrt{\mathrm{m}}$. This result was replicated in the F/A-18 bulkhead example, where the portion of the rate curve between 0.8 and 3.5 $\mathrm{MPa}\sqrt{\mathrm{m}}$ was used almost exclusively. It had previously been noted that the slope of this portion of the rate curve gave a Paris-like value of m=2.36, close to the value of m=2 which, when used in the simplest Paris type models, results in the log-linear crack growth curve shape seen in the actual experimental data for both the bulkhead and coupon examples.

The P-3 example shows that again, in the early life of the crack, the region below 2.0 $\mathrm{MPa}\sqrt{\mathrm{m}}$ was crucial, but that as the crack length grew above about 0.02" (0.5mm) different portions of the crack growth rate curve were being used (and were contributing significantly to the crack growth increment). This could explain why, away from the near threshold region into the traditionally better defined regions of the rate curve, predictions by models such as FASTRAN of crack growth above about 0.050" have in the past been able to show good correlation to experimental data. This has led to such traditional models being more successful in calculating inspection intervals and crack growth from rogue flaw sizes than predicting the life from a very small initial flaw size.

5.4 F-111 Calibration

Another case where other researchers had concluded that FASTRAN produced poor analysis results (or at least it was judged that the success of a calibration effort was uncertain within the timescale given for the work) was the F-111 program. Under this program a large number of coupons were tested in what was called the Loads Interpretation Truncation Validation (LITV) coupon testing program. The F-111 LITV coupon testing included 19 cases [43] covering a range of wing locations, scaling and truncation levels. Subsequent to this test program and subsequent to the issue of FASTRAN calibration in the F-111 EBA analysis raised in [4], a short investigation was conducted [44] to again study the robustness of calibrating FASTRAN using the F-111 data. That investigation concluded that, even when calibrated, the FASTRAN predictions were inconsistent (with experiment) and un-conservative.

An example taken from [44] was for the case of sequence FL3 which is for the FASS 226 location under the F-WELD spectrum with nominal truncation and nominal scaling. The crack growth rate data used in the original analysis was obtained from the Damage Tolerance Design Handbook [45]. The material is 2024-T851, and the rate data available were for R ratios of 0.1 and 0.5. To collapse the data to provide crack growth rate as a function of the effective stress intensity range, ΔK_{eff}, a constant constraint factor of α=1.5 was used.

This F-111 case was re-evaluated using an independent calibration of FASTRAN and the revised model was then applied firstly to this case and subsequently to the other 18 LITV cases. The first step required for a FASTRAN analysis is to collapse the data to provide rate as a function of the effective stress intensity range, ΔK_{eff}. Doing this requires consideration of the stress state (including specimen thickness) to select an appropriate constraint factor, α. The original analysis used a constant α of 1.5, and the result is plotted in Figure 44.

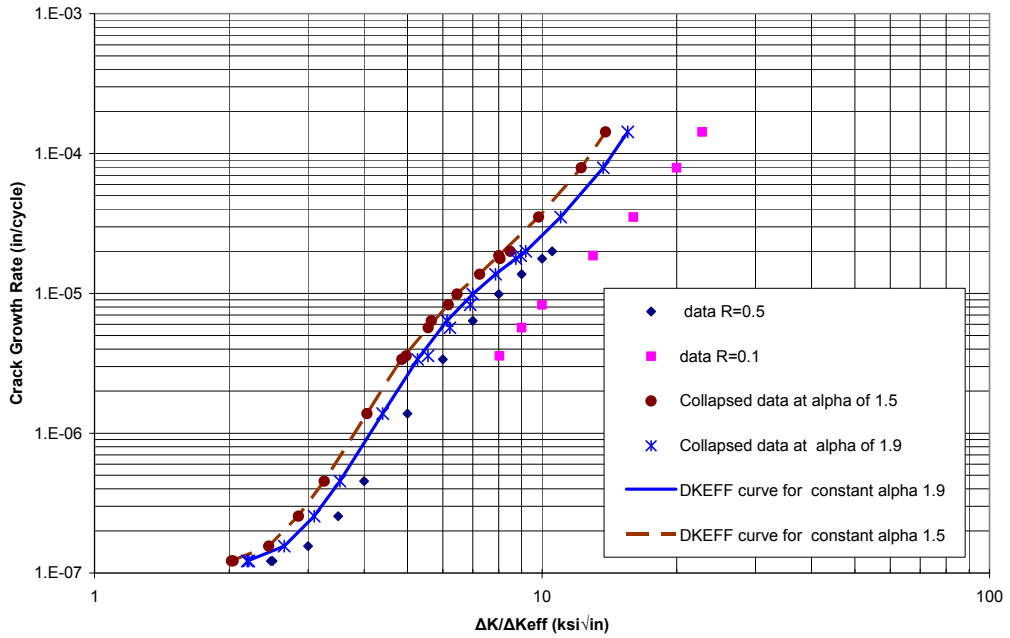

Figure 44 : Crack growth rate curve for 2024-T851 from [45] with derived ΔK_{eff} curves

The data collapsed reasonably well, i.e. the R-ratio shift which was evident in the 0.1 and 0.5 data was collapsed onto a single curve. However, the value of 1.5 for α is considered to be low considering the 8mm (0.31 inch) thickness of the LITV coupons. For a through-thickness crack the constraint factor is a function of the thickness and can be calculated precisely, but in many problems the value needs to be adjusted to account for the variation seen by an initially small crack as it progresses from partial to through-thickness. If the rate data has been obtained from specimen thicknesses different to the problem being examined then the correct value is even more uncertain. Using guidelines detailed in [46] it was determined that a value of α = 1.9 would be more applicable in the current case, and so the raw data were collapsed at that value. The result is also plotted in Figure 44. It is evident that the data also collapsed reasonably well at that value of constraint, so the analysis was then performed under those conditions.

The revised analysis for the FL3 case was then conducted using the revised rate curve and constraint value, a nominal initial crack size of 0.01 mm and the result is plotted in Figure 45. It is evident that the revised analysis compared much more favourably against the test data, particularly once the crack size exceeded 0.1 mm.

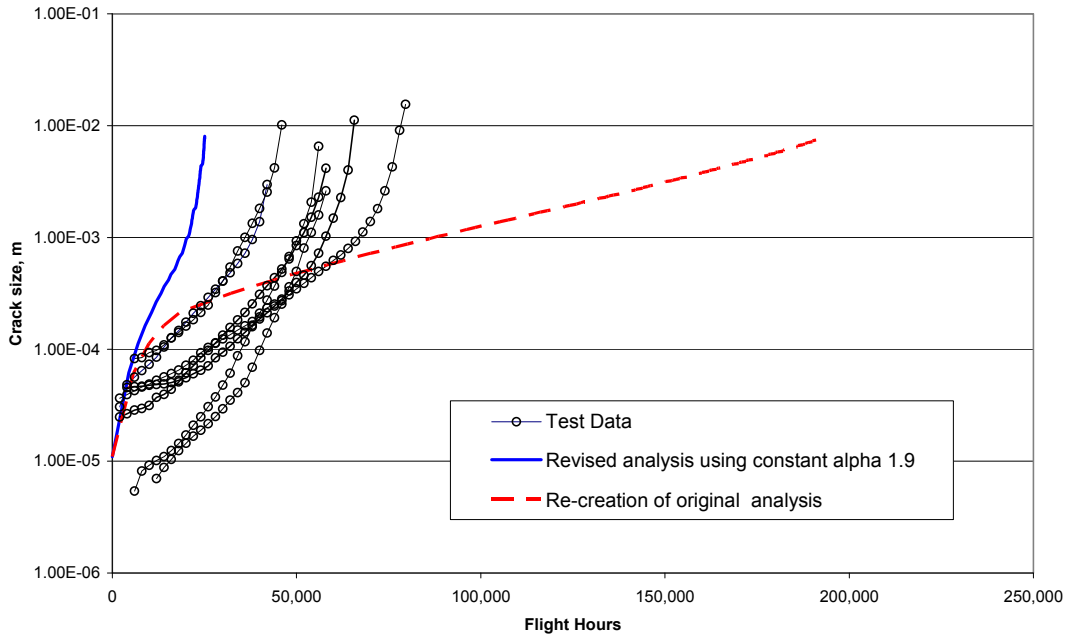

Figure 45: Crack growth comparison showing test data for FL3 from the F-111 LITV coupon test program compared with original and updated FASTRAN analyses

The next step was to apply this revised FASTRAN model to the other 18 cases from [43]. As the coupon geometry and material was fixed it was important to retain the same inputs to the model, with the only variation being the applied loading spectrum. It is reasonable to think that alpha may vary with different spectra and this may affect the performance of the model over a range of similar spectra. The complete results are detailed in Appendix B and show good to very good correlation for the majority of spectra. A minority of predictions were not good and further work would thus be needed to determine why. The results are not claimed to be a comprehensive validation of the code or a demonstration of the limits of its validity. However the examples do show that, within the scope of the F-111 location and spectra problem, near threshold crack growth rate data and stress-state constraint effects are again important.

The shape of the fractographically measured crack growth curves for the various LITV spectra varied from log-linear to a more general Paris-type power function, with at least one spectra, FL12 (Wing Splice F-WELD with CPLT) resulting in significantly delayed crack growth. The initial FASTRAN prediction was excessively conservative, however it was found that when a (crack growth rate) threshold adjustment was made to the particular parameter in the modelling equation, C3, the FASTRAN prediction could match the experimental results, see Figure 46. This suggests that if the threshold data issue was improved, FASTRAN could make better predictions of total crack growth life. Note however that the prediction with the modified threshold value is a 'post-diction' analysis. The challenge will be to replicate such a match to experiment in a 'blind' situation.

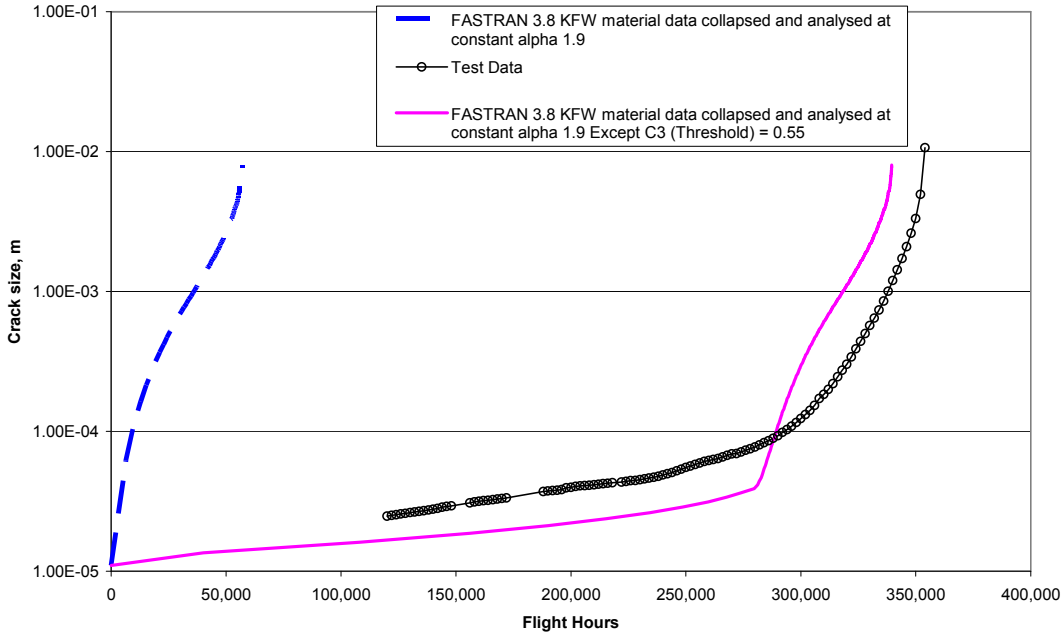

Figure 46: Crack growth comparison for FL12 with adjustments for threshold

From the above examples we can see that is it possible, with appropriate input data and calibration to match experimental results using a traditional model, in this case FASTRAN. For FASTRAN the choice of constraint factor requires particular attention. The F-111 LITV cases demonstrate that good results can be achieved even with a fairly simple constant alpha approach and with little consideration to the threshold region. With the use of variable constraint factors, as was done for the P-3 program, FASTRAN could be expected to produce improved results

At least one F-111 spectra showed clear delay in the development of established crack growth. This behaviour could be modelled by adjustments in the FASTRAN model for threshold effects. It could be expected that careful analysis of the threshold region and the initial crack size and shape could result in consistently improved predictions of total life from a physical initial flaw.

5.5 Calibration of Traditional Models within the EBA Methodology

The calibration of crack growth models has been shown to be important for obtaining satisfactory estimates of crack growth in traditional approaches. Given that the same traditional models are sometimes used in the EBA methodology to give predictions of relative severity between spectra, it is of interest to see whether calibration is similarly important.

The FASTRAN/CGAP modelling as part of the original F-111 wing lifing work in [22] was not conducted with material and other input parameters that were specifically tuned to the F-111 spectra. Instead, the F-111 program proceeded on the judgement that validation via fatigue test

results would underpin the final lifing advice. Material data was extracted from the literature and a fixed constraint value was used. Similarly, no specific calibration of FASTRAN was performed in an EBA review document [2] which used slightly different material and constraint data but produced F-111 crack growth predictions similar to those from [22]. It was noted that in some cases the FASTRAN predictions used in the process to derive relative spectra severities were very different to the actual experimental results. Examples are shown in Figure 47 and Figure 48.

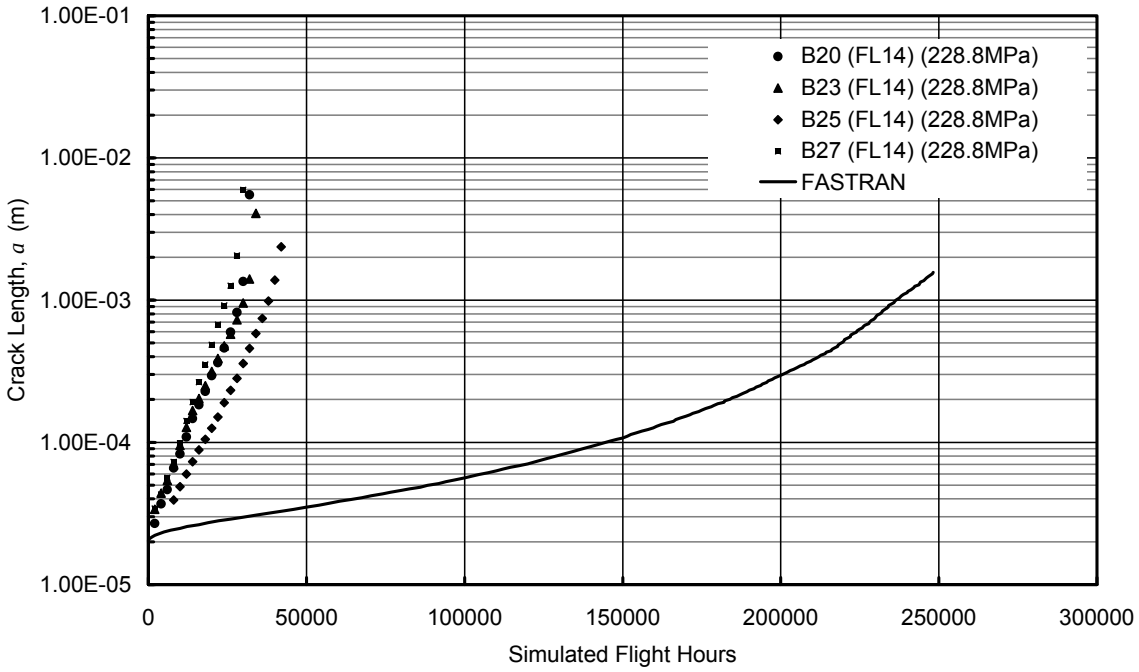

Figure 47: FASTRAN crack growth prediction under F-WELD at CSS 135 (FL14) and compared to experimental QF data obtained under F-WELD at CSS 135 (FL14) [2]

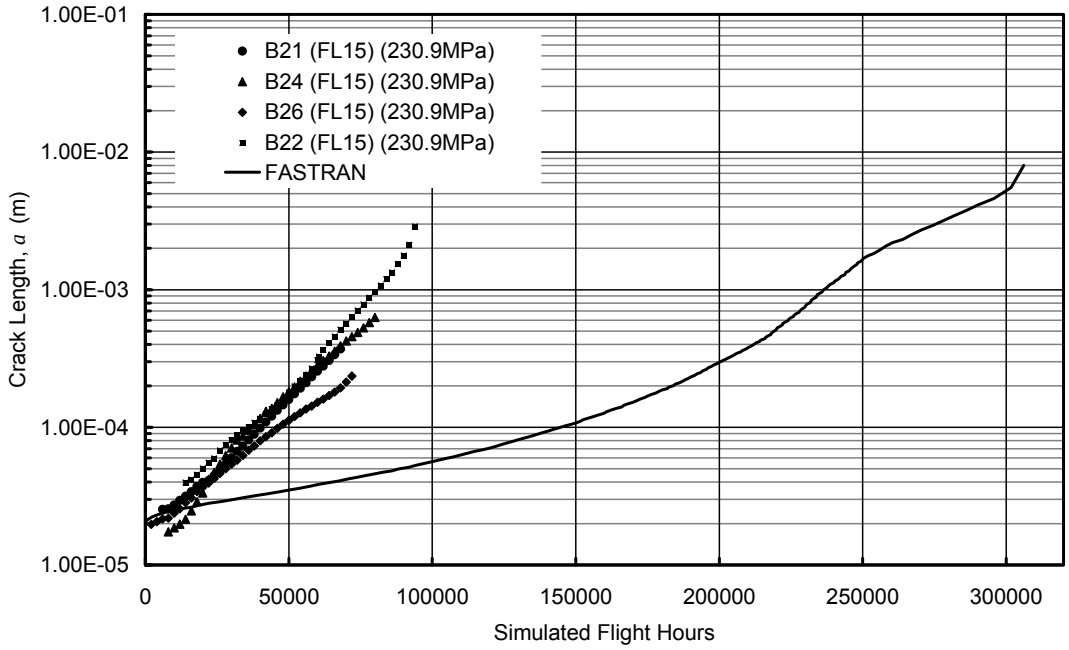

Figure 48: FASTRAN crack growth prediction under D20 at CSS 135 (FL15) and compared to experimental QF data obtained under D20 at CSS 135(FL15). [2].

Very similar results are obtained by the F-111 group in [22], see for example Figures 13 and 15 of that report. The difference between the experimental data and the uncalibrated FASTRAN predictions shown in Figure 47 and Figure 48 are summarised in Table 7.

Table 7: Summary of coupon results and FASTRAN life predictions (predictions of total life to a crack size of 2mm) for two spectra from [2]

F-111 Critical location	Spectra	LITV Coupon designation	Average. Coupon life (hours)	FASTRAN predictions (to 2mm) [2]
CSS 135	D20	FL15	~98000	~250,000
	F-WELD	FL14	~33000	~250,000
Ratios			3:1	1:1

Given the significant difference in life ratios between test and model we might anticipate that the EBA process will predict long for FL14 and short for FL15. When the process was undertaken this was exactly what happened, see Figure 47 and Figure 48, with the results summarised in Table 8.

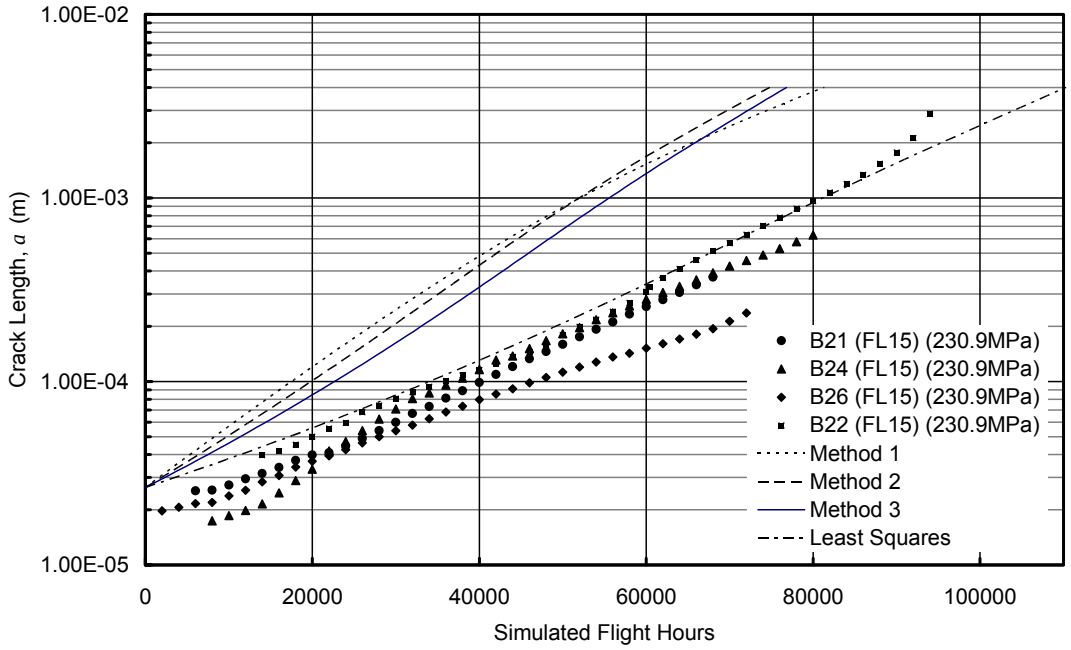

Figure 49: Four FASTRAN based EBA crack growth predictions created with Fl14 QF data to predict crack growth under FL15 and compared to experimental QF data obtained under D20 at CSS 135 (FL15) [2]

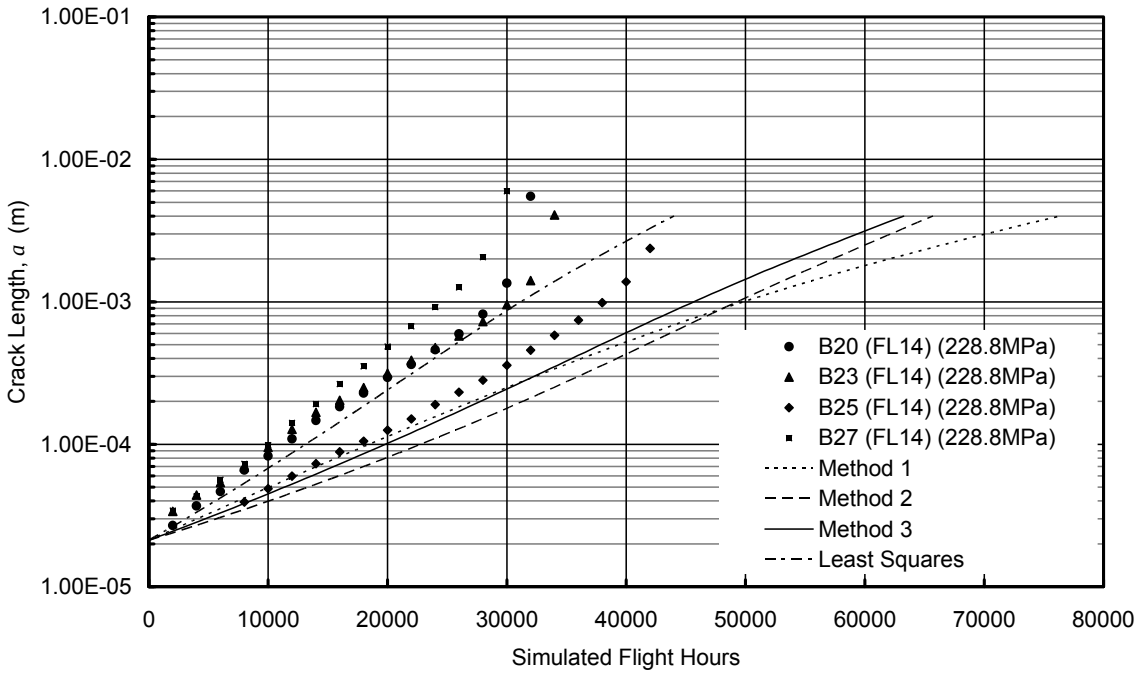

Figure 50: Four FASTRAN based EBA crack growth predictions created with FL15 QF data to predict crack growth under FL14 and compared to QF data obtained under FL14 [2]

Table 8: Summary of EBA based F-111 spectra to spectra predictions (predictions of total life to a crack size of 2mm) derived from [2]

F-111 Critical location	Spectra	LITV Coupon designation	Average. Coupon life (hours)	FASTRAN based EBA predictions	% diff to exp
CSS 135	D20	FL15	~98000	~65,000 (Figure 49)	-34%
	F-WELD	FL14	~33000	~54,000 (Figure 50)	+64%

The conclusion that can be drawn is that confidence in the EBA based relative spectra approach (as used for the F-111) to produce satisfactory results reduces as the discrepancy between the FASTRAN prediction and experiment increases in terms of either absolute life predictions or relative spectra severity. To further test this observation the EBA process applied to the F-111 could be repeated with a calibrated FASTRAN model to assess any improvements in the EBA predictions as also suggested in [22]. Equally, however, we cannot say that close agreement between experiment and prediction from the traditional tools needed in the EBA process to provide the relative spectra severity values is sufficient in itself to ensure a successful EBA based analysis. Other steps in the EBA curve fitting and analysis process (i.e. stress scaling, geometry and notch effects, EIFS determination etc) also need to work satisfactorily.

6. Discussion

6.1 Observations of Crack Growth Behaviour

The experimental crack growth data in Section 4 show a mixture of behaviours, from log-linear commencing at time zero to non-exponential behaviour. In terms of the source of the fatigue cracks, they were one of several known nucleation features discussed in Section 1.1, i.*e.*, surface (or very near surface) discontinuities as a result of etching or surface exposed hard phase precipitates. Both Al 7050 and Al 7075 alloys are observed to have hard precipitates of sizes up to 10 to 100 microns depending on product form. For material in which the surface has been treated by an etching procedure, etch pits from the DSTO process were determined to be of a similar size, consistent with the estimations of size of the initiating features seen in the coupon data presented in Section 4. A number of observations have been made, the most significant of these are:

a. Different CG rates observed for etched versus machined coupons. Fatigue in high strength aluminium alloys under aircraft spectra appears to be a surface initiating problem. As the different surface finishing techniques are traditionally thought to influence crack nucleation and initiation only, the observable difference in crack growth rate for the entire life of the F/A-18 coupons under the lower stress levels and also for the P-3 spectra coupons is of significance. The influence of multiple initiation sites for the etched coupons and the retention of etching fluid are possible reasons for this difference. For the thin coupons, where crack growth proceeds as a through thickness crack, the etch pits on the sides of the coupon may well be counteracting the normal retarding influence of the plane stress condition seen at these surfaces. The significance of these effects needs to be verified further as the etched and as-machined coupons have in some but not all cases different crack growth rates. Any adverse or unrepresentative effect on crack growth predictions would need to be checked during analysis on F-111, F/A-18, or any other aircraft where the aircraft surface is not etched but etched coupon results are being used in predictions.

b. Some coupon results show log-linear (exponential) growth from time zero, see Figure 7 and Figure 11. Others show a period of nucleation or delayed micro-growth that preceded the established growth, see Figure 8, Figure 12 and Figure 46. Other results show non-similar crack growth shapes for related spectra but with the same coupon geometry, whilst still others show variations attributable to the effect of changing stress state. For some spectra, fractography was successful back to very soon after the application of the initial load. For others, particularly the results with delayed growth, fractography was not able to identify the early history. As a result, it makes comprehensively answering the question, 'what is really going on at the bottom?' very difficult and thus modelling the very smallest of cracks a challenge.

6.1.1 Delayed Established Crack Growth

What has been observed from the crack growth results discussed in Section 4 is that, for some sequences and stress levels, crack growth beyond the initiating defect commences very rapidly. In other cases, the crack takes a considerable proportion of the eventual total crack growth life to

reach established crack growth. The different behaviour is idealised in Figure 17 and Table 1. For the high stress F/A-18 spectra, the very rapid transition to Stage 2 (a crack of size a_i) means that the prediction of total crack growth life lends itself to a crack growth analysis problem from an initial physical defect of size a_i. As shown in earlier sections, both experimentally-based and traditional fracture mechanics based methods could be suitable. For all other spectra the situation is sometimes not as simple, as flaw orientation and size, combined with complicating factors not yet fully understood such as load interaction and growth mechanisms at very small crack sizes, produces variability in the crack growth up to 0.1 mm. In some cases, there is a delay in the establishment of clearly observable crack growth. The current state of the art for traditional fracture mechanics based approaches does not yet provide reliable results for crack growth for these situations. Improvement is possible, but will only be successful if careful attention is paid to the threshold region by way of improved underlying data or improved modelling of the small crack region. In [1] Hu *et al* discussed the issues involved in modelling short crack behaviour and what further work was needed. In [47] several approaches to adjusting current models for the short crack regime were examined; however, the state of the art was described as unsatisfactory. The more recent results shown in Section 5 give promise that with improvements in threshold data and other aspects, the total life prediction capability of traditional models could be improved. This is discussed further in Section 6.3.

For experimentally based approaches such as EBA, more complexity by way of multiple or variable spectrum specific parameters would need to be introduced to model the delayed initiation period, counter-acting the current attractiveness of having only two unchanging, but spectrum specific, Paris-like constants for the whole crack growth life. Current approaches, which rely on strain or stress-life methods to predict the crack initiation phase, also remain valid options for the prediction of durability only.

The use of a physical value of a_i when using traditional models replicates the El Haddad adjustment for the modelling of small cracks described in page 54 of [1]. This involves replacing the minute fatigue crack at the boundary of the initiating feature (refer to Figure 17) with progression of a crack of size a_i. Whilst this matters little for the high stress situations where the transition from a crack like defect of size a_i to a naturally shaped crack of size a_i is very quick, it becomes further from reality as the micro-cracking period becomes longer. In this case, the artificial adjustment of stress intensity is compensating for unknowns in the local stress intensity and short crack growth behaviour.

6.2 Calibration of Traditional Crack Growth Models

The calibration of crack growth models prior to their application on specific problems is universally accepted good practice, but not always conducted. At the very least, the use of uncalibrated models due to data availability or work schedule constraints needs to be supported by subsequent experimental based validation. All our current crack growth models, be they based on adjusted summations of individual cycles or spectrum specific curve fits, are largely empirical. As such they do not accurately represent all the complex underlying mechanisms of crack growth and can only be used with confidence within the confines of the area for which they have been tested. Calibration (or at least validation) is unavoidable for the reasons given at the start of Section 5. The most important issue is thus transferability, with models performing

reliably and well over a larger range of problems being preferred. Quoting from one of the more well known texts on the subject of fracture mechanics [48] p146;

> 'If all models are simplifications, none can be preferred over another….they can all be made to work if the parameters are adjusted appropriately. All claims that one model is better than another are improper. Each model can be made to work if empirically adjusted; if it does not work it was not adjusted properly. Generality of the adjustment may be a problem. In that respect some models may be somewhat better than others. Clearly the adjustment parameters will be material dependent. *But, should they also depend strongly upon the stress history, as they do, then they cannot be used generally*. Attempt to make general use of these parameters then lead to false claims with regard to a model's adequacy'

One of the reasons quoted by those advocating the use of direct (VA) experiment-based approaches such as EBA for fatigue life prediction is that the traditional models were insufficiently accurate [21] or the EBA provided significant advantages [22] due to their direct use of experimental data from the variable amplitude sequence of interest. In Section 5.2.1.1 an experimentally based spectrum specific calibration was trialled using the FASTRAN model and F/A-18 low K_t coupon data. The results showed that FASTRAN could in fact provide good predictions of crack shape and duration over several related F/A-18 spectra, although the study was not complete enough to show such a technique was accurate enough for a full range of F/A-18 problems. The same issue for the F-111 is explored in Section 5.4 where an initial assessment of poor results is replaced by a re-assessment that shows, even with the use of a single constraint factor, FASTRAN results can be much improved over a range of F-111 spectra and that further improvements could be expected with more sophisticated calibration. This clearly shows the importance of the need to calibrate traditional models such as AFGROW and CGAP/FASTRAN models. The key in the current analysis, however, was the careful evaluation of the required constraint factors. This requirement does inject a degree of difficulty and uncertainty when calibrating and using the models, and this could lead to other disadvantages such as schedule or resource implications.

The separate consideration of absolute (total life) and relative (severity) prediction abilities of traditional tools suggests that only the second ability is needed when conducting an EBA based prediction of an untested spectra. The F-111 data considered in Section 5.5 shows however that this too can lead to errors. The problem then becomes one of building sufficient confidence through experimental validation that un-calibrated traditional models do reliably and accurately estimate relative spectrum effects. The use of traditional crack growth models to predict relative lives (severities) based on calculations of growth in the small crack regime in particular, when these same models are known to be deficient in this area, means that such an approach is risky in these cases.

In another separate example based on P-3 spectra assessed in [49], the EBA/FASTRAN relative spectra severity method was also not able to correctly predict the relative coupon lives under two spectra because the slopes of the two established crack growth curves were not proportional to the total coupon lives.

The conclusion is therefore, that since un-calibrated conventional models cannot generally be relied upon to give correct answers to new problems, calibration (and validation) becomes a necessity for the production of reliable results whether it is for EBA based purposes or for traditional analyses.

6.3 The Importance of Near-Threshold Crack Growth Rate Data

In Section 5.2.2, a FASTRAN analysis on an F/A-18 bulkhead location was re-evaluated and the original poor correlation with experiment was shown to be the result of using inaccurate underlying rate data in the near-threshold region obtained by extrapolation. The issue of accurate underlying crack growth rate data was further explored in Section 5.3. A modification was made to FASTRAN to collect the ΔK_{eff} value for each cycle pair used within the program to calculate increments of crack growth. The additional output could thus reveal which part of the constant amplitude derived crack growth rate versus ΔK_{eff} curve was being used within the model. The results show that different parts of the rate curve were being accessed by the model for different spectra, but for all spectra the near threshold portion of the rate curve was important. Note however that this assessment of ΔK_{eff} and resulting crack growth increment per cycle is what is being calculated by FASTRAN which may or may not equate to what happens physically. However the closeness between experiment and analysis demonstrates some reasonableness, at least at the engineering level, between a crack growth model based on $\frac{da}{dn} = f(\Delta K)$ and reality.

The F/A-18 centre bulkhead example showed that FASTRAN was almost exclusively using the crack growth rate data between ΔK_{eff} values of 1 and 3 MPa$\sqrt{m}$ as originally surmised in Section 5.2.2. The slope of the crack growth rate curve in this region was calculated as (m=) 2.36, close to the value of m=2 for log-linear crack growth, again showing consistency between experimental crack growth results and constant amplitude data used by FASTRAN. There is thus no inconsistency between the often observed exponential crack growth behaviour seen in many aircraft problems and constant amplitude crack growth rate data as it indicates that these problems are dominated by the near threshold ΔK_{eff} region.

The examples in this report show that the performance of traditional tools for crack growth prediction can be improved with the use of more accurate constant amplitude rate data. Given that the near-threshold region of the curve below 3.5 MPa$\sqrt{m}$ is the key for both F/A-18 type examples for the majority of their entire crack growth lives, and for the P-3 example in the early part of the predicted fatigue life, accurate data in this region would seem to be crucial for improved crack growth predictions generally. Then there is the issue of the threshold itself and the effect of large numbers of small cycles at or near this point. Given the sensitivity of the P-3 results to changes in a_i, and the effect of threshold adjustment to the F-111 FL12 results, defining the point at which the crack driving force does not exceed the crack growth resistance of the material would seem to be crucial. Work to improve the definition of constant amplitude rate curves in this region is currently being undertaken by DSTO and this work should be continued.

7. Conclusions

Using data from recent DSTO experimental programs on the F/A-18, F-111 and P-3 this report has made observations of crack growth behaviour and undertaken re-analysis of selected examples using a traditional model. The findings have been discussed and the key conclusions drawn from this exploration are as follows:

1. From the cases demonstrated in this report, properly calibrated traditional CG models can currently predict the total crack growth curve for F/A-18 and (most) F-111 spectra in aluminium alloys. The very quick transition from an initial material feature to a crack of equivalent size, under combat aircraft type load spectra and stress levels, means that little accuracy is lost by making use of the 'El Haddad' equivalent approach of using the size of the surface breaking initial material flaw as a value for a_i.

2. For maritime and transport aircraft spectra (and at least one F-111 spectra, FL12) the problem of predicting the total crack growth life is more difficult. The period of delay in developing an established crack has so far limited the successful use of traditional models to the prediction of crack growth above damage tolerance flaw sizes, although examples in this report suggest improvements can be made. Equally, the inability to model the 'initiation' period and the established growth period with a single set of Paris or Paris-like rate parameters means that both simple traditional models and simple direct experimentally based methods such as EBA will not be successful. Further advances in fractography or other techniques such as atomic simulation that can measure or describe the growth of the smallest of cracks may reveal behaviour that can then be modelled to improve predictions in this region.

3. Understanding which parts of the crack growth rate curve are important for crack growth predictions made using conventional models can help to focus attention on improving the accuracy of the regions of the input crack growth rate curve that will give the most benefit to the life prediction problem at hand.

4. The improvement of rate data in the near-threshold region is important for different spectra types. For high stress F/A-18 type spectra, the near-threshold data is crucial for most of the crack growth period and using improved data along with an a_i value consistent with the size of the initial flaw results in good predictions of total life and crack growth shape. For transport type spectra, the near-threshold crack growth rate data is also important for early crack growth and thus predictions of total life. Traditional predictions above damage tolerance flaw sizes, necessary for determining inspection intervals, use the currently better founded regions of the crack growth rate curve and remain satisfactory.

5. Traditional crack growth models require calibration before they are able to be used with confidence. This report provides examples of how improvements can be made. This report (and earlier reports) also show that, despite their use within the EBA based process being restricted to providing estimates of relative severity between spectra, differences between predictions from the traditional model and experiment can lead to inaccurate overall EBA predictions. Accuracy of predictions of relative severity by traditional models is not in itself

sufficient, however, for ensuring the overall accuracy of experimentally based prediction methods such as EBA.

6. It appears from examples in this report that improved threshold and near threshold constant amplitude data can resolve the discrepancies seen between (particularly) log-linear experimental data and past predictions from conventional models. As a consequence, log-linear (exponential) crack growth behaviour can be considered a special case (albeit a very common special case) of the general crack growth behaviour in Al alloys under aircraft type spectra that is described, in its first order, by the material crack growth rate versus ΔK behaviour.

7. Oversimplification of the underlying crack growth rate data such as the traditional Paris (single m value) equation and its modifications such as Forman has the potential to introduce large errors into fatigue life prediction. More sophisticated representations should be used in more complicated work such as comparing different models or for predictions against experiment such as in coupon or full scale fatigue test interpretation programs lest incorrect conclusions are drawn. Its use in initial analytical fatigue design, along with appropriate analysis based uncertainty factors may well be acceptable. However, if the work schedule and resources permit, it still remains important to develop a good physics based model for fatigue design.

7.1 Future Work

This work builds upon previous investigations within the DSTO Methods and Standards Group that have attempted to understand and examine alternative crack growth models including the DSTO EBA method [50, 51]. It is part of a general and ongoing effort within the Task to examine and identify the most appropriate CG tools (along with their limitations and boundaries of applicability) for different problems. It links with the 'problem space/method space' initiative first raised by DGTA, and more current demands for support from the DSTO platform tasks under titles such as 'define the limits of applicability of LEFM fatigue crack growth analyses for highly stressed combat airframes' and 'provide expert advice on various fatigue analysis methods for C130'. Remaining unaddressed issues include the effect of notches and notch plasticity. For the Methods and Standards Group, work needs to be done on a number of fronts including:

a. Expand the behavioural analysis and continue the efforts to define and refine boundaries of applicability for different fatigue and crack growth methods and models.

b. Continue to improve the predictive ability of traditional crack growth models in the small/short/micro crack regime.

c. Reflect the current evaluations on fatigue life and crack growth modelling in advice on fatigue life methodologies and airworthiness standards that are most appropriate for different aircraft types.

d. Develop a better understanding of the effect of notch plasticity, both through theory and experiment, and improve traditional modelling capability to deal with notch plasticity and constraint effects.

The issue of accurate rate data at or near the threshold level is the key to improving the prediction of spectra results in the small crack region and the current work in DSTO should be supported. This includes the development of marker banding techniques that can assist with fractographic analysis at very small crack sizes and for spectra with low stresses.

8. Acknowledgements

This report has drawn a considerable amount of data from the DSTO F/A-18, F-111 and P-3 programs, the ready availability of which is a major resource for DSTO and the authors thank those programs. Thanks also go to Marcus McDonald for his careful review of the report.

9. References

1. Hu W., T.Y.C., Walker K. F., Mongru D., Amaratunga R., and Jackson P., *A Review and Assessment of Current Airframe Lifing Methodologies and Tools in AVD, DSTO-RR-0321*. December 2006.
2. Wallbrink, C., Amaratunga. R., Hu, W., et al., *An Evaluation of the Effective Block Approach Using P-3 and F-111 Crack Growth Data, DSTO-TR-2195*. September 2008.
3. P. Jackson, D.M., C Wallbrink, K Walker, W Hu, *Exploration of Questions regarding Crack Growth behaviour under Practical Combinations of Aircraft Spectra, Stress levels and Notch Types, DSTO-DP-XXXX*. 2009.
4. Jackson, P., Mongru, D., Wallbrink, C., Walker, K., Hu, W., *Exploration of Questions regarding Crack Growth behaviour under Practical Combinations of Aircraft Spectra, Stress levels and Notch Types, DSTO-DP-XXXX*. 2009.
5. Molent L, *The Lead Crack Fatigue Lifing Framework, DSTO-RR-0353*. April 2010.
6. Schijve, J., *Fatigue of structures and materials in the 20th century and the state of the art.* International Journal of Fatigue, 2003. **25**: p. 679-702.
7. McDonald, M., Molent, L., and Green, A.J., *Assessment of Fatigue Crack Growth Prediction Models for F/A-18 Representative Spectra and Material*, DSTO, Editor. 2006.
8. Navarro, A. and E.R.d.l. Rios, *Short and long fatigue crack growth: A unified model.* Philosophical Magazine A, 1988. **57**(1): p. 15 - 36.
9. Ritchie, R.O., *Near-threshold fatigue-crack propagation in steels.* International Metallurgical Review, 1979. **20**: p. 205-230.
10. Walker, K., *The effect of Stress Ratio During Crack Propagation and Fatigue for 2024-T3 and 7075-T6 Aluminum.* Effects of Environment and Complex Load History of Fatigue Life, 1970. **Spec. Tech. Publ. 462, ASTM**: p. 1-14.
11. Forman, R.G., V.E. Kearney, and R.M. Engle, *Numerical analysis of crack propagation in cyclic-loaded structures.* Trans. ASME, Journal of Basic Engineering, 1967. **89, Series D**: p. 459-464.
12. Newman, J.C., Wu, X.R., Venneri, S.L., and Li, C.G., *Small-Crack Effects in High-Strength Aluminium Alloys*, NASA, Editor. 1994, NASA.
13. Yoder, G.R., *On Microstructural Control of Near Threshold Fatigue Crack Growth in 7000 Series AluminumAlloys NRL-MR-4787, US Navy.* Apr 1982.
14. Wanhill, R.J., *Low Stress Intensity Fatigue Crack Growth in 2024-T3 and T351.* Eng. Fract. Mech., 1988. **30**(2): p. 233-260.
15. Wanhill, R.N., J., *Low Stress Intensity Fatigue Small-Crack Growth in 2024-T3 and T351.* Eng. Fract. Mech., 19881994. **30**(2): p. 233-260.
16. R. O. Ritchie, S.S., *Small Fatigue Cracks: A Statement of the Problem and Potential Solutions, Materials Science and Engineering 1986, 84, 11.*
17. Ritchie, R.O., Suresh, S., *Small Fatigue Cracks: A Statement of the Problem and Potential Solutions, Materials Science and Engineering 1986, 84, 11.*
18. Grandt, A.F., *Fundamentals of structural integrity, damage tolerant design and nondestructive evaluation*. 2004: John Wiley and Sons USA.
19. Gallagher, J.P., *Estimating Fatigue Crack lives for Aircraft: techniques.* Experimental mechanics, 1976. **16**(11): p. 425-433.
20. Gallagher, J.P., Stalnaker, H. D., *Developing Normalizes Crack Growth Curves for Tracking Damage in Aircraft*, in *Journal of Aircraft*. 1978. p. 114-120.

21. McDonald, M., Molent, L., and Green, A.J., *Assessment of Fatigue Crack Growth Prediction Models for F/A-18 Representative Spectra and Material, DSTO-RR-0312*. April 2006.
22. Zhuang, W., Boykett, R., Phillips, M., and Molent, L., *Effective Block Approach for Damage Tolerance Analyses of F-111 D/F Model Wing Structures, DSTO-TR-2124*. May 2008.
23. Huynh, J., Molent, L., and Barter, S., *Fatigue Crack Growth Predictions for 7050 Aluminium Alloy with Different Stress Concentration Factors, DSTO-RR-0330*. July 2007.
24. Barter, S., *Fatigue Crack Growth in 7050-T7451 Aluminium Alloy Thick Section Plate with a Surface Condition Simulating Some Regions of the F/A-18 Structure, DSTO-TR-1458*. July 2003.
25. Barter, S., and Huynh, J, *Fatigue Crack Growth in 7050-T7451 Aluminium Alloy Open Hole Coupons, DSTO-TN-0677*. 2006.
26. Huynh, J., and Barter, S., *Fatigue Crack Growth in 7050-T7451 Aluminium Alloy Notched Coupons, DSTO-TR-1966*. March 2007.
27. Diab, H., and Goldsmith, R., *Fractography Results of F-111 Loads Interpretation and Truncation Validation (LITV) Coupon Test Program, DSTO-TR-2000*. June 2007.
28. Veul, R.P.G., and Ubels, L.C., *Results of the FMS Spectra Coupon Test Prorgam Performed within the Framework of the P-3C Service Life Assessment Program, NLR-CR-2003-488*. December 2003.
29. Lockheed-Martin, *P-3C FSFT Fatigue and Damage Tolerance Analysis CDRL A009, N00019-99-C-1386*. October 2002.
30. Teunisse, B., Phillips, M., Jackson, P., Matricciani, E., Hu, W., Amaratunga, R., Hartley, D., Mongru, D., *Computer programs and Methodology used for DSTO P-3C SLAP Test Interpretation, DSTO-TR-1834*. March 2006.
31. Pell R.A., M.l., and Green A. J., *The Fractographical Comparison of F/A-18 Aluminium Alloy 7050-T7451 Bulkhead Representative Coupons Tested Under Two Fatigue Load Spectra at Several Stress Levels, DSTO-TR-1547*. Feb 2004.
32. McDonald, M., Molent, L., *Fatigue Assessment of the F/A-18 Horizontal Stabilator Spindle, DSTO-TR-1620. September 2004.*
33. Jones, R., L. Molent, and S. Pitt, *Crack growth of physically small cracks.* International Journal of Fatigue, 2007.
34. Jones, R., Molent, L., Pitt, S., and Soires, E. *Recent developments in fatigue crack growth modelling*. in *European Conference on Fracture*. 2006.
35. Jones, R., Pitt, S., and Peng, D., *The generalised Frost-Dugdale approach to modelling fatigue crack growth.* Engineering Failure Analysis, 2008.
36. Jones, R., L. Molent, and S. Pitt. *Crack growth of physically small cracks*. in *Proceedings of International Conference on Fatigue Damage of Structural Materials VI*. 2006. Hyannis, USA.
37. Molent, L., Dixon, B., and Barter, S. *The FINAL program of enhanced teardown for agile aircraft structure*. in *8th NASA/FAA/DOD Conference on Aging Aircraft*. 2005. Palm Springs CA USA.
38. Sharp, P.K., R. Byrnes, and G. Clark, *Examination of 7050 Fatigue Crack Growth Data and its Effect on Life Prediction*. 1998, Aeronautical and Maritime Research Laboratory DSTO. p. 48.
39. Hsu, C., Chan, K. K., and Yu, J., *Effects of thickness on plasticity-induced fatigue crack closure: analysis and experiment.* ASTM STP 1343, 1999.
40. Newman, J.C., Yamada, Y., and Newman, J.A., , *Crack-closure behaviour of 7050 Aluminium Alloy near threshold conditions for wide range in load ratios and constant Kmax tests", presented*

at ASTM/ESIS Fatigue and Fracture Mechanics Symposium, Vancouver, Canada, May 2009. 2009.

41. Mongru, D., *Direct Current Potential Drop System Calibration of 1015-T6 Notched and Centre Crack Growth Coupons*. 2009, DSTO: Melbourne.
42. Barter, S.A., *Fatigue Crack Growth in 7050T7451 Aluminium Alloy Thick Section Plate with Surface Condition Simulating Some Regions of the F/A-18 Structure*. 2003.
43. Diab, H., and Goldsmith, R., *Fractography results of F-111 loads interpretation and truncation validation (LITV) coupon test program*. 2007, DSTO.
44. Zhuang, W., *Investigation of the robustness of the FASTRAN calibration*. 2009.
45. Anon, *Damage Tolernat Design Handbook*. 1983.
46. Newman, J.C., *A crack-closure model for predicting fatigue crack growth under aircraft spectrum loading. In: Chang, J. B. and Hudson, C. M. (eds.) Methods and Models for Predicting Fatigue Crack Growth under Random Loading, ASTM STP 748. ASTM 53-84*. 1981.
47. Walker., K.F., *Evaluation of the C* Model for Addressing Short Fatigue Crack Growth. DSTO-TR-2185*. October 2008.
48. Broek, D., *The practical use of fracture mechanics*. 1988: Kluwer Academic Publishers.
49. Mongru, D., et al., *Evaluation of Alternative Life Assessment Approaches Using P-3 SLAP Test Results, DSTO-TR-2418*. 2010.
50. Wallbrink, C., et al., *An evaluation of the effective block approach using P-3 and F-111 crack growth data*. 2007, DSTO. p. 84.
51. Hu, W., et al., *A Review and Assessment of Current Airframe Lifing Methodologies and Tools in AVD*. 2006, DSTO.

Appendix A: Coupon Test Programs and Coupon Types

A number of different programs were sourced to provide the crack growth data upon which the observations were made.

A.1. Coupon Types

The following provides diagrams of each coupon type described in this report.

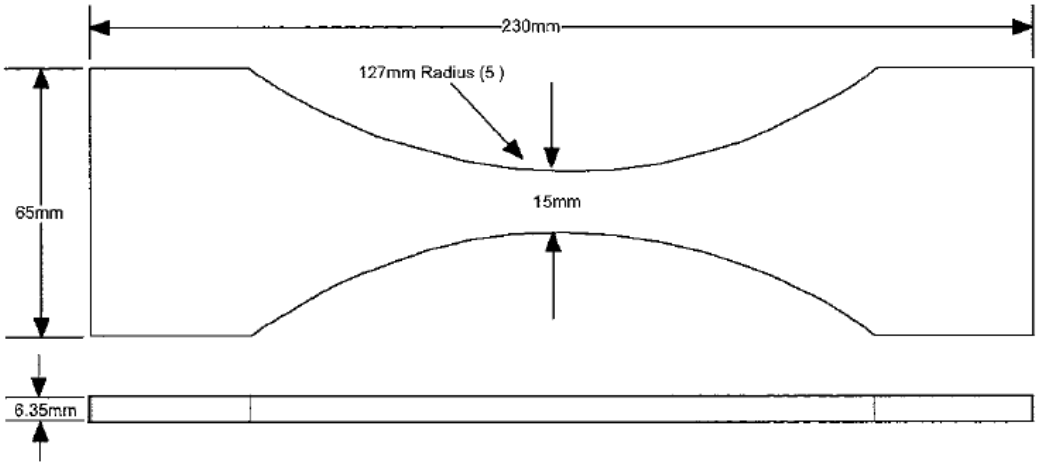

Figure A-1: F/A-18 Low Kt Coupon

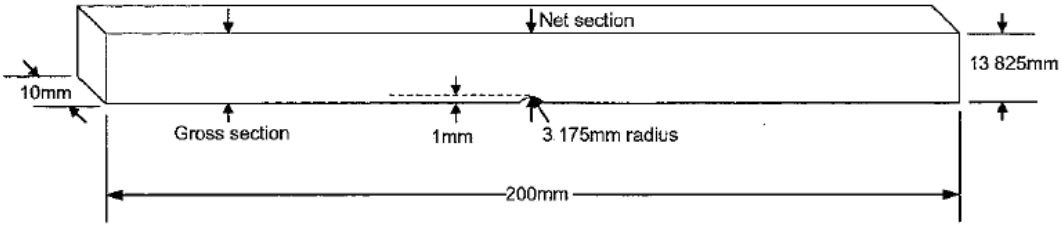

Figure A-2: F/A-18 Mid Kt Coupon

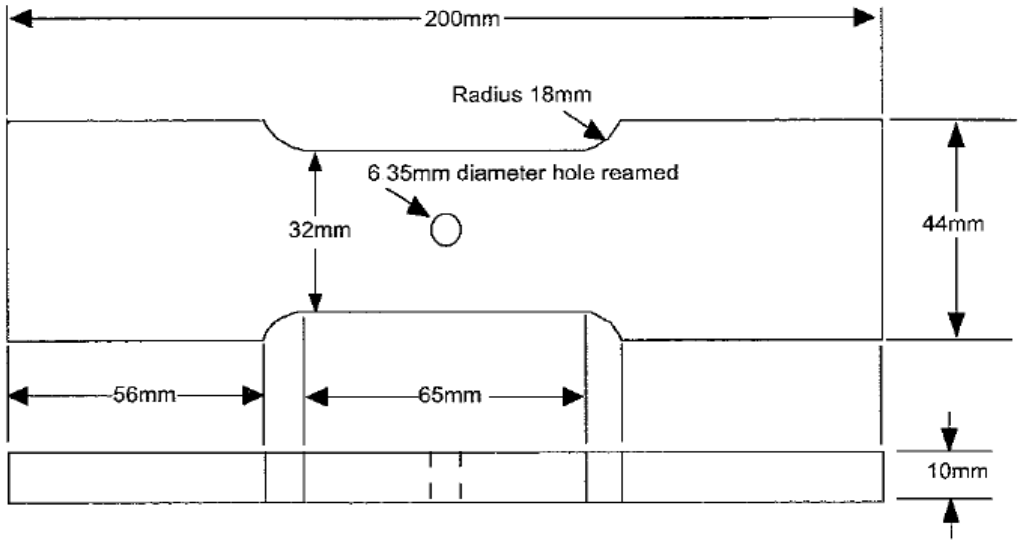

Figure A-3: F/A-18 'High' Kt Coupon

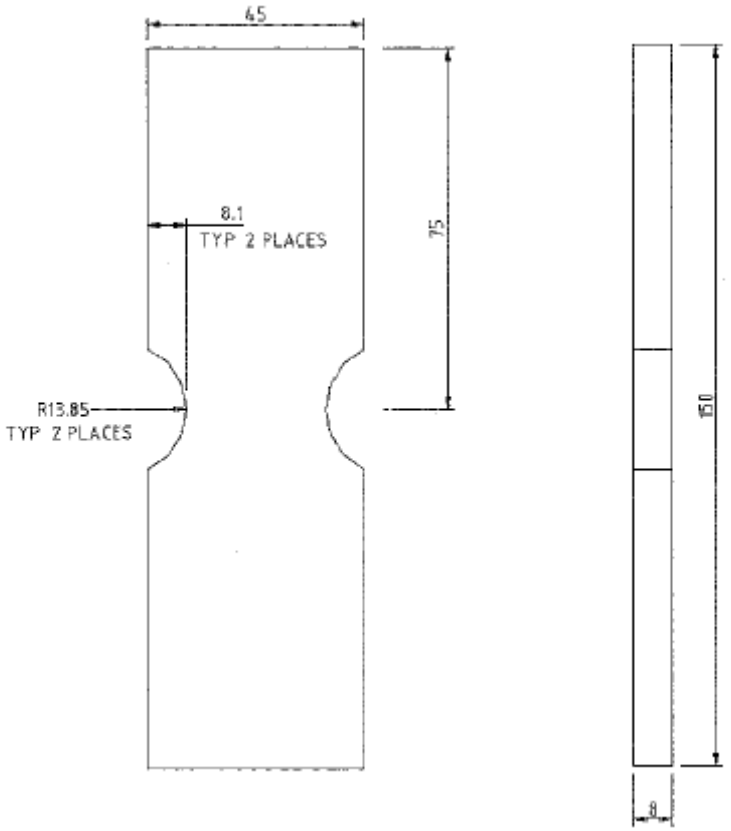

Figure A-4: F-111 LITV Double Notched Coupon

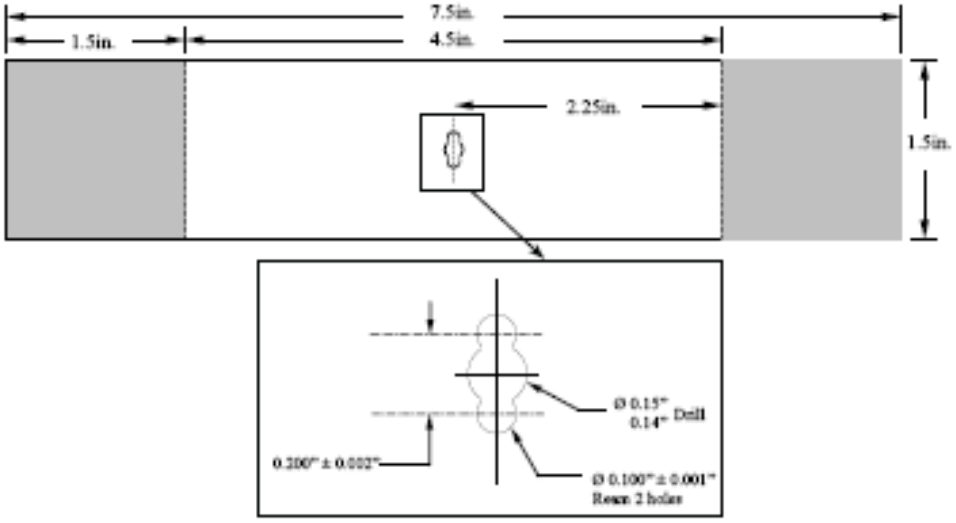

Figure A-5: P-3 High Kt Double-Ear Coupon

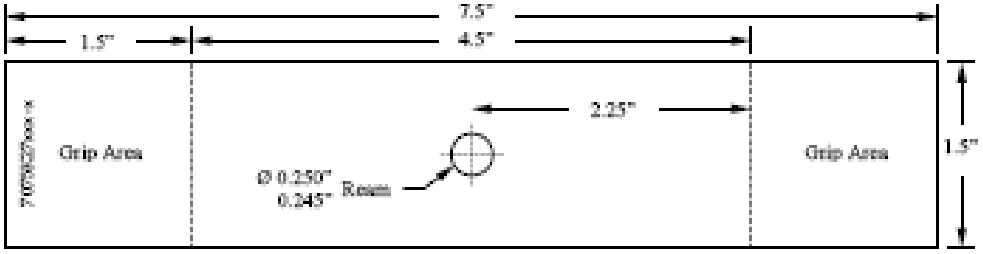

Figure A-6: P-3 Open Hole Coupon

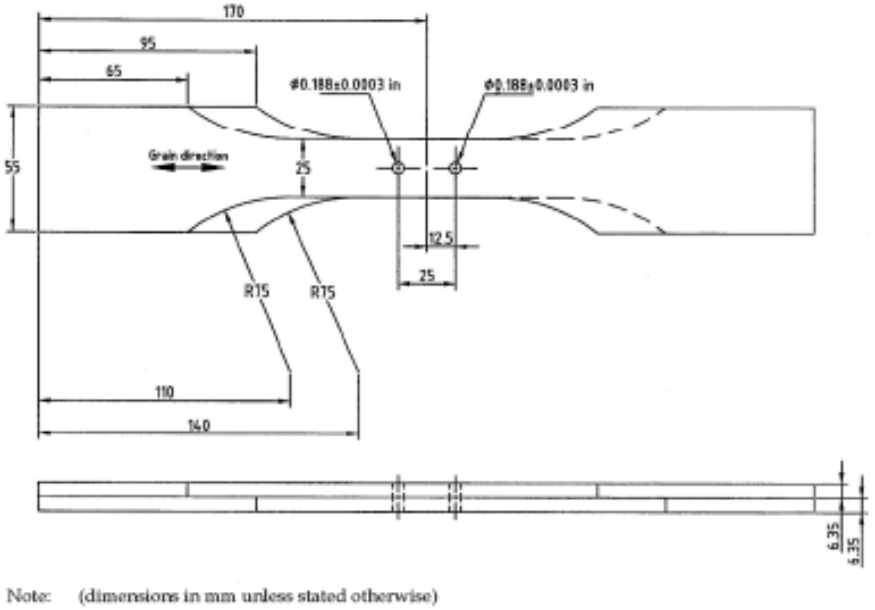

Figure A-7: P-3 Low-Load Transfer Joint Coupon

A.2. Coupon Test Matrix

The following table summarises the variable amplitude spectra coupon test programs examined in this discussion paper giving the coupon Kt values and the range of peak stresses covered by the variable amplitude spectra

Table A-1 Summary of coupon test matrices

Program	**Coupon Type**	**A_{gross} / A_{net}**	**Kt gross**	**Kt net**	**Applied remote stress range**		**Net stress range**	
					MPa	ksi	MPa	ksi
F/A-18	low K_t	1.0	1.04	1.04	280-467	41-68	280-467	41-68
	mid K_t	1.08	2.26	2.1	180-300	26-44	194-324	28-47
	high K_t	1.25	3.32	2.66	124-200	18-29	155-250	23-36
F-111	LITV double notch	1.56	2.4	1.55	179-235	26-34	280-367	40-53
P-3 SLAP	Double-ear	1.25	5	4	138-214	20-31	173-267	25-39
Ad-hoc	Double-ear (P-3)	1.25	5	4	138-214	20-31	173-267	25-39
	Double-ear (F-111)	1.25	5	4	242-254	35-37	302-317	44-46
	Open hole (F-111)	1.2	3.24	2.7	242-254	35-37	290-305	42-44
	Double-ear (F/A-18)	1.25	5	4	140-150	20-22	175-188	25-28

Appendix B: Revised FASTRAN Analysis Comparisons for F-111 LITV Coupon Testing

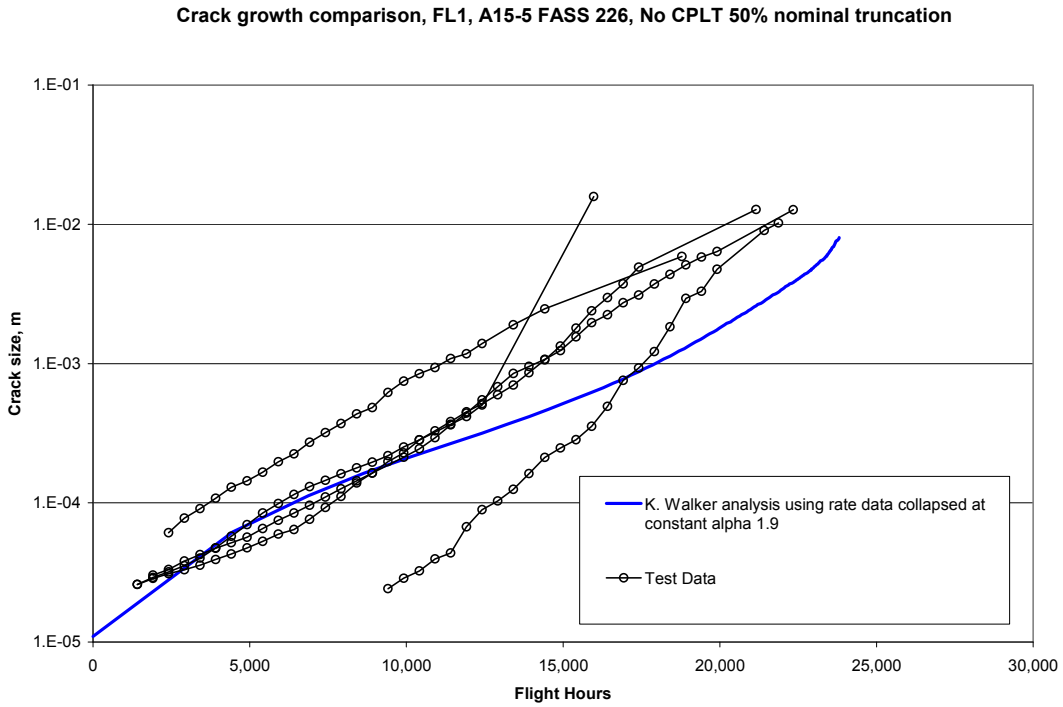

Figure B- 1 Crack Growth Comparison FL1, A15-5 FASS 226, No CPLT, 50% nominal truncation

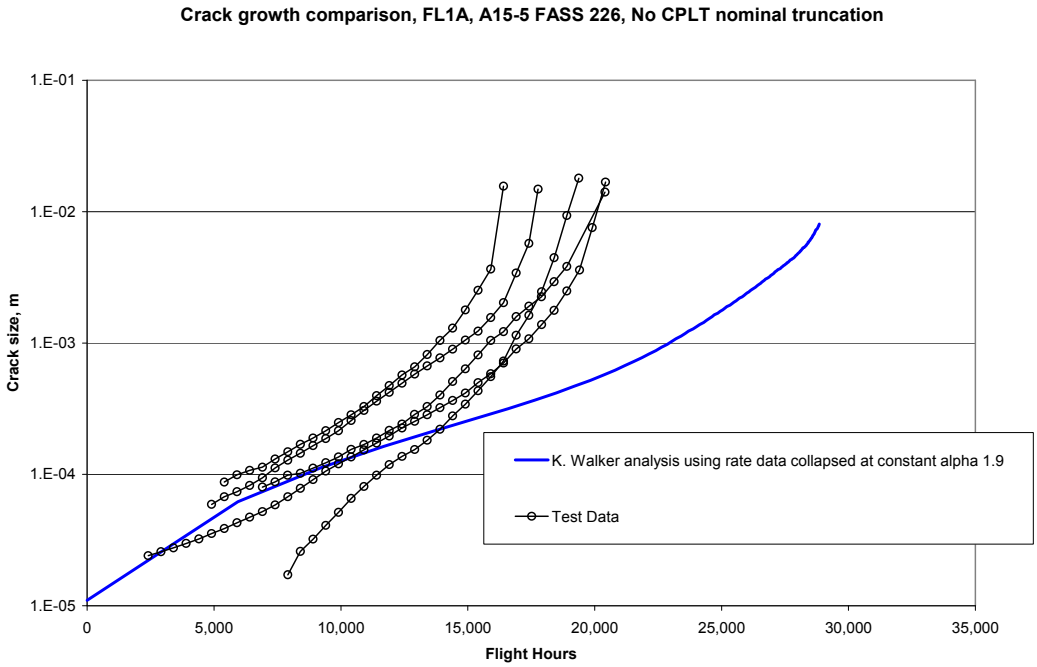

Figure B- 2 Crack growth Comparison FL1A, A15-5 FASS 226 No CPLT, nominal truncation

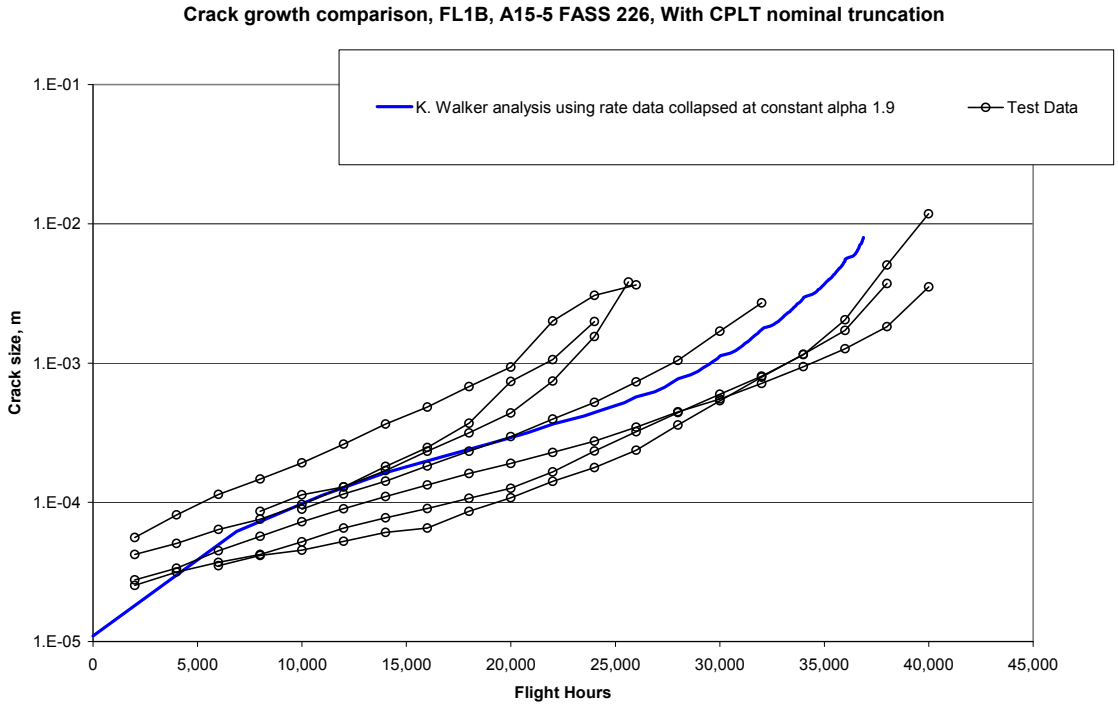

Figure B- 3 Crack growth Comparison FL1B, A15-5 FASS 226 With CPLT, nominal truncation

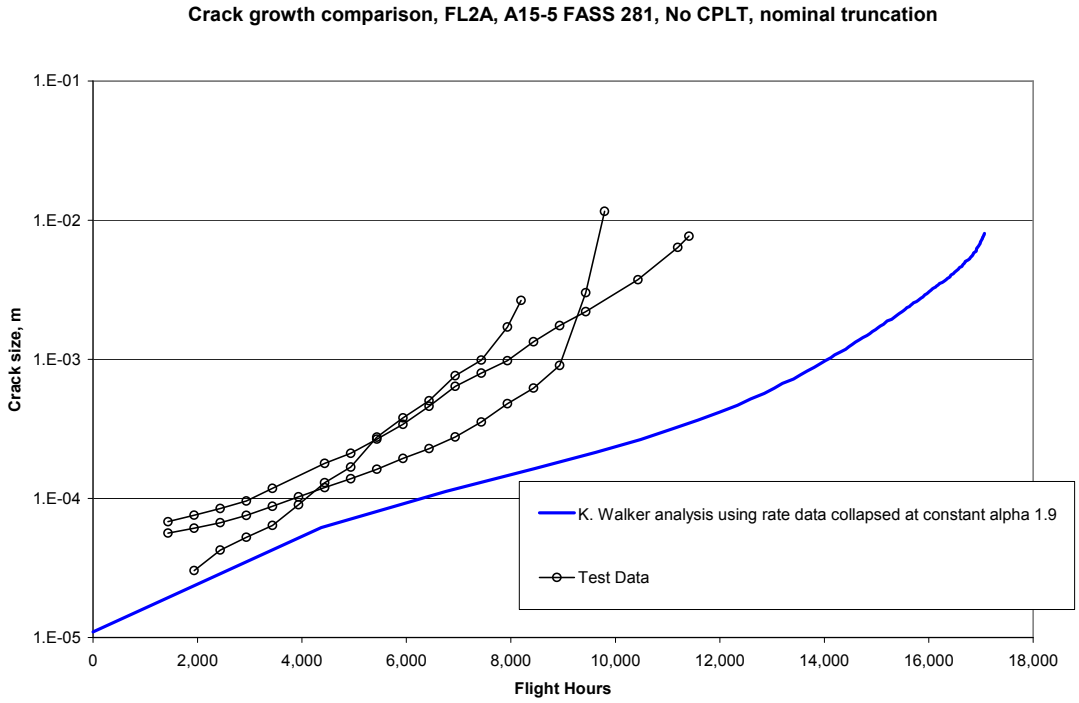

Figure B- 4 Crack growth Comparison FL2A, A15-5 FASS 281 No CPLT, nominal truncation

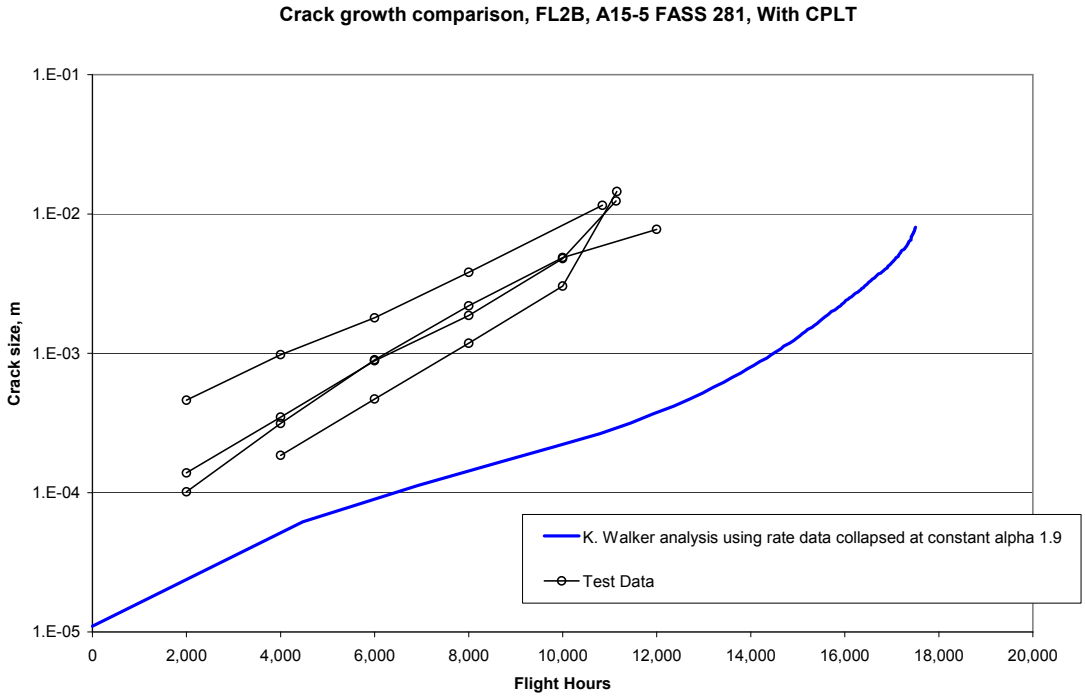

Figure B- 5 Crack growth Comparison FL2B, A15-5 FASS 281 with CPLT

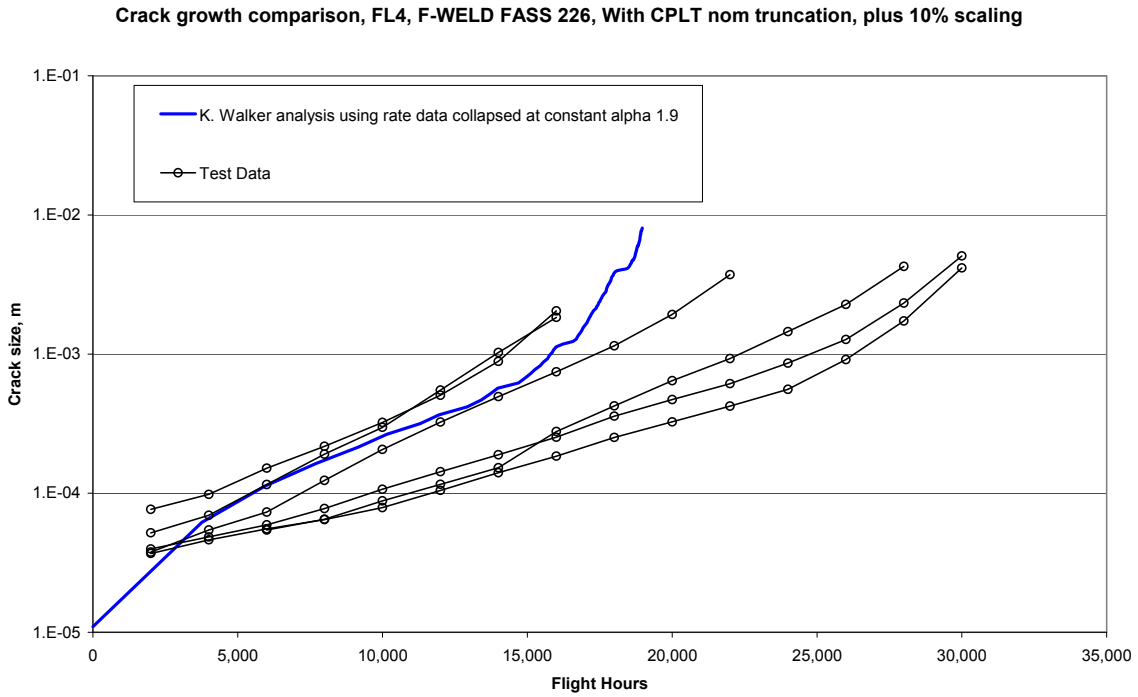

Figure B- 6 Crack growth Comparison FL4, F-WELD FASS 226, with CPLT nominal truncation plus 10% scaling (Note – all these coupon results are considered suspect and were rejected [26]. However, the results are shown here regardless and are for information only).

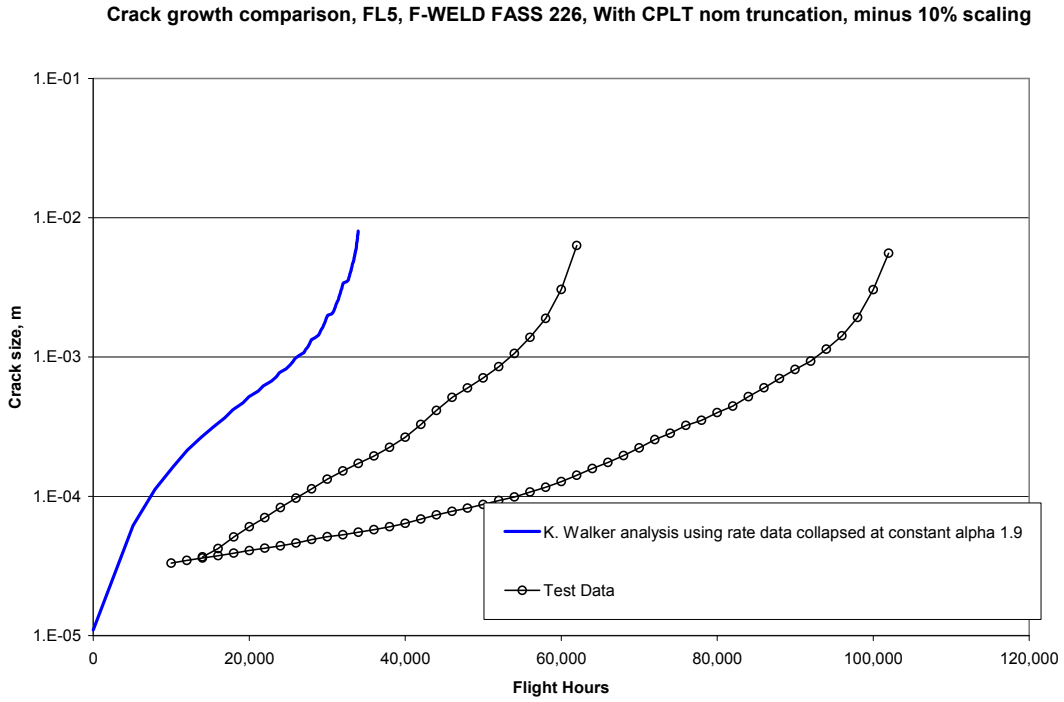

Figure B- 7 Crack growth Comparison FL5, F-WELD FASS 226, with CPLT, nominal truncation, minus 10% scaling

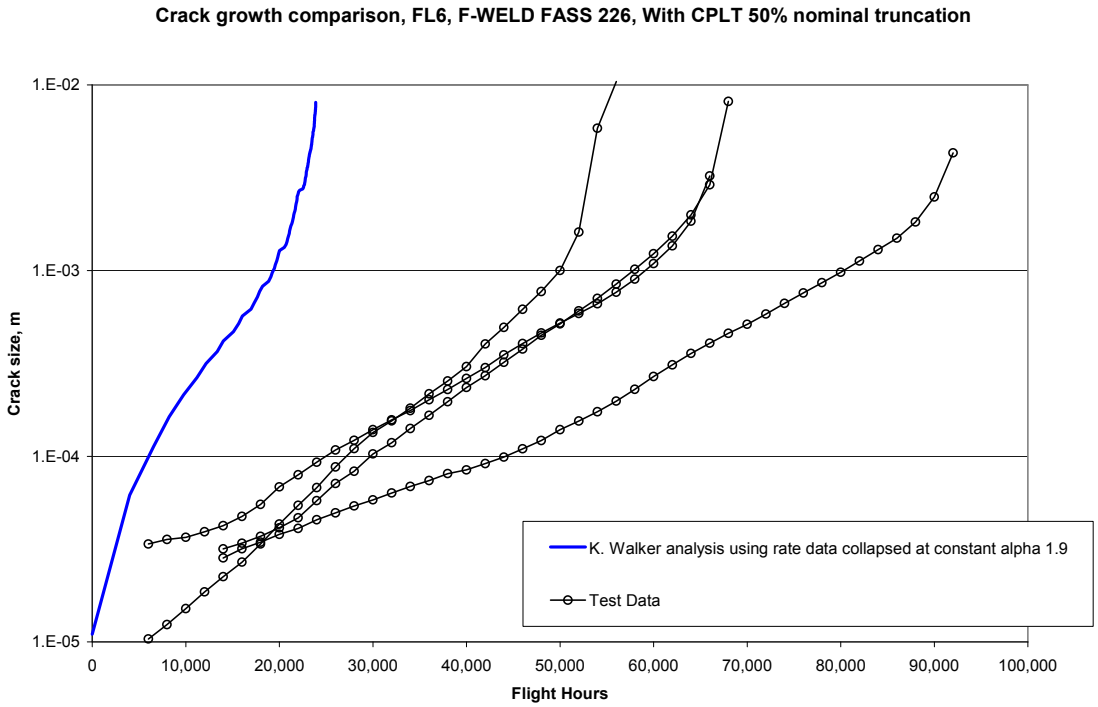

Figure B- 8 Crack growth Comparison FL6, F-WELD FASS 226, with CPLT, 50% nominal truncation

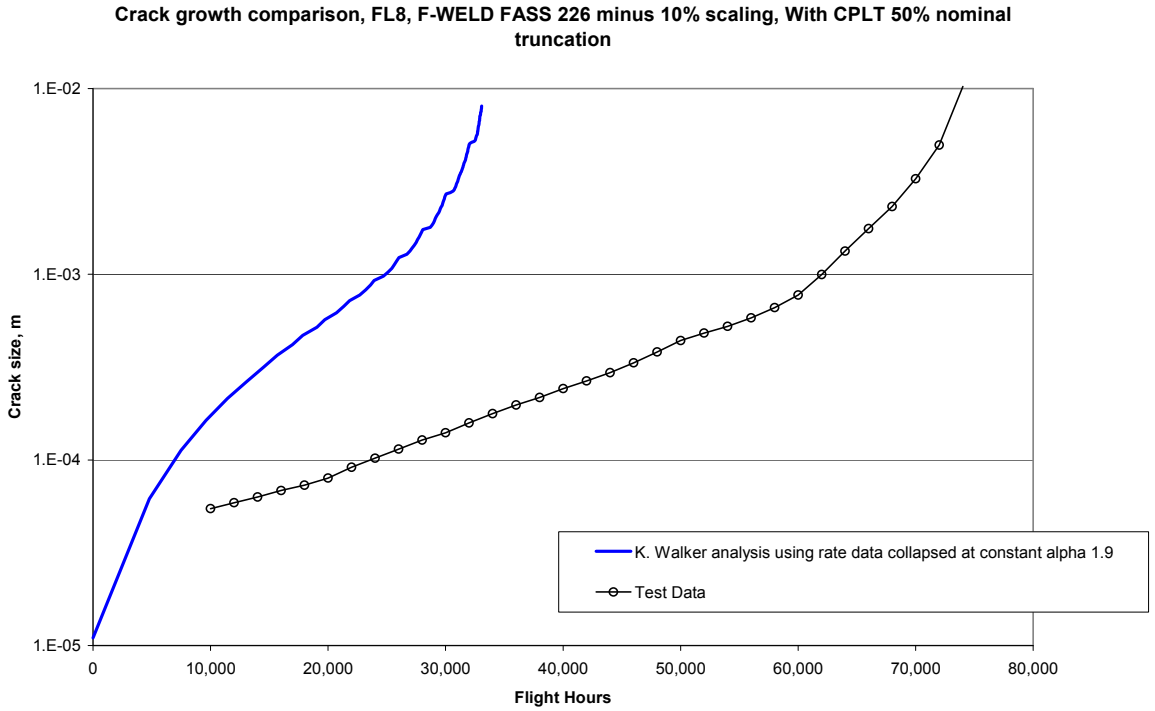

Figure B- 9 Crack growth Comparison FL8, F-WELD FASS 226, with CPLT, minus 10% scaling, 50% nominal truncation

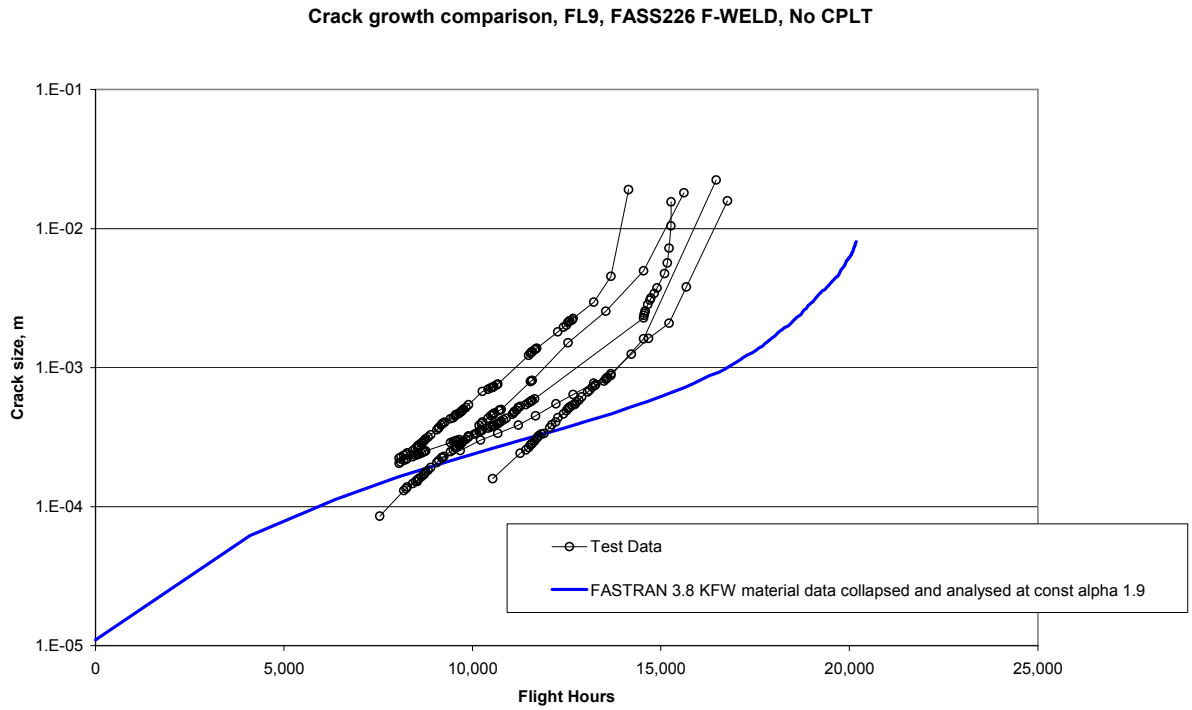

Figure B- 10 Crack growth Comparison FL9, FASS 226 F-WELD, no CPLT

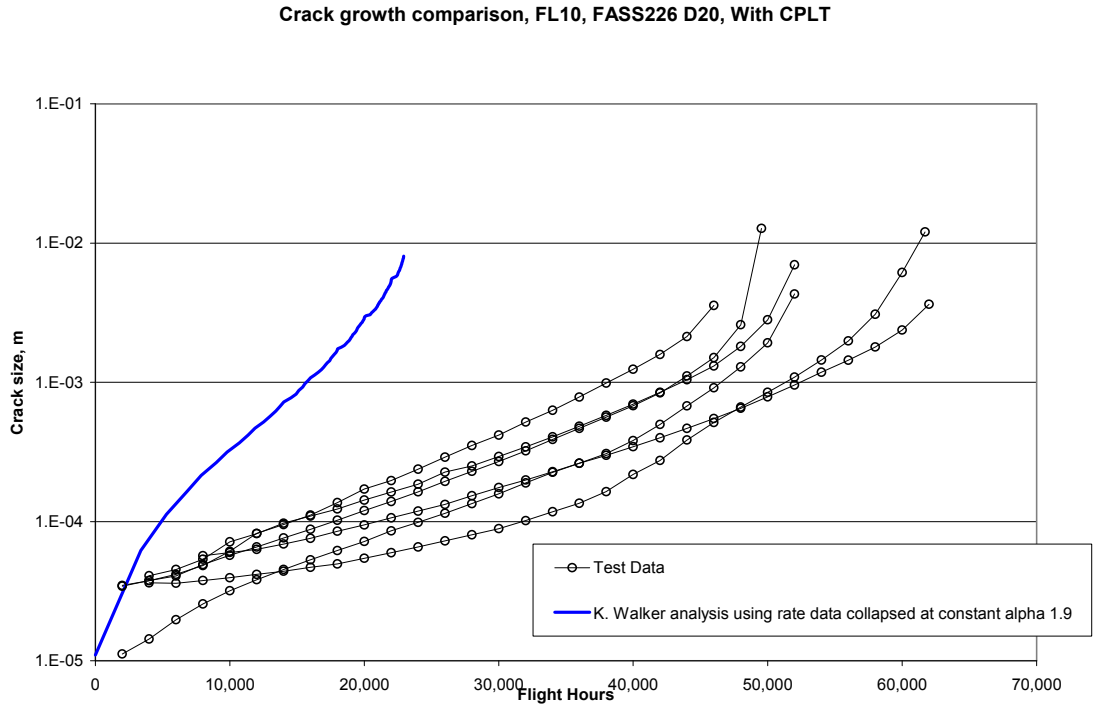

Figure B- 11 Crack growth Comparison FL10, FASS 226 D20, with CPLT

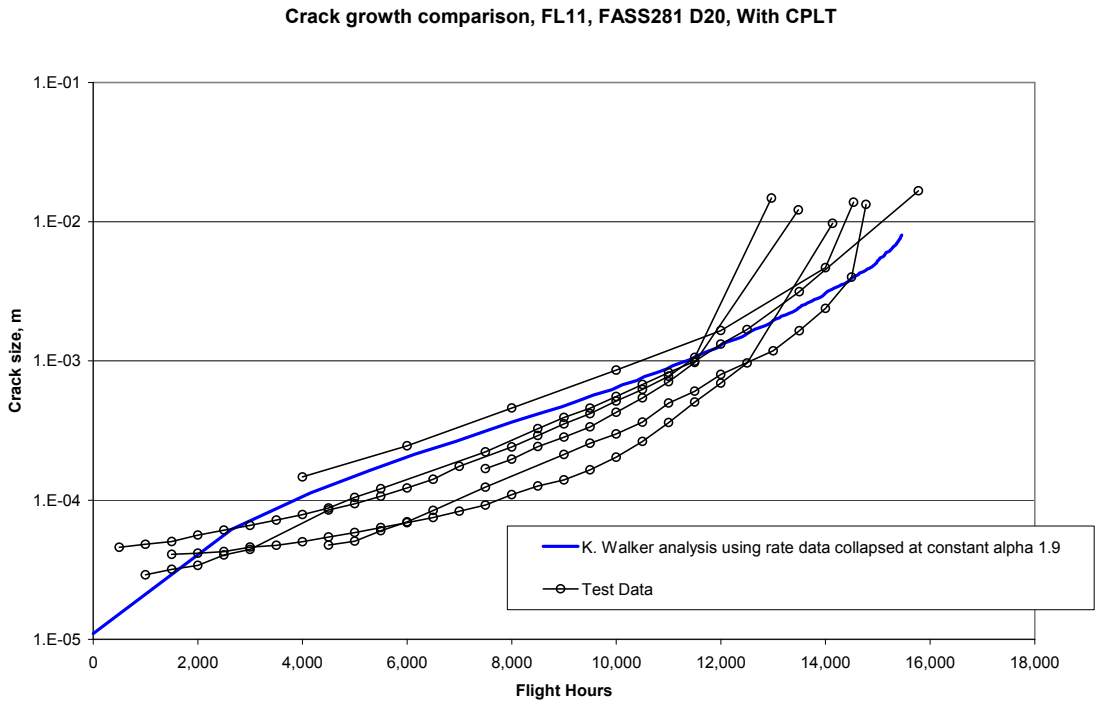

Figure B- 12 Crack growth Comparison FL11, FASS 281 D20, with CPLT

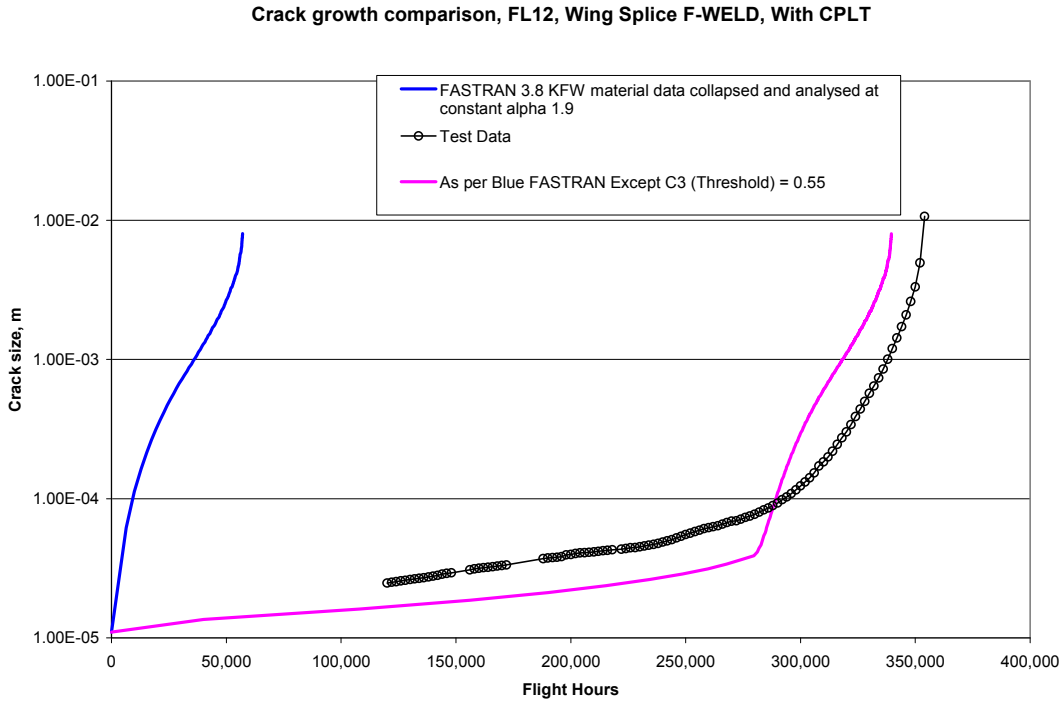

Figure B- 13 Crack growth Comparison FL12, Wing Splice F-WELD, with CPLT

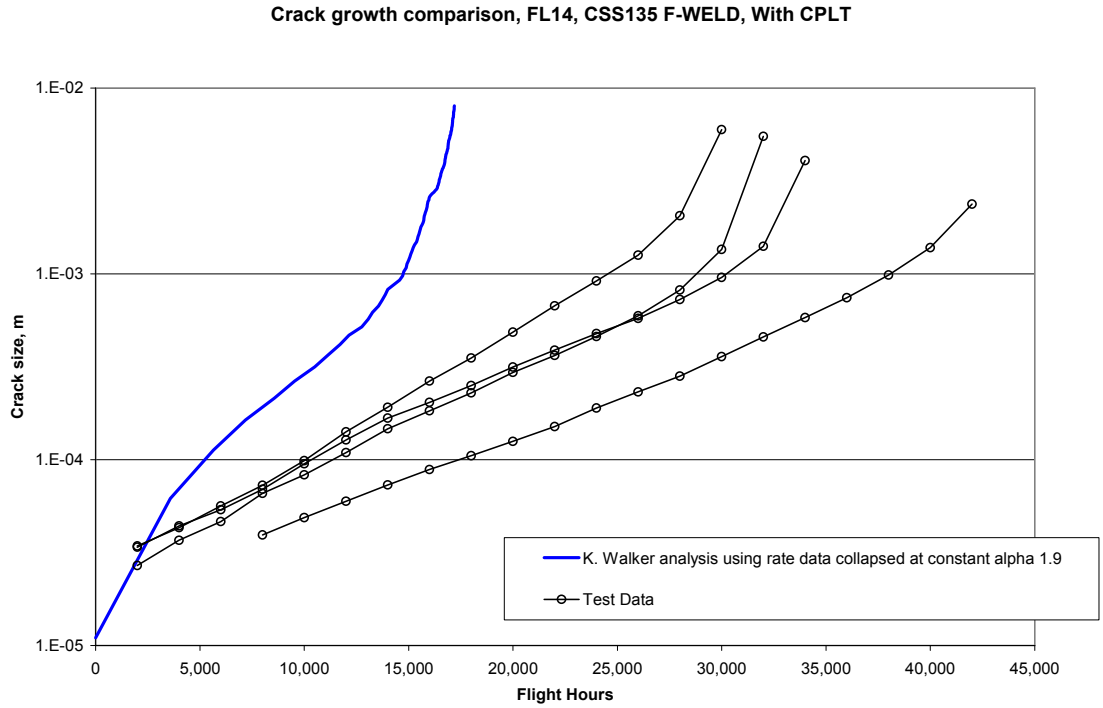

Figure B- 14 Crack growth Comparison FL14, CSS135 F-WELD, with CPLT

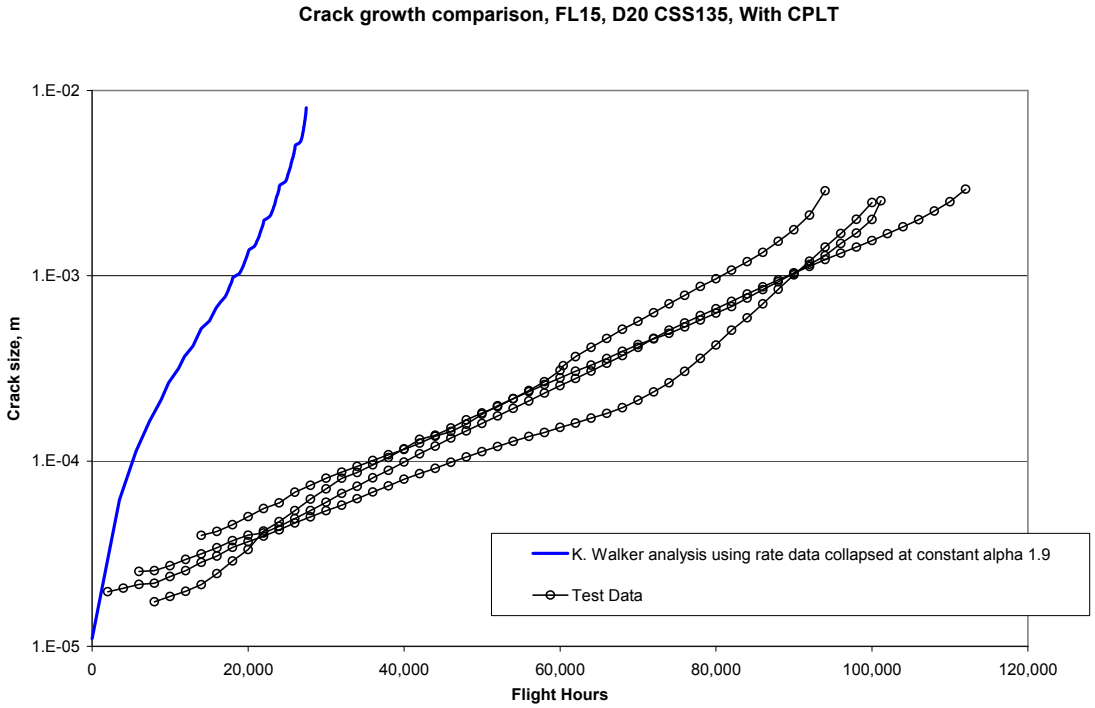

Figure B- 15 Crack growth Comparison FL15, D20 CSS135, with CPLT

This page is intentionally blank

DEFENCE SCIENCE AND TECHNOLOGY ORGANISATION
DOCUMENT CONTROL DATA

1. PRIVACY MARKING/CAVEAT (OF DOCUMENT)

2. TITLE

Exploration of Questions Regarding Modelling of Crack Growth Behaviour under Practical Combinations of Aircraft Spectra, Stress Levels and Materials

3. SECURITY CLASSIFICATION (FOR UNCLASSIFIED REPORTS THAT ARE LIMITED RELEASE USE (L) NEXT TO DOCUMENT CLASSIFICATION)

Document	(U)
Title	(U)
Abstract	(U)

4. AUTHOR(S)

P. Jackson, C. Wallbrink, K. Walker, D. Mongru and W. Hu

5. CORPORATE AUTHOR

DSTO Defence Science and Technology Organisation
506 Lorimer St
Fishermans Bend Victoria 3207 Australia

6a. DSTO NUMBER	6b. AR NUMBER	6c. TYPE OF REPORT	7. DOCUMENT DATE
DSTO-RR-0368	AR-015-0368	Research Report	July 2011

8. FILE NUMBER	9. TASK NUMBER	10. TASK SPONSOR	11. NO. OF PAGES	12. NO. OF REFERENCES
2010/1088618/1	AIR 07/283	DGTA	85	51

13. DSTO Publications Repository

http://dspace.dsto.defence.gov.au/dspace/

14. RELEASE AUTHORITY

Chief, Air Vehicles Division

15. SECONDARY RELEASE STATEMENT OF THIS DOCUMENT

Approved for public release

OVERSEAS ENQUIRIES OUTSIDE STATED LIMITATIONS SHOULD BE REFERRED THROUGH DOCUMENT EXCHANGE, PO BOX 1500, EDINBURGH, SA 5111

16. DELIBERATE ANNOUNCEMENT

No Limitations

17. CITATION IN OTHER DOCUMENTS Yes

18. DSTO RESEARCH LIBRARY THESAURUS http://web-vic.dsto.defence.gov.au/workareas/library/resources/dsto_thesaurus.shtml

crack growth, fatigue, structural integrity, aircraft, modelling

19. ABSTRACT

Qustions regarding the most appropriate crack growth modeling tools in aircraft structural analysis have been asked of the Fatigue Methods and Standards Group within AVD Continuing the Group's previous endeavours along these lines this report commences by stating the questions that will be explored and then individually examining the issues using both experimental data from coupon tests run under typical aircraft spectra and results from various crack growth prediction models. The findings, particularly those regarding the likely boundaries of applicability of different crack growth modelling techniques are then discussed. Conclusion are drawn regarding the implications of the findings of the work for fatigue practicioners within DSTO and for future work within the Standards and Methods Group.